Brain Network Correlates of Recovery of Consciousness and Non-Invasive Brain Stimulation

Danielle Nadin

Integrated Program in Neuroscience

Faculty of Medicine and Health Sciences

McGill University, Montreal

Submitted March 2021

A thesis submitted to McGill University in partial fulfillment of the requirements of the degree of Master of Science.

Table of Contents

Table of Figures

Chapter 2

Chapter 3

Chapter 4

Appendix 1

Table of Tables

Abstract

Brain-injured individuals may survive but become behaviorally unresponsive and are then said to be in a disorder of consciousness (DoC). Some of these patients are transiently aware of themselves and their surroundings (i.e. are conscious), while the rest are completely unconscious. This distinction is critical, as it has implications for end-of-life decision-making and access to care. Yet, 15 to 41% of patients who are minimally conscious are misdiagnosed as unconscious (Kondziella et al., 2016; Schnakers et al., 2009a). While neuroimaging methods such as positron emission tomography are available for prognosis, they are not accessible to all patients due to cost and medical contraindications. Further, there are no recommended treatment options for DoC patients beyond 4-16 weeks post-injury (Giacino et al., 2018). There is therefore a need for novel approaches to the prognosis and treatment of DoC.

First, we investigated the relationship between 3-node functional motifs derived from high-density electroencephalogram (EEG) networks and states of anesthetic-induced unconsciousness in healthy adults (n=9). Node participation in a motif composed of long-range, source-sink connections was disrupted during states of anesthetic-induced unresponsiveness. Participation in a loop-like motif composed of short-range connections was disrupted during high levels of anesthesia and returned to its baseline state prior to recovery of responsiveness. Second, we measured the association between 3-node functional network motifs and recovery of consciousness in three cases of DoC. At baseline, the topography of node participation in motifs was similar to healthy controls in patients who eventually recovered. The ability of topographic network properties to reconfigure in response to an anesthetic perturbation was also associated with recovery. Third, we measured the effects of transcranial direct current stimulation (tDCS) applied to the left dorsolateral prefrontal cortex of healthy adults on scalp and source EEG networks to inform the eventual treatment of DoC. We found no statistically significant impact of 1 or 2 mA tDCS on brain networks as compared to sham stimulation.

Taken together, these three studies highlight the usefulness of graph theoretical measures derived from high-density EEG for the prognostication of DoC and the neurophysiological assessment of tDCS response. This work raises several avenues for future exploration in the areas of prognosis and treatment of DoC, such as perturbation studies, optimized tDCS targeting algorithms and tDCS dose-response studies in DoC populations.

Résumé

Les personnes atteintes de lésions cérébrales peuvent survivre, mais devenir non-répondantes, et sont alors considérées comme ayant un trouble de la conscience. Certain-e-s de ces patient-e-s sont temporairement conscient-e-s d'eux/elles-mêmes et de leur environnement, tandis que les autres sont complètement inconscient-e-s. Cette distinction est essentielle, car elle a des implications sur la prise de décision en fin de vie et sur l'accès aux soins. Pourtant, 15 à 41% des patient-e-s dont la conscience est minimale sont diagnostiqué-e-s à tort comme étant inconscient-e-s (Kondziella et al., 2016; Schnakers et al., 2009a). Bien que des méthodes de neuroimagerie telles que la tomographie par émission de positons soient disponibles pour la pronostication, elles ne sont pas accessibles à tou-te-s les patient-e-s en raison de coûts et de contre-indications médicales. De plus, il n'y a pas d'options de traitement recommandées pour ces patient-e-s au-delà de 4 à 16 semaines après la lésion (Giacino et al., 2018). Il y a donc un besoin pour de nouvelles approches pour le pronostic et le traitement des troubles de la conscience.

Tout d'abord, nous avons étudié la relation entre les motifs fonctionnels à 3 nœuds dérivés d'électroencéphalogrammes (EEG) à haute densité et les états d'inconscience induites par l'anesthésie chez des adultes en santé (n = 9). La participation de nœuds dans un motif composé de connexions source-puits à longue portée était interrompue durant les états de non-réponse induites par l'anesthésie. La participation dans un motif cyclique composé de connexions à courte portée était interrompue pendant les niveaux élevés d'anesthésie et est revenue à son état de base avant que les participant-e-s récupèrent leur capacité de répondre aux commandes. Deuxièmement, nous avons mesuré l'association entre les motifs fonctionnels à 3 nœuds et la récupération de la conscience dans trois cas de troubles de la conscience. Au niveau de base, la topographie de la participation de nœuds dans les motifs était similaire à celle de sujets sains chez les patients qui ont éventuellement récupéré conscience. La capacité des propriétés topographiques du réseau cérébral à se reconfigurer en réponse à une perturbation anesthésique était également associée à la récupération de conscience. Troisièmement, nous avons mesuré les effets de la stimulation transcrânienne à courant continu (tDCS) appliquée au cortex préfrontal dorsolatéral gauche d'adultes en santé (n=15) sur les réseaux cérébraux au niveau du cuir chevelu et du cortex pour informer le traitement éventuel des troubles de la conscience. Nous n'avons trouvé aucun impact

statistiquement significatif de la tDCS à 1 ou 2 mA sur les réseaux cérébraux par rapport à la stimulation placébo.

Prises ensemble, ces trois études mettent en évidence l'utilité des mesures proposées par la théorie des graphes dérivées de l'EEG haute densité pour le pronostic des troubles de la conscience et l'évaluation neurophysiologique de la réponse à la tDCS. Ces travaux soulèvent plusieurs pistes d'exploration future dans les domaines du pronostic et du traitement des troubles de la conscience, telles que les études de perturbation, les algorithmes de ciblage optimisé de la tDCS et les études de dosage de la tDCS chez les patients avec des troubles de la conscience.

Acknowledgements

I would first like to acknowledge the unwavering support of my supervisor, Dr. Stefanie Blain-Moraes. From unexpected delays to being completely derailed by COVID-19, you have remained flexible and positive as we navigated this thesis. Thank you for encouraging my involvement in projects other than my own and activities outside the lab, which have made my master's experience all the richer. You are everything a supervisor should be, and while I look forward to the next steps in my career, it is bittersweet to leave such a wonderful lab. Thank you to everyone in the BIAPT Lab for making these past years such a fun learning experience. A special thank you to Dr. Catherine Duclos for allowing me to accompany you on many trips to meet participants and to Yacine Mahdid for the thousands of lines of code without which none of this would have worked. Thank you to Dr. Marie-Hélène Boudrias; you provided me with the first research experience which sparked my interest in this work and motivated to me to complete this master's.

Thank you to the numerous collaborators whose time, advice, clinical and technical expertise made this work possible. To Drs. Mohamed Badawy, Justin Létourneau and Gilles Plourde, thank you for welcoming me into your ICUs and operating rooms for data collection, and for providing a clinical perspective to this work. To Drs. Christophe Grova and Umit Aydin, thank you for sharing your methods with me and for walking me through them. To Dr. Trey Avery and the rest of the EGI team who have visited us in Montreal, thank you for helping us make the most of our tools, and for getting us unstuck at many points along the way. Thank you to Dr. Reza Farivar for lending us equipment and getting this project over the finish line during a pandemic. To Béatrice Pelletier-De Koninck, thank you for sharing statistical advice; you simplified my life ten-fold!

To the Black In Neuro team, thank you for enriching my time in neuroscience. You have turned one of the arguably worst times to be writing a thesis into some of the greatest months of my life. To the participants and their families who shared a little piece of their lives with me, thank you for your trust and your generosity. To my own friends and family, thank you for the late nights, phone calls, meltdowns, highs and lows of these past few years. This would not have been possible or worthwhile without you. My master's has been generously supported by the Canadian Institutes of Health Research and the Fonds de la recherche en santé du Québec; thank you to the taxpaying public for trusting me with your hard-earned dollars.

Contribution of Authors

In Chapter 2, Danielle Nadin analyzed the data, interpreted the findings and constructively reviewed and edited the manuscript. Michael Avidan[1], Dr. Max Kelz[2] and Dr. George Mashour[3] designed the study. Dr. Vijay Tarnal[3], Dr. Paul Picton[3], Dr. Giancarlo Vanini[3], Dr. Goodarz Golmirzaje[3]. Dr. Ellen Janke[3] and Dr. Stefanie Blain-Moraes[4,5] collected the data. Yacine Mahdid[5,6], Dr. Catherine Duclos[4,5] and Dr. Stefanie Blain-Moraes[4,5] analyzed the data and interpreted the findings. Dr. Catherine Duclos[4,5] and Dr. Stefanie Blain-Moraes[4,5] wrote the first draft of the manuscript. Dr. George Mashour[3] also constructively reviewed the manuscript.

In Chapter 3, Danielle Nadin collected, analyzed and interpreted the data. She also wrote the first draft of the manuscript. Dr. Stefanie Blain-Moraes[4,5] and Dr. Gilles Plourde[7,8] designed the study. Dr. Catherine Duclos[4,5], Alexander Rokos[5,6], Dr. Caroline Arbour[9,10], Mohamed Badawy[7,8] and Justin Létourneau[7,8] collected the data. Yacine Mahdid[5,6] helped to analyze the data. Dr. Catherine Duclos[4,5], Yacine Mahdid[5,6] and Dr. Stefanie Blain-Moraes[4,5] helped interpret the data and provide constructive feedback and edits to the manuscript.

In Chapter 4, Danielle Nadin designed the study, collected, analyzed and interpreted the data, and wrote the manuscript. Dr. Stefanie Blain-Moraes[4,5] and Dr. Marie-Hélène Boudrias[4,5] designed the study. Dr. Stefanie Blain-Moraes[4,5] interpreted the data and provided constructive feedback and edits to the manuscript.

1. Department of Anesthesiology, Washington University School of Medicine, St. Louis, MO, USA
2. Department of Anesthesiology, Perelman School of Medicine, University of Pennsylvania, Philadelphia, PA, USA
3. Center for Consciousness Science and Department of Anesthesiology, University of Michigan Medical School, Ann Arbor, MI, USA
4. School of Physical and Occupational Therapy, McGill University, Montreal, Canada
5. Montreal General Hospital, McGill University Health Centre, Montreal, Canada
6. Integrated Program in Neuroscience, McGill University, Montreal, Canada
7. Montreal Neurological Hospital and Institute, McGill University Health Center, Montreal, QC
8. Department of Anesthesia, McGill University, Montreal, QC
9. Centre de recherche, CIUSSS du-Nord-de-l'Île-de-Montréal, Montreal, QC
10. Faculty of Nursing, Université de Montréal, Montreal, QC

Introduction

Following a brain injury, some patients are completely or inconsistently behaviorally unresponsive, and are said to have unresponsive wakefulness syndrome (UWS) or to be in a minimally conscious state (MCS), respectively. The standard diagnostic tool for such disorders of consciousness (DoC) is the clinical consensus of the patient's medical team, as well as neurobehavioral assessments such as the gold-standard JFK Coma Recovery Scale – Revised (CRS-R). Importantly, clinical consensus leads to a misdiagnosis rate of up to 41%, with patients in MCS being misdiagnosed with UWS (Schnakers et al., 2009a). Even when the CRS-R is used, 15% of patients are misdiagnosed (Kondziella et al., 2016). The distinction between UWS and MCS is critical, as only patients in MCS are transiently aware of themselves and their environment (i.e. are conscious). Being misdiagnosed as UWS may severely impact end-of-life decision-making, as well as the allocation of rehabilitation resources.

Further, prediction of recovery trajectories (i.e. prognostication) is often primarily based on diagnosis, age at injury, etiology of injury and neurobehavioral assessment, and is subject to similar challenges as diagnosis. Neuroimaging techniques such as positron emission tomography (PET) (Stender et al., 2016) and functional magnetic resonance imaging (fMRI) (Song et al., 2018) have achieved high prognostic accuracy, specificity and sensitivity, but this has yet to be done in a clinically-appropriate manner using electroencephalography (EEG). EEG is an interesting technique in this context, as, in addition to being non-invasive, it is portable, inexpensive and easy to set up at the bedside. There is therefore a need to explore novel EEG metrics for disorder of consciousness prognosis (Problem 1).

Beyond diagnostic and prognostic inaccuracy, there are limited treatment options for patients with DoC. The current recommendation of the American Academy of Neurology is to prescribe the drug amantadine to promote recovery in adult traumatic brain injury patients 4-16 weeks post-injury (Giacino et al., 2018). This drug is thought to act by enhancing dopamine signalling in prefrontal and striatal circuits involved in arousal and attention (Giacino et al., 2012). Beyond this acute time window, there is no recommend treatment. There is growing evidence supporting non-invasive brain stimulation (NIBS) as a potential treatment for DoC. Transcranial direct current stimulation (tDCS) is one such technique which applies a weak electric current to the surface of the scalp to modulate the resting membrane potentials of neurons. In the anodal configuration, neurons are

depolarized to facilitate firing (Stagg & Nitsche, 2011). Multiple double-blinded, randomized sham-controlled trials have demonstrated a positive effect of single or multiple sessions of anodal tDCS to the left dorsolateral prefrontal cortex (L-DLPFC) on behavioral responsiveness in DoC patients (Angelakis et al., 2014; Martens et al., 2018; Thibaut et al., 2014, 2017). However, there is substantial heterogeneity in the responsiveness of patients to tDCS, which is influenced by gray matter atrophy, brain metabolism, etiology of brain injury, time since injury and the number of stimulation sessions received (Estraneo et al., 2017; Thibaut et al., 2015). In addition to the limited evidence for why some patients respond to tDCS and some do not, it is unclear what electrophysiological mechanism underlies the effect of tDCS on the brains of patients with DoC.

While PET, fMRI and EEG have been used to try to understand the mechanism of tDCS-response, and to distinguish tDCS responders from non-responders (Thibaut et al., 2015), few studies have done so using high-density EEG (HD-EEG). HD-EEG-derived brain networks allow for higher spatial-resolution and more complex graph theoretical analyses (Bai et al., 2018; Hermann et al., 2020; Hill et al., 2019; Wu et al., 2019). In addition, only two studies have investigated the impact of L-DLPFC tDCS on connectivity in the source space, where greater insight on the specific brain regions affected by stimulation can be gained as compared to scalp-level analyses (Hermann et al., 2020; Hill et al., 2019). Thus, HD-EEG network analysis, particularly in the source space, is an underused tool that may prove useful in measuring the effects of tDCS on the brain (Problem 2).

This thesis will address issues in prognosticating and treating DoC by 1) evaluating a novel EEG-based metric for prognostication (Aim 1); and 2) investigating the brain network mechanisms of tDCS response using HD-EEG in healthy controls, in order to better understand this technique prior to applying it in DoC populations (Aim 2). These aims were achieved through three studies.

In Study 1, we validated functional network motifs – which are specific patterns of connectivity between a subset of nodes in a network – as a marker of anesthetic-induced unconsciousness in a cohort of healthy controls. We hypothesized that the spatial organization of node participation in motifs would change across states of anesthesia, and that this would information about the neural correlates of consciousness complementary to what can be gleaned from more commonly used graph theoretical network properties.

In Study 2, we explored functional network motifs as prognostic markers in three cases of disorders of consciousness. We hypothesized that DoC prognosis would be associated with the spatial organization of node participation in motifs. We anticipated that the spatial information provided by network motifs would be more predictive of patient outcome compared to more commonly used clinical measures, spectral properties and metrics which dilute spatial information by averaging across the whole brain network.

In Study 3, we investigated the impact of 1 and 2 mA anodal tDCS to the L-DPLFC on scalp and source space brain networks constructed using HD-EEG in a group of healthy controls. We hypothesized that a single session of 1 mA anodal tDCS would have similar effects on the EEG spectral content and graph theoretical network properties as compared to 2 mA anodal tDCS. We posited that the neurophysiological effects of tDCS at both stimulation intensities would translate to behavior, i.e. that stimulation of the L-DLPFC would increase accuracy and reduce reaction time on a working memory task.

Chapter 1: Literature Review

Disorders of Consciousness

Consciousness

Levels of consciousness are frequently described along three axes: wakefulness, awareness, and connectedness (Martial et al., 2020). Wakefulness (or arousal) refers to the presence of spontaneous eye opening, while awareness refers to subjective experiences of oneself or their surroundings, such as perception, thoughts, and emotions. The gold standard for measuring awareness is response to verbal command. While response to command is sufficient to determine awareness, it is not necessary; in other words, if a person is unresponsive, it cannot be concluded that they are unaware. Finally, connectedness refers to a connection with the external environment and stimuli. Some states of consciousness, like certain stages of sleep, may allow for internal awareness, but are disconnected due to a lack of connection with the outside world.

Mechanism

DoC can develop following acquired brain injury (e.g. stroke; anoxic, hypoxic or traumatic brain injury), infection (e.g. meningitis) or as a long-term result of a neurodegenerative disorder (e.g. Alzheimer's disease) (Monti, Laureys, et al., 2010). In the acute stage of acquired brain injury, patients are typically comatose and/or maintained in a pharmacological coma, where they are neither wakeful or aware, and neither spontaneous or evoked arousal is possible (Giacino et al., 2014). Upon emergence from coma or withdrawal of sedation, patients who survive may begin to recover or transition to a liminal state, where they are neither fully conscious nor unconscious. These states, called DoC, are characterized by wakefulness (e.g. spontaneous eye-opening), but inconsistent or completely absent awareness (e.g. evoked response to command).

Diagnosis & prognosis

DoC can be broadly categorized into MCS and UWS (formally known as vegetative state). In both cases, patients exhibit wakefulness in the form of reflexive behaviors, such as eye-opening, blinking and swallowing. In MCS, patients can also inconsistently demonstrate awareness by responding to verbal commands, while, in UWS, patients are completely unresponsive. Misdiagnosis may occur when fully unresponsive patients have undiagnosed disabilities (e.g.

blindness, deafness) or conditions (e.g. hydrocephaly) which make it difficult or impossible for them to respond appropriately to behavioral assessment (Monti, Laureys, et al., 2010). Further, the fluctuating nature of MCS may also lead to misdiagnosis if assessments are unknowingly performed when patients are in pain, asleep or experiencing a lower level of consciousness (Monti, Laureys, et al., 2010). As a consequence, 15 to 41% of MCS patients are misdiagnosed with UWS (Peterson et al., 2015; Schnakers et al., 2009a). This diagnosis, which labels them as unconscious when they are not, can have significant impacts on clinical decision-making and care.

In North America, diagnoses and prognoses are made based on neurobehavioral assessments, while functional neuroimaging and EEG are recommended when neurobehavioral results are ambiguous (Giacino et al., 2018). If neuroimaging and neurobehavioral assessments disagree, alternate diagnoses may be considered and rehabilitative care may be modified, but it is still recommended that neurobehavioral assessment be repeated regularly (Giacino et al., 2018). While the CRS-R is recommended to assist with diagnosis and prognosis, this assessment is not widely used due its length and requirement of regular, daily administration (Personal communication, C. Arbour, 2020). In Europe, qualitative clinical EEG (e.g. sleep patterns, EEG reactivity) and quantitative HD-EEG analyses are recommended in the absence of command-following ability, along with functional neuroimaging evaluations using PET and fMRI (Kondziella et al., 2020). Unlike in North America, if neuroimaging and neurobehavioral assessments disagree, the highest level of consciousness determined by either method should be presumed (Kondziella et al., 2020).

Transcranial Direct Current Stimulation

Mechanism

tDCS is a NIBS technique which modulates cortical excitability via the application of a weak electric current through electrodes placed on the surface of the scalp. Current is sent through one or multiple positive anodes and received by one or multiple negative cathodes. In the anodal configuration, anodes are placed over a targeted area, and cortical excitability in this area is increased by depolarizing neural resting potentials, consequently increasing the likelihood of action potential firing (Stagg & Nitsche, 2011). Long-term effects of tDCS are thought to occur through a long-term potentiation-like mechanism which acts primarily through glutamatergic NMDA-receptor dependent and GABAergic pathways (Stagg & Nitsche, 2011).

Stimulation dosage and montage

While it was formerly believed that anodal tDCS always results in increased cortical excitability and that cathodal tDCS (when the cathode is placed of the target region) always results in decreased cortical excitability (Stagg & Nitsche, 2011), recent evidence suggests that this is not always the case. When applied at 2 mA for 20 min, cathodal tDCS has been shown to increase, rather than decrease, cortical excitability (Batsikadze et al., 2013; Mosayebi Samani et al., 2019). Further, dose-dependent effects of tDCS are non-linear, with low intensity stimulation ($\leq$ 1 mA) showing equal or greater effects on cortical excitability as compared to high intensity stimulation ($>$ 1 mA) in the primary motor cortex (Agboada et al., 2019; Jamil et al., 2017). This may account for the large inter-individual variability observed in tDCS studies, which employ a varied and often inconsistent range of stimulation parameters (Bikson et al., 2018).

The field is also moving towards high-density and targeted stimulation montages. Traditionally, tDCS has been delivered through large sponge electrodes (typically 25 to 35 cm^2), with one electrode placed over the targeted area and the other placed over the supraorbital area. Target areas have long been determined using the 10-20 system, which estimates the location of brain areas based on landmarks like the bridge of the noise and the periauricular points (Jasper, 1958). More recently, high-density electrode montages using small circular electrodes have been shown to increase stimulation focality and intensity by $\geq$ 80% as compared to traditional montages (Dmochowski et al., 2011). Targeting algorithms have also been employed to take into consideration subjects' brain anatomy and head shape in order to determine the optimal electrode placement to stimulate a region of interest. The literature points to a trade-off between the intensity of the electric field at the target site, and the focality of stimulation to that target site, with algorithms at each end of this spectrum (Dmochowski et al., 2011; Fernández-Corazza et al., 2020). Open source software are available to perform targeting, taking a participant's MRI, the stimulation electrode size and composition, and the targeted brain area as input (Y. Huang et al., 2018)

Treatment for disorders of consciousness

There is growing evidence supporting tDCS as a potential treatment for DoC. Multiple double-blinded, randomized sham-controlled trials have demonstrated a positive effect of single or multiple sessions of anodal tDCS to the L-DLPFC on behavioral responsiveness (Angelakis et al., 2014; Martens et al., 2018; Thibaut et al., 2014, 2017). However, at the individual level, there is

substantial heterogeneity in the responsiveness of patients to tDCS. Gray matter atrophy, brain metabolism, brain injury etiology, time since injury and the number of stimulation sessions received have all been shown to contribute to this variability (Estraneo et al., 2017; Thibaut et al., 2015).

In addition to the limited evidence for why some patients respond to tDCS and some do not, it is unclear what electrophysiological and cognitive mechanisms underly the effect of tDCS on the brains of DoC patients. In healthy controls, anodal tDCS applied over the L-DLPFC has been shown to increase working memory performance, as measured by reduced reaction time and increased accuracy on memory tasks (Boggio et al., 2006; Fregni et al., 2005; Teo et al., 2011), hinting that working memory enhancement may be one dimension of cognition through which tDCS promotes behavioral recovery in DoC. At the neurological level, preserved brain metabolism and grey matter (Thibaut et al., 2015), functional and structural integrity in the stimulated area (Minjoli et al., 2017) and other consciousness-related brain areas (e.g. precuneus, thalamus) (Thibaut et al., 2019) appear necessary for positive tDCS response.

Electroencephalographic Network Analysis & Source Localization

Network analysis

Several types of networks can be constructed using signals from the brain, including structural, functional, and effective networks. Structural networks describe the anatomical connections in the brain, such as white matter tracts. Effective networks refer to causal relationships in the brain, reflecting information transfer. Finally, functional networks describe statistical correlations between co-activated regions of the brain. The presence of functional connectivity therefore does not imply that structural or causal connections are also present.

EEG signals can be used to construct a graph where the nodes are scalp electrodes, and the edges are functional relationships between nodes. These functional relationships can be measured using simple correlations or more complex measures in the time-frequency domain. Because these statistical relationships are not grounded in anatomical or causal relationships, it is important to account for potentially spurious connections. Since electric fields generated by neural activity spread through the brain, cerebrospinal fluid, ventricles, and head tissues, activation in one brain area may be recorded by several, spatially dispersed scalp electrodes. In these cases, simple

correlations between these scalp electrodes will be spuriously elevated due to this spreading phenomenon, called volume conduction (Lachaux et al., 1999). Since volume conduction is instantaneous (i.e. there is no time delay between neuronal activation and measurement of the electric field at dispersed scalp electrodes), connectivity metrics which discard the instantaneous portion of the signal can help reduce the effects of volume conduction. Specifically, the weighted and directed phase lag index (wPLI and dPLI, respectively) (Cornelis J. Stam et al., 2007; Vinck et al., 2011) and the orthogonalized amplitude envelope correlation (AEC) (Brookes et al., 2012), which look at the non-instantaneous phase and amplitude relationships of signals over time, correct for volume conduction, and will be employed in this thesis.

It has been demonstrated that wPLI and dPLI are sensitive to neurophysiological changes related to consciousness (Blain-Moraes et al., 2015, 2016, 2017), but very few studies to date have used these measures to evaluate the EEG network effects of tDCS. One group has shown changes in network centrality following tDCS in a group of DoC patients (Thibaut et al., 2018), while another reported no impact of tDCS on network measures (Mancini et al., 2016). Similarly, orthogonalized AEC has not been explored in the context of tDCS and DoC, but is of interest as this measure has been shown to result in networks similar to resting state networks measured using fMRI (Brookes et al., 2012; Hipp et al., 2012).

Source localization

Source localization creates a representation of cortical activity by projecting recordings from scalp electrodes into the cortical space. This technique allows for inferences to be made about which anatomical brain regions are functionally connected, providing more information than scalp-level functional connectivity. As EEG signals are primarily generated by the synchronized firing of populations of pyramidal neurons perpendicular to the cortical surface (Gloor, 1985), activity within the brain is modeled using a finite number of source dipoles placed along the cortical surface (on the order of 8000 to 15 000 dipoles). As the number of source dipoles is much larger than the number of scalp electrodes, this is an ill-posed problem, with multiple possible solutions (Hassan et al., 2014). An optimal solution can be obtained by posing mathematical constraints on the problem, such as the location and orientation of source dipoles, as well as the conductivity of head and brain tissues, governed by Maxwell's equations (Hämäläinen et al., 1993).

In the context of measuring the effects of tDCS, source-localized EEG is still an underused tool. In healthy individuals, current density in the L-DPLFC has been correlated with tDCS response (J.-H. Kim et al., 2014), but others have also reported no impact of tDCS on resting state EEG networks in the source space (Hill et al., 2019). One study showed that DoC patients who exhibited behavioral improvement following anodal tDCS applied to the L-DLPFC also had increased power and parietal-occipital connectivity in the alpha and theta bands (Hermann et al., 2020). This effect was correlated with electric field strength in the stimulated prefrontal cortex, suggesting a causal effect of tDCS on behavioral responsiveness (Hermann et al., 2020).

Chapter 2: Brain Network Motifs are Markers of Loss and Recovery of Consciousness

Catherine Duclos, Ph.D.*,[1,2] Danielle Nadin, B.Sc.*,[1,2], Yacine Mahdid, B.Sc.,[1,2] Vijay Tarnal, M.D.,[4] Paul Picton, M.D.,[4] Giancarlo Vanini, M.D.,[4] Goodarz Golmirzaie, M.D.,[4] Ellen Janke, M.D.,[4] Michael S. Avidan, M.B.B.Ch.,[5] Max B. Kelz, M.D., Ph.D.,[6] George A. Mashour, M.D., Ph.D.,[4] Stefanie Blain-Moraes, Ph.D.[1,2]

* These authors contributed equally to the work

1. School of Physical and Occupational Therapy, McGill University, Montreal, Canada
2. Montreal General Hospital, McGill University Health Centre, Montreal, Canada
3. Integrated Program in Neuroscience, McGill University, Montreal, Canada
4. Center for Consciousness Science and Department of Anesthesiology, University of Michigan Medical School, Ann Arbor, MI, USA
5. Department of Anesthesiology, Washington University School of Medicine, St. Louis, MO, USA
6. Department of Anesthesiology, Perelman School of Medicine, University of Pennsylvania, Philadelphia, PA, USA

Corresponding author: Stefanie Blain-Moraes, Ph.D. Montreal General Hospital, Room L11-132, 1650 Cedar Ave, L11-132 Montréal, Québec, H3G 1A4 Canada. Tel: 514-398-1325 stefanie.blain-moraes@mcgill.ca

In order to validate the use of 3-node functional motifs as a potential prognostic marker in patients with disorders of consciousness, we investigated the association of motifs with states of anesthetic-induced unconsciousness. This manuscript was published in *Scientific Reports*.

Reference: Duclos, C.*, Nadin, D.*, et al. (2021). Brain network motifs are markers of loss and recovery of consciousness. *Scientific Reports*, *11*: 3892. https://doi.org/10.1038/s41598-021-83482-9.

* These authors contributed equally to the work.

Abstract

Motifs are patterns of inter-connections between nodes of a network, and have been investigated as building blocks of directed networks. This study explored the re-organization of 3-node motifs during loss and recovery of consciousness. Nine healthy subjects underwent a 3-h anesthetic protocol while 128-channel electroencephalography (EEG) was recorded. In the alpha (8–13 Hz) band, 5-min epochs of EEG were extracted for: Baseline; Induction; Unconscious; 30-, 10- and 5-min pre-recovery of responsiveness; 30- and 180-min post-recovery of responsiveness. We constructed a functional brain network using the weighted and directed phase lag index, on which we calculated the frequency and topology of 3-node motifs. Three motifs (motifs 1, 2 and 5) were significantly present across participants and epochs, when compared to random networks ($p<0.05$). The topology of motifs 1 and 5 changed significantly between responsive and unresponsive epochs (*p-values*<0.01; Kendall's W = 0.664 (motif 1) and 0.529 (motif 5)). Motif 1 was constituted by long-range chain-like connections, while motif 5 was constituted by short-range, loop-like connections. Our results suggest that anesthetic-induced unconsciousness is associated with a topological re-organization of network motifs. As motif topological re-organization may precede (motif 5) or accompany (motif 1) the return of responsiveness, motifs could contribute to the understanding of the neural correlates of consciousness.

Introduction

The field of network neuroscience has yielded powerful insight into the way the brain is structurally and functionally connected. The application of graph theoretical analysis to neuroimaging techniques has provided evidence that the brain has features of a complex small-world network, with functional modules and densely connected hubs (Bullmore & Sporns, 2009; Sporns, 2018). The development of measures quantifying properties of the brain network has led to a better understanding of the anatomical and functional architecture that drives various brain states, including anesthetic-induced unconsciousness. Both electroencephalography (EEG) and functional magnetic resonance imaging (fMRI) studies have shown that propofol-, sevoflurane-, and ketamine- induced unconsciousness induce a functional disconnection of anterior and posterior regions of the cortex (Bonhomme et al., 2016; Boveroux et al., 2010; Jordan et al., 2013; H. Lee et al., 2013; Palanca et al., 2015; Ranft et al., 2016), while propofol and sevoflurane also induce an anteriorization of alpha power from the occipital to the frontal cortex (Akeju et al., 2014; John et

al., 2001; Purdon et al., 2013). Graph theoretical analysis has demonstrated that global and topological properties of brain networks are altered during anesthetic-induced unconsciousness (Blain-Moraes et al., 2017; Hashmi et al., 2017; U. Lee et al., 2011; Moon et al., 2015; Schroeter et al., 2012). While these advances have led to a clearer understanding of how anesthetic-induced unconsciousness creates conditions incompatible with information processing and transfer (U. Lee & Mashour, 2018), the majority of these measures describe macro-scale global network properties, using a single-number value, rather than meso- or micro-scale node-based values describing changes in brain functioning.

Motifs are patterns of inter-connections between the nodes of complex networks, with a probability of occurrence that is significantly higher than in randomized networks (Milo et al., 2002). As such, functional motifs have been investigated as the basic building blocks of directed networks (Milo et al., 2002; Sporns & Kötter, 2004). The distribution of motifs across a brain network is organized to support information integration and segregation – key properties associated with consciousness (Tononi, 2004, 2012; Wei et al., 2017). Shin *et al.* showed that motif frequency changes across anesthetic induction, maintenance and recovery, and that some motifs are state-specific (2013). Conversely, Kafashan *et al.* showed that sevoflurane-induced unconsciousness disrupts motifs of weaker correlation strength within and between resting-state networks, but preserves motifs with higher correlation strength (2016). These findings reveal changes in the building blocks of a network, on a nodal level, across states of consciousness, and suggest that motifs may reflect the granular network alterations of anesthesic-induced unconsciousness. However, the temporal and topological relationship between motifs, induction of and emergence from anesthetic-induced unconsciousness has yet to be established.

This exploratory study tested the hypothesis that loss and recovery of anesthetic-induced unconsciousness causes a re-organization of network motifs. More specifically, we aimed to determine the temporal association between network motifs and the behavioral return of responsiveness. Nine healthy adults underwent a controlled, 3-h anesthetic protocol, during which high-density EEG was acquired. In the alpha frequency band (8–13 Hz), five-minute epochs of EEG were analyzed across the anesthetic protocol, for: Baseline; Induction; Unconsciousness; 30-, 10-, and 5-min prior to recovery of responsiveness (ROR); as well as 30- and 180-min post-ROR (Fig. 1). We hypothesized that different global states of consciousness (Bayne et al., 2016) have a

characteristic motif frequency and topology, and that motifs can effectively distinguish consciousness from anesthetic-induced unconsciousness. Given that motifs may constitute the building blocks of functional networks, we also hypothesized that the motifs associated with consciousness would be disrupted upon anesthetic-induced unconsciousness and would recover prior to the return of behavioral responsiveness. As nodal measures of functional brain networks, we hypothesized that motif frequency and topology would be useful measures to complement global network properties in the study of the neural correlates of consciousness.

Results

Nine healthy participants underwent a 3-h anesthetic protocol at surgical levels while 128-channel EEG was recorded. The anesthetic protocol was comprised of a 15-min propofol induction followed by a 3-h period of isoflurane inhalation at 1.3 minimum alveolar concentration (MAC). Five-minute epochs of EEG were extracted for the following time points: 1) Baseline; 2) Induction; 3) Unconscious; 4) 30 min pre-recovery of responsiveness (ROR); 5) 10-min pre-ROR; 6) 5-min pre-ROR; 7) 30 min post-ROR; and 8) 180 min post-ROR (Fig. 1). Half of these epochs (1,2,7,8) therefore represented periods of behavioral responsiveness and half (3-6) represented periods of behavioral unresponsiveness.

Motifs are present across all states of consciousness, but their frequency cannot distinguish between responsive and unresponsive states

The total frequency of occurrence of the five unidirectional 3-node motifs (Fig. 2) was compared against 100 null networks to assess motif significance. Across all eight epochs, the frequency of motifs 1, 2 and 5 was significantly higher than in null networks, though this significance varied across epochs and participants (Fig. 3). In the alpha band, motif 1 was significantly present across epochs and participants (alpha: 98.6%), followed by motif 2 (95.8%) and motif 5 (91.7%). As motifs 3 and 4 did not appear significantly more frequently than in null networks, they were removed from subsequent analyses. The frequency of significant motifs (i.e. 1, 2 and 5) was compared across all epochs. The null hypothesis (H_0) here was no significant difference in motif frequency across responsive and unresponsive epochs could not be rejected with the Friedman test ($p > 0.05$). A Bayesian repeated-measures ANOVA yielded anecdotal evidence for H_0 for motif 1 ($BF_{10} = 0.879$); moderate evidence for motif 2 ($BF_{10} = 0.212$); and anecdotal evidence for H_0 for

motif 5 ($BF_{10} = 0.908$), suggesting that there was insufficient evidence to conclude that the total number of motifs changed across the experiment.

Reconfiguration of motif topology marks changes in states of consciousness

On average across all participants, in the alpha band, nodes that participated in motifs 1 and 5 during conscious wakefulness were consolidated into circumscribed brain areas, with motif 1 dominant in central regions (Fig. 4A) and motif 5 dominant in posterior and peripheral regions (Fig. 4C). Nodes that participated in motif 2 were scattered across the brain and did not cluster into a single spatial pattern. The topologic distribution of motif 1 changed significantly from Baseline ($\chi^2(7) = 27.887$, p < 0.001, W = 0.664) across all four unresponsive epochs: Unconscious (p = 0.002); 30-min pre-ROR (p = 0.0065);10-min pre-ROR (p = 0.001); and 5-min pre-ROR (p = 0.00575) (Fig. 4A). The topologic distribution of motif 5 changed significantly from Baseline ($\chi^2(7) = 20.400$, p = 0.005, W = 0.529) during the Unconscious epoch (p = 0.0014) and 30-min pre-ROR (p = 0.0021) (Fig. 4C). The topologic distribution of motif 2 did not differ significantly from Baseline at any epoch. Individual patterns of motif topology and re-organization varied slightly from this average pattern (Fig. 4E). Topological reorganization was more visually apparent in individual subjects than on average for 7 of the 9 participants (see Supplementary Material Fig. 1 for examples of individual participant figures). Topological re-organization in the theta band was similar to that observed in the alpha band, while there was no clear re-organization in the delta or beta bands (see Supplementary Material Figures 2, 3 and 4 for delta, theta, and beta results, respectively).

Topologic distribution of source nodes and alpha power

We assessed phase-based lead-lag relationships in every motif to identify which nodes were origins of information flow (i.e. “sources”), and which were destinations of information (i.e. “sinks”). This source node analysis was only conducted for motif 1, given that all nodes in motif 5 are both the source and destination of information flow. Source nodes in motif 1 were located predominantly in anterior regions during Baseline, and shifted towards dominance in central regions during the Unconscious, 30- and 10-min pre-ROR epochs (Fig. 4B). Sources returned to anterior dominance upon recovery of responsiveness.

We investigated the association between the topologic distribution of alpha power and the changes in anterior-posterior dominance observed in motifs across states of consciousness. Alpha power was consolidated in posterior regions during Baseline, 30- and 180-min post-ROR (Fig. 4D). An increase in frontal alpha power is visually apparent during the Induction, Unconscious, 30-, 10- and 5-min pre-ROR epochs. There was a small-to-medium, significant positive correlation between alpha power, and the frequency of motif 1 ($R = 0.26$, $p < 0.001$) and motif 5 ($R = 0.22$, $p < 0.001$).

Network motifs reflect changes in long-range and short-range functional connections

The average total Euclidian distances between nodes within a given motif were pooled across all participants and epochs and the distribution was plotted on a histogram (Fig. 4, panel F). Nodes participating in motif 1 formed long-range connections (median total distance = 10.0 cm, range = 8.21 to 14.0 cm), while nodes participating in motif 5 formed short-range connections (median total distance = 4.21 cm, range = 2.91 to 8.55 cm). Nodes in motif 1 can either be connected to 1 other node (in the case of sources) or 2 other nodes (in the case of sinks) within the motif; individual connection distances therefore range between 4.11 and 14.0 cm in length. Nodes participating in motif 5 are always connected to 2 nodes; individual connection distances range between 1.45 and 4.28 cm in length.

Global network properties do not consistently distinguish between responsive and unresponsive states

We compared four global network properties (i.e. global efficiency, clustering coefficient, modularity and binary small-worldness) across the eight 5-min epochs. We did not have sufficient evidence to conclude that global efficiency was significantly different from Baseline at any time point according to Friedman's test. A Bayesian repeated-measures ANOVA showed that the model including epoch as a factor was slightly more likely than the null model ($BF_{10} = 14.985$); however, there was only anecdotal evidence for decreases in global efficiency from Baseline during the Unconscious epoch ($BF_{10,U} = 1.349$) and 5-minutes pre-ROR ($BF_{10,U} = 1.112$) (Fig. 5A). The clustering coefficient changed significantly across epochs ($\chi^2(7) = 34.667$, $p < 0.001$, $W = 0.470$). Specifically, this measure significantly increased from Baseline at Unconscious, 30-, 10-, and 5-min pre-ROR epochs ($p < 0.01$, Fig. 5B). Changes in binary small-worldness were driven by

changes in the clustering coefficient; this metric was therefore also significantly changed from Baseline ($\chi^2(7) = 34.481$, $p < 0.001$, $W = 0.448$). Specifically, it was increased from Baseline at the Unconscious epochs, as well as 30-, 10-, and 5-min pre-ROR ($p < 0.05$, not plotted due to redundancy). Modularity changed significantly across epochs ($\chi^2(7) = 32.481$, $p < 0.001$, $W = 0.277$) and was significantly increased from Baseline at 30-, and 5-min pre-ROR ($p < 0.01$, Fig. 5C). Only clustering coefficient and binary small-worldness statistically distinguished the Unconscious epoch from Baseline.

Network efficiency and clustering topology do not spatially reorganize across states of consciousness

To further explore our negative findings for global network properties, efficiency and clustering coefficient were plotted on a topographic head map at a nodal level (i.e. prior to averaging across all nodes to obtain global network measures). Unlike network motifs, we observed no consistent spatial organization of efficiency, or any reorganization of efficiency and clustering coefficient across states of consciousness, even at the individual subject level (see Supplemental Fig. 5 for a sample individual participant).

Discussion

We investigated motifs in human directed functional EEG networks to identify statistically significant motifs associated with states of consciousness, and to reveal the temporal changes in these basic network building blocks across loss and recovery of consciousness. The directed functional networks were constructed from high-density EEG data recorded from human participants before, during and after anesthetic-induced unconsciousness using surgical levels of anesthesia, without the confounds of surgical stress, inflammatory burden or polypharmacy that often accompany anesthesia research. This protocol enabled us to assess consciousness-related transitions in brain networks. Networks were constructed from four epochs of behavioral responsiveness and four epochs of behavioral unresponsiveness. Three classes of 3-node motifs (i.e. ID = 1, 2 and 5) were significantly more likely to be embedded in these brain networks compared to null networks. These motifs were topologically distributed in distinct patterns that re-organized with changes in levels of consciousness. Motif 1 consisted of two source nodes connected to a shared sink node. This motif was constituted by long-range connections, with sources predominant in anterior and central regions during conscious wakefulness, and dominant

in posterior regions during unresponsive states. The topological distribution of nodes participating in motif 1 significantly reorganized during all four unresponsive epochs. Motif 5 consisted of three interconnected nodes linked by short-range connections. Nodes participating in motif 5 were concentrated in posterior and peripheral brain regions during Baseline conscious wakefulness; anterior nodes increased their participation in this motif during the Unconscious and 30-min pre-ROR epochs. The topologic distribution of motif 5 nodes returned to Baseline patterns by 10-min pre-ROR, and maintained this pattern through all subsequent epochs.

It is instructive to examine the characteristics of the significant motifs in finer detail. The three statistically significant motifs investigated in this study can be divided into two sub-types, according to their structure: chain-like motifs (ID = 1 and 2) and loop-like motifs (ID = 5). In the chain-like motifs, two nodes that are not directly linked are integrated through an intermediate third node. These chain-like motifs have been implicated in the communication between functional modules of the brain, both in humans and macaques (Leonardo L. Gollo & Breakspear, 2014; Shen et al., 2012; Wei et al., 2017). Other studies have linked hub regions – which play an important role in the information integration of the brain network – to the intermediate apex of these chain-like motifs, and suggest that densely inter-connected hubs (the rich club) form a stable synchronization core through these chain-like motifs (L. L. Gollo et al., 2015). Our analysis of motif 1 is highly consistent with these previous observations. We demonstrated that motif 1 consists of long-range connections, with posterior sinks (i.e. the intermediate apex) during all responsive epochs and anterior sinks during all unresponsive epochs. This reconfiguration of modular architecture is consistent with, and provides a potential functional mechanism for, the anteriorization of network hubs observed during anesthetic-induced unconsciousness (M. Kim et al., 2016). The significant topological disruption of this motif across all unresponsive epochs is also consistent with previous studies associating the disruption of long-range functional connectivity with loss of consciousness (Chennu et al., 2014; Schroeter et al., 2012), lending credibility to our analysis. The loop-like motifs form a tight loop for information processing, enabling local integration to achieve functional specification. The loop-like motif in our analysis (ID = 5) consisted of short-range connections that were dominant in posterior and peripheral regions in the Baseline epoch, and shifted to a peripheral anterior-dominance during unconsciousness. The fact that this motif was no longer significantly distinct from its Baseline

pattern 10-min prior to the return of responsiveness suggests that the re-establishment of short-range connections may be necessary but not sufficient for behavioral responsiveness.

If consciousness is a pre-requisite for intentional behavior (Dehaene & Naccache, 2001), then networks sustaining consciousness may return prior to the ability to understand and willingly respond to a command. The dissociation between consciousness and responsiveness has recently been established on the level of brain network dynamics, where network changes were linked to state of consciousness rather than behavioral responsiveness (Julia S Crone et al., 2020). Our findings regarding the temporal course of motif topological reconfiguration may also suggest that distinct network processes underly consciousness and responsiveness. Although the topology of motifs 1 and 5 were spatially complementary and although they were both significantly disrupted during unconsciousness, motif 1 did not return to Baseline patterns until the recovery of responsiveness, while motif 5 returned at least 10 min prior to the recovery of responsiveness. Motif 1 therefore appears to accompany behavioral responsiveness, and to be a marker of both the cognitive capacity to understand and respond to a command, and the motor ability to execute that command. In contrast, motif 5 returned prior to behavioral responsiveness, suggesting that it may constitute a marker of consciousness and a pre-requisite of behavioral responsiveness. Moreover, motif 5 may be a potential indicator of the imminent return to responsiveness, which would be of significant clinical value in monitoring for intraoperative awareness (Avidan et al., 2011), and in assessing pathological unconsciousness such as unresponsive wakefulness syndrome and minimally conscious state (Schnakers et al., 2009b).

We explored several other potential explanations regarding the mechanism driving the re-organization of network motifs across states of consciousness. First, we investigated the hypothesis that the observed motif re-organization was associated with anterior-posterior shifts in alpha power across states of consciousness. The anteriorization, or "frontal dominance" of alpha power has long been associated with anesthetic-induced unconsciousness (Feshchenko et al., 2004; John et al., 2001; Purdon et al., 2013; Tinker et al., 1977), and the reorganization of motifs 1 and 5 exhibited a similar anterior-posterior shift in dominance across states of consciousness. There were small-to-medium correlations between alpha power and motif topology, indicating that the shift in alpha power may be a contributing factor to the observed shift in motif distribution. Alternatively, it is possible that both alpha power and motif topology are independent markers that reflect anesthetic-

induced reconfiguration of network dynamics. Though the mechanisms of alpha-power anteriorization are still not well understood, they are posited to reflect alterations in cortico-thalamic interactions – essential for consciousness processing and cognitive function (Berger & Garcia, 2016; Blumenfeld, 2010; Castaigne et al., 1981; Giattino et al., 2017) – caused by the effect of anesthetic drugs on various thalamic nuclei (Ching et al., 2010; Vijayan et al., 2013). Conversely, simulations with model complex networks have shown that nodes with larger degrees (e.g. network hubs) have larger amplitudes (Moon et al., 2015). As the apex of motif 1 has also been co-located with network hubs (Wei et al., 2017), the correlation of alpha power and motif topology may simply reflect two epiphenomenal markers of anesthetic-induced shifts in network hub location. Second, we investigated the hypothesis that changes in motif topology were driven by anesthetic-induced changes in motif frequency across the experiment. Anesthetic-induced unconsciousness has been associated with a decrease in the strength of directed functional connectivity across brain regions (Blain-Moraes et al., 2014, 2015; Moon et al., 2015), which could potentially be accompanied by a decrease in motif frequency. However, the total frequency of each motif was not statistically different between any of the 8 epochs or across states of consciousness (conscious vs. unconscious), eliminating this as a plausible explanation for the observed changes in motif topologic distribution.

Our results highlight the value of network motifs as a complementary node-based measure to global network properties. Global network properties have proven useful in characterizing altered states of consciousness or changes in responsiveness (Blain-Moraes et al., 2017; Chennu et al., 2014, 2016; Julia Sophia Crone et al., 2014; Dell'Italia et al., 2018; Hashmi et al., 2017; M. Lee et al., 2017; U. Lee et al., 2011; Luppi et al., 2019; Schroeter et al., 2012; Vecchio et al., 2017). Here, we showed that some global network properties were altered as of result of anesthesia, and recovered prior to or in parallel with the return of behavioral responsiveness. Similar to previous findings (Blain-Moraes et al., 2017; Liang et al., 2020), we showed that unresponsive brain networks have increased clustering coefficients and modularity during some unresponsive epochs, though only clustering coefficients and binary small-worldness were statistically distinct from Baseline during the Unconscious epoch, and across all unresponsive epochs. Our Bayesian analysis suggests that the lack of statistically significant differences for global efficiency and modularity (during the Unconscious epoch) is a result of our small sample size and the high variability between subjects. Unlike these global network properties, the topologies of motifs 1 and 5 were significantly different from Baseline during the Unconscious epoch (and other subsequent unresponsive epochs), in spite

of the small sample size and high variability. These different may suggest that macro-scale (i.e. global) versus meso-scale (i.e. node-based) network properties reflect divergent information (Betzel et al., 2018), and highlights the complementary information that motifs can provide in describing brain network correlates of consciousness.

The results of this study must be interpreted in light of several limitations. First, this was a small study of young healthy volunteers, and the patterns of motif distributions observed herein may not generalize to surgical patients of varying ages and comorbidities, nor to brain-injured patients. Secondly, loss and recovery of consciousness were indirectly assessed through behavioral responsiveness. It is therefore impossible to confirm whether participants were truly unconscious during all epochs of unresponsiveness, or whether they retained awareness but had a loss of motor control or of the cognitive abilities necessary for understanding commands and initiating proper responses. Given the MAC of 1.3 during the 3-h anesthetic period, we are confident that study participants were deeply anesthetized during the anesthetic protocol and during the Unconscious epoch, which took place in the first 5 min following the end of isoflurane administration. However, unresponsiveness is not equivalent to unconsciousness (Sanders et al., 2012), and awareness may still be present despite unresponsiveness. There have been accounts of intraoperative awareness and no method has yet proven to be completely effective in detecting consciousness (i.e. awareness) during an anesthetic state (Mashour et al., 2011). Thirdly, the Unconscious epoch represents the first 5 min after isoflurane has been turned off, rather than during isoflurane administration. However, in these 5 min immediately after the 3-h anesthetic period at surgical levels, participants were unresponsive, and remained completely unresponsive for over 30 min. This was a state of unresponsiveness where patients still had high levels of isoflurane concentration in their brain and blood, without the direct effect of isoflurane administration. Fourthly, as our directed functional network was constructed using directed phase lag index (dPLI), our analysis was limited to motifs with unidirectional connections between nodes. In the class of 3-node motifs, this restricted the scope of our analysis to 5 of the 13 potential 3-node motifs. While the patterns of motif distribution described in this paper remain valid, it is possible that the motifs highlighted herein are in fact a subgraph (i.e. a graph formed by a subset of the vertices of a larger graph) of bidirectional motifs. Constructing the directed functional network with a metric such as symbolic transfer entropy would enable non-complementary measures of bi-directional interactions between nodes, and merits future work (Staniek & Lehnertz, 2008). Sixth, our interpretation of the topologic distribution of

motif 1 as a marker of the recovery of responsiveness is limited by the study design, where the first available resting-state epoch following the recovery of responsiveness occurs 30 min after the return of responsiveness. Analysis of the networks constructed from epochs immediately following the recovery of responsiveness are warranted to confirm the relationship of this motif distribution to an individual's global state of consciousness (Bayne et al., 2016). Finally, our analysis was conducted on the level of the EEG sensors, which can record changes in brain activity that do not occur proximal to the electrodes under analysis; it is possible that the topologic changes in motifs reflect distant cortical interactions that are widely projected to many cortical sites. Future work should use source reconstruction or current source density analysis to model the data in source space to further illuminate the neurophysiological underpinnings of motif configurations and their causal relationship to states of consciousness.

This study provides preliminary evidence that changes in states of consciousness induce a structured re-organization in the topology of functional network motifs. Though motif frequency remains constant under anesthetic-induced unconsciousness, the motif topology associated with conscious wakefulness shifts during unconsciousness and returns either prior to, or in parallel with the recovery of responsiveness, in a motif-specific manner. As such, motifs could improve the monitoring, identification and prognostication of consciousness. As nodal properties of functional networks, motifs may complement global network properties in the study of the neural correlates of consciousness.

Methods

Participants

Nine healthy volunteers (5 males; 24.4 ± 1.0 years old) were recruited at the University of Michigan, as part of the Reconstructing Consciousness and Cognition study (NCT01911195) (Maier et al., 2017). A tenth participant was initially recruited but was subsequently excluded from all analyses due to excessive noise artifacts in the EEG. The study was approved by the Institutional Review Board of the University of Michigan (HUM0071578). All methods were performed in accordance with relevant guidelines and regulations, and written informed consent was obtained from all participants. As this was an observational study, it was not registered in a clinical trial registry. Participants were included if they were between 20 and 40 years old, had a BMI < 30

kg/m^2, satisfied the criteria for the American Society of Anesthesiologists Physical status I or II (Vacanti et al., 1970), had an easily visualized uvula and were able to provide signed informed consent. Participants were excluded if they had physical indication of a difficult airway, family history of problems with anesthesia, obstructive sleep apnea, neuropsychiatric disorders, hypertension, cardiovascular disease, reflux, sleep disorders, postoperative nausea or vomiting, motion sickness, or reactive airway disease. Participants were also excluded for pregnancy, past or current use of psychotropic medications, current tobacco or alcohol use exceeding 2 drinks/day, positive urine toxicology test, allergy to eggs, egg products, or soy.

Anesthetic protocol

Participants underwent a 3-h anesthesia protocol at surgical levels. As previously described (Maier et al., 2017), participants underwent a standard clinical preoperative history and physical examination on the day of the study. The anesthetic protocol took place in an operating room. Standard electrocardiogram, non-invasive blood pressure cuff, pulse oximeter, and capnography were used for constant monitoring during the protocol. Patients were pre-oxygenated by face mask prior to induction of general anesthesia with a stepwise increasing infusion rate of propofol: 100 mcg/kg/min × 5 min increasing to 200 mcg/kg/min × 5 min, and then to 300 mcg/kg/min × 5 min. After 15 min of propofol administration, inhalation of 1.3 age-adjusted minimum alveolar concentration (MAC) of isoflurane was started (Nickalls & Mapleson, 2003). Loss of consciousness occurs generally around 0.3 MAC (Eger, 2001), 1.0 MAC can abolish evoked related potentials (Lotto et al., 2004), and 1.3 MAC produces suppression of the sympathetic nervous system (Daniel et al., 1998; Knapp, 2017). Consequently, 1.3 MAC reflects surgical anesthesia and is deemed a deep anesthetic state (Knapp, 2017). A laryngeal mask was inserted orally, a nasopharyngeal temperature probe was placed, and the propofol infusion was discontinued. Anesthetized subjects received 1.3 age-adjusted MAC inhaled isoflurane anesthesia for 3 h. Blood pressure was maintained within 20% of baseline pre-induction values using a phenylephrine infusion or intermittent boluses of ephedrine, as necessary. To prevent post-anesthetic nausea and vomiting, participants received 4 mg of intravenous ondansetron 30 min prior to discontinuation of isoflurane.

At the end of the 3-h anesthetic period, isoflurane was discontinued and we started an audio loop command that was played every 30 s, asking the participant to squeeze their left or right hand twice

(randomized order). Recovery of consciousness was estimated through return of responsiveness, which was defined as the earliest instance in which participants correctly responded to two consecutive audio loop commands. The laryngeal mask was removed when deemed medically safe by the attending anesthesiologists.

Electroencephalographic acquisition and preprocessing

EEG was acquired using a 128-channel system from Electrical Geodesics, Inc. (Eugene, OR) with all channels referenced to the vertex (Cz). Electrode impedance was maintained below 50 kΩ prior to data collection and data were sampled at 500 Hz. Throughout the experiment, data were visually monitored by a trained investigator to ensure continued signal integrity. All data preprocessing was performed in EEGLAB (Delorme & Makeig, 2004). Five-minute epochs of EEG were extracted for the following time points: 1) Baseline; 2) Induction; 3) Unconscious; 4) 30 min pre-recovery of responsiveness (ROR); 5) 10 min pre-ROR; 6) 5 min pre-ROR; 7) 30 min pre-ROR; and 8) 180 min post-ROR (Fig. 1). Four of these epochs were associated with a state of responsiveness (epochs 1, 2, 7, 8) and four were associated with a state of unresponsiveness (epochs 3, 4, 5, 6). EEG data were bandpass filtered between 0.1 and 50 Hz. Non-scalp channels were discarded, leaving 99 channels for the subsequent analyses. All noisy channels were visually identified and removed, then the data were re-referenced to an average reference. Eye-blinks were removed using Independent Component Analysis (ICA). Finally, all epochs with noise or non-physiological artifacts were visually identified and removed. We then band-pass filtered the cleaned EEG data into delta (1–4 Hz), theta (4–8 Hz), alpha (8–13Hz), and beta (13–30 Hz) frequency bands. Analyses of the alpha band were presented in the main body of the paper, while analyses of other frequency bands are included in the supplementary material.

Functional connectivity

To construct a functional brain network from EEG data, we used the weighted phase lag index (wPLI) (Vinck et al., 2011), and the directed phase lag index (dPLI) (C. J. Stam & van Straaten, 2012) (Fig. 6), which are robust methods to avoid volume conduction confounds in the data (Cornelis J. Stam et al., 2007). This was done using custom MATLAB scripts (version R2018b).

wPLI was calculated using the following formula:

$$wPLI_{ij} = \frac{\left|E\{\mathcal{J}(C_{ij})\}\right|}{E\{\left|\mathcal{J}(C_{ij})\right|\}} = \frac{\left|E\{\left|\mathcal{J}(C_{ij})\right| sgn(\mathcal{J}(C_{ij}))\}\right|}{E\{\left|\mathcal{J}(C_{ij})\right|\}}$$

where $\mathcal{J}(C_{ij})$ is the imaginary part of cross-spectrum C_{ij} between signals i and j (Vinck et al., 2011). The cross-spectrum C_{ij} is defined as $Z_i Z_{j*}$, where Z_i is the complex value Fourier spectra of the signal i for each frequency, and Z_j* is the complex conjugate of Z_j. C_{ij} can be written as $Re^{i\theta}$, where R is magnitude and θ is the relative phase between signal i and j (Vinck et al., 2011). A wPLI value of 1 indicates complete phase locking between the two signals (i.e. that the instantaneous phase of one signal is leading the other). Conversely, a wPLI value of 0 indicates no consistent phase-lead or -lag relationship. To know the direction of the phase-lead/phase-lag relationship between channels i and j in the wPLI matrix, we calculated the dPLI (C. J. Stam & van Straaten, 2012). First, the instantaneous phase of each EEG channel was extracted using a Hilbert transform. The phase difference $\Delta\varphi_t$ between all the channels was then calculated where $\Delta\varphi_t = \varphi_{i,t} - \varphi_{j,t}$, t = 1,2,…,N, where N is the number of samples in one epoch, and i and j include all channels. dPLI was then calculated using the following formula:

$$dPLI_{ij} = \langle H(\Delta\varphi_t) \rangle$$

where H(x) represents the Heaviside step function, where H(x) = 1 if x > 0, H(x) = 0.5 if x = 0 and H(x) = 0 otherwise. Thus, if on average signal i leads signals j, dPLI will be between 0.5 and 1, and if signal j leads signal i, dPLI will be between 0 and 0.5. If there is no phase-lead/phase-lag relationship between signals, dPLI = 0.5.

For both the wPLI and dPLI matrices, we controlled for noise-induced phase relationships using surrogate datasets in which we randomized the phase relationship between two channels, while maintaining their spectral properties. More specifically, using the instantaneous phase for each channel pair i and j, we maintained the phase time series for i and scrambled the time series for j from 0 to x, by swapping it for the time series from x to n, where n is the number of samples in one epoch, and 0 < x < n. Data segments used to generate surrogate wPLI/dPLI matrices were 10 s in length, and each was permuted 20 times to generate a distribution of values representing the spurious connectivity. The wPLI and dPLI values of the original, non-shuffled EEG data were compared to this distribution of surrogate data using a Wilcoxon signed rank test and were set to 0

(wPLI) or 0.5 (dPLI) if they did not achieve statistical significance. Statistical significance was set to $p < 0.05$.

Network motifs

In a directed network, a motif is a subnetwork consisting of N nodes and at least (N-1) edges linking the nodes in a path (Milo et al., 2002; Sporns & Kötter, 2004). In this study, we investigated network motifs of N = 3 using a unidirectional network, for which 5 motifs are possible (Fig. 2). Each EEG electrode represented a single node; a 3-node motif therefore represents a specific pattern of interconnection between any three electrodes on the scalp (i.e. motifs are not constrained to connections between neighboring electrodes). While motifs comprised of other numbers of nodes are possible, we restrict the analysis in this paper to N = 3 due to the exponential increase in computational complexity that co-occurs with increasingly higher numbers of nodes.

Network motifs were computed using custom MATLAB scripts and the Brain Connectivity Toolbox (Rubinov & Sporns, 2010). Prior to computing the network motifs, we normalized the dPLI matrix into a non-symmetrical phase-lead matrix, in order to remove redundant information. Given the nature of the dPLI matrix, a value at position (i,j) is necessarily the opposite of a value at position (j,i). We therefore set any value that was below 0.5 in the dPLI matrix, corresponding to a non-phase-leading value, to 0. The remaining non-zero values were normalized between 0 and 1. This normalized phase-lead matrix was then used to calculate the frequency of participation of each node in each motif (Rubinov & Sporns, 2010).

Two levels of surrogate analysis were used to calculate whether the probability of occurrence of motifs was beyond chance (i.e. whether a motif is significantly present). First, we corrected for the surrogate number of motifs calculated at each node as follows: using BCT (Rubinov & Sporns, 2010), we generated 100 null networks that preserved the degree and strength distribution from the normalized phase lead matrix. For each of the 100 null networks, we calculated the mean frequency of each motif, for each node. Second, we corrected for the surrogate number of motifs across each network: for each motif, we calculated the total aggregate frequency of motifs in the network by summing across all nodes. We then calculated a network Z-score per motif against the distribution of the total motifs in the 100 null networks as follows:

$$Z_i = \frac{N_i^{real} - < N_i^{null} >}{std(N_i^{null})}$$

where N_i^{real} is the aggregate frequency of motif *i* across the network and N_i^{null} is the aggregate motif frequency of the 100 null networks (Wei et al., 2017). If Z_i was greater than 1.96, the motif was considered to be significant in the network; if not, it was considered non-significant and set to a frequency of 0.

Analysis of global network properties

The functional brain network was constructed using the wPLI of all pairwise combinations of electrode channels. We constructed a binary adjacency matrix A*ij* using a threshold of 35%: if the wPLI*ij* value of nodes *i* and *j* was within the top 35% of all wPLI values, A*ij* = 1; otherwise, A*ij* = 0. We chose a binarized approach to be coherent with the majority of studies assessing global network properties, which have also used a binarized approach to construct their graph (Blain-Moraes et al., 2017; H. Kim et al., 2018, 2018; H. Kim & Lee, 2019; M. Kim et al., 2016; Moon et al., 2015; Shin et al., 2013). The 35% threshold was selected because it was previously shown to be the optimal threshold to avoid an isolated node in the EEG network during baseline (H. Kim et al., 2018). From the binary adjacency matrix, we calculated global network properties using the Brain Connectivity Toolbox (BCT) (Rubinov & Sporns, 2010), including global efficiency, clustering coefficient, and modularity (Fig. 6). Global efficiency is the inverse of the average shortest path length ($\frac{1}{L_w}$), where L_W is the average of the shortest path lengths (L*ij*) between all pairs of nodes in the network (Dell'Italia et al., 2018). The clustering coefficient, calculated by averaging the clustering coefficients of all individual nodes (C*i*), represents the degree to which nodes of a graph tend to cluster together, such that higher values imply networks with highly clustered or regular structures (Watts & Strogatz, 1998). The modularity of the network represents the strength of division of a network into modules, such that high modularity implies a network with strong within-module connections and weak between-module connections (Newman, 2006). Modularity was calculated using the Louvain algorithm. Finally, small-world organization is characterized by high levels of clustering and short path lengths, meaning that all nodes of a network are linked through relatively few intermediate steps, though they are only directly connected to a few, mainly neighboring, nodes (Bullmore & Sporns, 2009). Binary small-

worldness is therefore the ratio of the clustering coefficient to the average path length, after both metrics are normalized against random networks (Humphries & Gurney, 2008). Global efficiency and clustering coefficient were normalized by taking the ratio between the true network metric and the average metrics computed for 10 random binary networks, which were generated by shuffling the empirically-generated network's edges 10 times while preserving the degree distributions, as previously done (Maslov & Sneppen, 2002; Milo et al., 2002).

Topological configuration of network motifs across states of anesthetic-induced unconsciousness

The distribution of nodes participating in each motif was visualized on a topographic head map, using the *topoplot* function of EEGLAB (Delorme & Makeig, 2004). Changes in the topologic distribution of participating nodes were assessed using cosine similarity on the topographic head maps, defined as:

$$s = \frac{b_i \cdot b_j}{\| b_i \| \| b_j \|}$$

where b_i and b_j are vectors containing motif frequencies for states *i* and *j* (Shin et al., 2013). Cosine similarity ranges from -1 to 1, where 1 indicates identical topological distribution, -1 indicates completely opposite topological distribution, and 0 indicates orthogonality or decorrelation. This measure was computing using custom MATLAB scripts.

Post hoc analyses

Once significant motifs were identified, we conducted two additional analyses to further interpret our results.

Topological distribution of source nodes within a motif

Using the dPLI, we conducted a source node analysis, in which we assessed the lead-lag relationships in every motif to identify which nodes were origins of information flow (i.e. "sources"), and which were destinations of information (i.e. "sinks"). Nodes that were phase-leading other nodes within a motif on their phase relationship were considered sources. Across the total frequency of participation of each node in a given motif, the total number of times that the node behaved as a source was calculated. This measure was referred to as "source total". To assess

the topological distribution of sources within the network, the source total for each node was normalized by computing its Z-score relative to all other node source totals in a given network. These Z-scores were then plotted on a topographic map to visualize the relative distribution of sources within the network. This analysis was performed using the BCT and custom MATLAB scripts.

Topological distribution of alpha power

We investigated the topological distribution of alpha power as a possible explanation for the changes in anterior-posterior dominance observed in motifs across states of consciousness. The Pearson correlation between the motif frequency and the raw alpha power ($\mu V/Hz^2$) for each node in the network was calculated. Alpha power was averaged across 10-second windows and computed using a multi-taper power spectral density estimate (number of tapers = 3, time-bandwidth product = 2, spectrum window size = 3 seconds) from the Chronux package (Mitra, 2007; Mitra et al., n.d.). Correlation between alpha power and the frequency of participation of each node within a network was quantified by computing the Pearson's correlation (R) between x and y, where x is the motif frequency and y is the power for a given node, across all participants, time points and nodes, constructed using custom MATLAB scripts.

Distance distribution of motif connections

For each node u, we summed the Euclidean distance (d) between u and all of its connected nodes v_i within a given motif, where i = {1,2} (i.e. up to two connected nodes). We repeated this for every motif j in the network, and then normalized by the motif frequency for that node (f_u). Thus, for each node, we obtain the total distance between a node and all its connections within a motif, averaged across all the motifs that node participates in, according to the following formula:

$$average\ total\ distance = \frac{\sum_{j=1}^{n}\sum_{i=1}^{2} d(u, v_i)}{f_u}$$

where $d(u, v_i)$ is the Euclidian distance between points u and v_i.

We pooled the average total distances for motifs 1 and 5 across all participants and epochs and plotted their distribution using a histogram. To obtain individual connection distances, we divide the average total distance by the number of connections a node has.

Statistical analyses

Due to our small sample size and high variability between participants, total motif frequency (i.e. the sum of motif frequency across all nodes), cosine similarity of motif topologies relative to Baseline, and global network properties (i.e. global efficiency, clustering coefficient, binary-small worldness and modularity) were compared across epochs using a non-parametric Friedman's test. Effect size was measured using Kendall's coefficient of concordance (W). When Friedman's test was significant, *post hoc* Bonferroni-corrected Conover's tests were performed, comparing all variables between Baseline and all other epochs (i.e. 7 comparisons). All tests were two-tailed with statistical significance set to $p < 0.05$.

When negative findings were observed for Friedman's test, a Bayesian repeated-measures ANOVA was performed to investigate whether these negative findings were meaningful. Negative findings were considered to not be meaningful when the Bayes factor was greater than 1 (BF_{10}, where 0 is the null model and 1 is the model including epoch as a factor).

Statistical analyses were conducted using JASP (version 0.12.2.0)

References

Akeju, O., Westover, M. B., Pavone, K. J., Sampson, A. L., Hartnack, K. E., Brown, E. N., & Purdon, P. L. (2014). Effects of Sevoflurane and Propofol on Frontal Electroencephalogram Power and Coherence. Anesthesiology: The Journal of the American Society of Anesthesiologists, 121(5), 990–998.

Avidan, M. S., Jacobsohn, E., Glick, D., Burnside, B. A., Zhang, L., Villafranca, A., Karl, L., Kamal, S., Torres, B., O'Connor, M., Evers, A. S., Gradwohl, S., Lin, N., Palanca, B. J., & Mashour, G. A. (2011). Prevention of Intraoperative Awareness in a High-Risk Surgical Population. New England Journal of Medicine, 365(7), 591–600.

Bayne, T., Hohwy, J., & Owen, A. M. (2016). Are There Levels of Consciousness? Trends in Cognitive Sciences, 20(6), 405–413.

Berger, M., & Garcia, P. (2016). Anesthetic Suppression of Thalamic High Frequency Oscillations: Evidence that the Thalamus is More than Just a Gateway to Consciousness? Anesthesia and Analgesia, 122(6), 1737–1739.

Betzel, R. F., Medaglia, J. D., & Bassett, D. S. (2018). Diversity of meso-scale architecture in human and non-human connectomes. Nature Communications, 9(1), 346.

Blain-Moraes, S., Lee, U., Ku, S., Noh, G., & Mashour, G. A. (2014). Electroencephalographic effects of ketamine on power, cross-frequency coupling, and connectivity in the alpha bandwidth. Frontiers in Systems Neuroscience, 8(114).

Blain-Moraes, S., Tarnal, V., Vanini, G., Alexander, A., Rosen, D., Shortal, B., Janke, E., & Mashour, G. A. (2015). Neurophysiological Correlates of Sevoflurane-induced Unconsciousness. Anesthesiology: The Journal of the American Society of Anesthesiologists, 122(2), 307–316.

Blain-Moraes, S., Tarnal, V., Vanini, G., Bel-Behar, T., Janke, E., Picton, P., Golmirzaie, G., Palanca, B. J. A., Avidan, M. S., Kelz, M. B., & Mashour, G. A. (2017). Network Efficiency and Posterior Alpha Patterns Are Markers of Recovery from General Anesthesia: A High-Density Electroencephalography Study in Healthy Volunteers. Frontiers in Human Neuroscience, 11, 328.

Blumenfeld, H. (2010). Neuroanatomy through clinical cases. Sinauer Associates Sunderland.

Bonhomme, V., Vanhaudenhuyse, A., Demertzi, A., Bruno, M.-A., Jaquet, O., Bahri, M. A., Plenevaux, A., Boly, M., Boveroux, P., Soddu, A., Brichant, J. F., Maquet, P., & Laureys, S. (2016). Resting-state Network-specific Breakdown of Functional Connectivity during Ketamine Alteration of Consciousness in Volunteers. Anesthesiology, 125(5), 873–888.

Boveroux, P., Vanhaudenhuyse, A., Bruno, M.-A., Noirhomme, Q., Lauwick, S., Luxen, A., Degueldre, C., Plenevaux, A., Schnakers, C., Phillips, C., Brichant, J.-F., Bonhomme, V., Maquet, P., Greicius, M. D., Laureys, S., & Boly, M. (2010). Breakdown of within- and between-network Resting State Functional Magnetic Resonance Imaging Connectivity during Propofol-induced Loss of Consciousness. Anesthesiology, 113(5), 1038–1053.

Bullmore, E., & Sporns, O. (2009). Complex brain networks: Graph theoretical analysis of structural and functional systems. Nature Reviews Neuroscience, 10, 186.

Castaigne, P., Lhermitte, F., Buge, A., Escourolle, R., Hauw, J. J., & Lyon-Caen, O. (1981). Paramedian thalamic and midbrain infarcts: Clinical and neuropathological study. Annals of Neurology, 10(2), 127–148.

Chennu, S., Finoia, P., Kamau, E., Allanson, J., Williams, G. B., Monti, M. M., Noreika, V., Arnatkeviciute, A., Canales-Johnson, A., Olivares, F., Cabezas-Soto, D., Menon, D. K.,

Pickard, J. D., Owen, A. M., & Bekinschtein, T. A. (2014). Spectral Signatures of Reorganised Brain Networks in Disorders of Consciousness. PLOS Computational Biology, 10(10).

Chennu, S., O'Connor, S., Adapa, R., Menon, D. K., & Bekinschtein, T. A. (2016). Brain Connectivity Dissociates Responsiveness from Drug Exposure during Propofol-Induced Transitions of Consciousness. PLOS Computational Biology, 12(1).

Ching, S., Cimenser, A., Purdon, P. L., Brown, E. N., & Kopell, N. J. (2010). Thalamocortical model for a propofol-induced α-rhythm associated with loss of consciousness. Proceedings of the National Academy of Sciences, 107(52), 22665–22670.

Crone, Julia S, Lutkenhoff, E. S., Vespa, P. M., & Monti, M. M. (2020). A systematic investigation of the association between network dynamics in the human brain and the state of consciousness. Neuroscience of Consciousness, 2020(niaa008).

Crone, Julia Sophia, Soddu, A., Höller, Y., Vanhaudenhuyse, A., Schurz, M., Bergmann, J., Schmid, E., Trinka, E., Laureys, S., & Kronbichler, M. (2014). Altered network properties of the fronto-parietal network and the thalamus in impaired consciousness. NeuroImage: Clinical, 4, 240–248.

Daniel, M., Weiskopf, R. B., Noorani, M., & Eger, E. I. (1998). Fentanyl Augments the Blockade of the Sympathetic Response to Incision (MAC-BAR) Produced by Desflurane and Isoflurane: Desflurane and Isoflurane MAC-BAR without and with Fentanyl. Anesthesiology, 88(1), 43–49.

Dehaene, S., & Naccache, L. (2001). Towards a cognitive neuroscience of consciousness: Basic evidence and a workspace framework. Cognition, 79(1), 1–37.

Dell'Italia, J., Johnson, M. A., Vespa, P. M., & Monti, M. M. (2018). Network Analysis in Disorders of Consciousness: Four Problems and One Proposed Solution (Exponential Random Graph Models). Frontiers in Neurology, 9.

Delorme, A., & Makeig, S. (2004). EEGLAB: an open source toolbox for analysis of single-trial EEG dynamics including independent component analysis. Journal of Neuroscience Methods, 134(1), 9–21.

Eger, E. I. I. (2001). Age, Minimum Alveolar Anesthetic Concentration, and Minimum Alveolar Anesthetic Concentration-Awake. Anesthesia & Analgesia, 93(4), 947–953.

Feshchenko, V. A., Veselis, R. A., & Reinsel, R. A. (2004). Propofol-Induced Alpha Rhythm. Neuropsychobiology, 50(3), 257–266.

Giattino, C. M., Gardner, J. E., Sbahi, F. M., Roberts, K. C., Cooter, M., Moretti, E., Browndyke, J. N., Mathew, J. P., Woldorff, M. G., Berger, M., Investigators, the M.-P., Berger, M., Brigman, B. E., Browndyke, J. N., Bullock, W. M., Carter, J., Chapman, J., Colin, B., Cooter, M., … Young, C. (2017). Intraoperative Frontal Alpha-Band Power Correlates with Preoperative Neurocognitive Function in Older Adults. Frontiers in Systems Neuroscience, 11.

Gollo, L. L., Zalesky, A., Hutchison, R. M., van den Heuvel, M., & Breakspear, M. (2015). Dwelling quietly in the rich club: Brain network determinants of slow cortical fluctuations. Philos Trans R Soc Lond B Biol Sci, 370(1668).

Gollo, Leonardo L., & Breakspear, M. (2014). The frustrated brain: From dynamics on motifs to communities and networks. Philosophical Transactions of the Royal Society B: Biological Sciences, 369(1653), 20130532.

Hashmi, J. A., Loggia, M. L., Khan, S., Gao, L., Kim, J., Napadow, V., Brown, E. N., & Akeju, O. (2017). Dexmedetomidine Disrupts the Local and Global Efficiencies of Large-scale Brain Networks. Anesthesiology, 126(3), 419–430.

Humphries, M. D., & Gurney, K. (2008). Network 'Small-World-Ness': A Quantitative Method for Determining Canonical Network Equivalence. PLoS ONE, 3(4), e0002051.

John, E. R., Prichep, L. S., Kox, W., Valdes-Sosa, P., Bosch-Bayard, J., Aubert, E., Tom, M., & Gugino, L. D. (2001). Invariant reversible QEEG effects of anesthetics. Consciousness and Cognition, 10(2), 165–183.

Jordan, D., Ilg, R., Riedl, V., Schorer, A., Grimberg, S., Neufang, S., Omerovic, A., Berger, S., Untergehrer, G., Preibisch, C., Schulz, E., Schuster, T., Schröter, M., Spoormaker, V., Zimmer, C., Hemmer, B., Wohlschläger, A., Kochs, E. F., & Schneider, G. (2013). Simultaneous Electroencephalographic and Functional Magnetic Resonance Imaging Indicate Impaired Cortical Top–Down Processing in Association with Anesthetic-induced Unconsciousness. Anesthesiology, 119(5), 1031–1042.

Kafashan, M., Ching, S., & Palanca, B. J. (2016). Sevoflurane Alters Spatiotemporal Functional Connectivity Motifs That Link Resting-State Networks during Wakefulness. Frontiers in Neural Circuits, 10, 107.

Kim, H., Hudetz, A. G., Lee, J., Mashour, G. A., Lee, U., & Re, Cc. S. G. (2018). Estimating the Integrated Information Measure Phi from High-Density Electroencephalography during States of Consciousness in Humans. Frontiers in Human Neuroscience, 12, 42–42.

Kim, H., & Lee, U. (2019). Criticality as a Determinant of Integrated Information Φ in Human Brain Networks. Entropy, 21(10), 981.

Kim, M., Mashour, G. A., Moraes, S.-B., Vanini, G., Tarnal, V., Janke, E., Hudetz, A. G., & Lee, U. (2016). Functional and Topological Conditions for Explosive Synchronization Develop in Human Brain Networks with the Onset of Anesthetic-Induced Unconsciousness. Frontiers in Computational Neuroscience, 10(1).

Knapp, R. M. (2017). A Deeper Look at Anesthesia Depth. Anesthesiology, 127(5), 904–905.

Lee, H., Mashour, G. A., Noh, G.-J., Kim, S., & Lee, U. (2013). Reconfiguration of Network Hub Structure after Propofol-induced Unconsciousness. Anesthesiology: The Journal of the American Society of Anesthesiologists, 119(6), 1347–1359.

Lee, M., Sanders, R. D., Yeom, S.-K., Won, D.-O., Seo, K.-S., Kim, H. J., Tononi, G., & Lee, S.-W. (2017). Network Properties in Transitions of Consciousness during Propofol-induced Sedation. Scientific Reports, 7(1), 16791.

Lee, U., & Mashour, G. A. (2018). Role of Network Science in the Study of Anesthetic State Transitions. Anesthesiology, 129(5), 1029–1044.

Lee, U., Muller, M., Noh, G.-J., Choi, B., & Mashour, G. A. (2011). Dissociable network properties of anesthetic state transitions. Anesthesiology, 114(4), 872–881.

Liang, Z., Cheng, L., Shao, S., Jin, X., Yu, T., Sleigh, J. W., & Li, X. (2020). Information Integration and Mesoscopic Cortical Connectivity during Propofol Anesthesia. Anesthesiology, 132(3), 504–524.

Lotto, M. L., Banoub, M., & Schubert, A. (2004). Effects of Anesthetic Agents and Physiologic Changes on Intraoperative Motor Evoked Potentials. Journal of Neurosurgical Anesthesiology, 16(1), 32–42.

Luppi, A. I., Craig, M. M., Pappas, I., Finoia, P., Williams, G. B., Allanson, J., Pickard, J. D., Owen, A. M., Naci, L., Menon, D. K., & Stamatakis, E. A. (2019). Consciousness-specific dynamic interactions of brain integration and functional diversity. Nature Communications, 10(1), 4616.

Maier, K. L., McKinstry-Wu, A. R., Palanca, B. J. A., Tarnal, V., Blain-Moraes, S., Basner, M., Avidan, M. S., Mashour, G. A., & Kelz, M. B. (2017). Protocol for the reconstructing consciousness and cognition (ReCCognition) study. Frontiers in Human Neuroscience, 11, 284.

Mashour, G. A., Orser, B. A., Avidan, M. S., & Warner, D. S. (2011). Intraoperative Awareness: From Neurobiology to Clinical Practice. Anesthesiology, 114(5), 1218–1233.

Maslov, S., & Sneppen, K. (2002). Specificity and stability in topology of protein networks. Science, 296(5569), 910–913.

Milo, R., Shen-Orr, S., Itzkovitz, S., Kashtan, N., Chklovskii, D., & Alon, U. (2002). Network motifs: Simple building blocks of complex networks. Science, 298(5594), 824–827.

Mitra, P. (2007). Observed brain dynamics. Oxford University Press.

Mitra, P., Bokil, H., Maniar, H., Loader, C., Mehta, S., Hill, D., Mitra, S., Andrews, P., Baptista, R., Gopinath, S., Nalatore, H., & Kaur, S. (n.d.). Chronux.

Moon, J.-Y., Lee, U., Blain-Moraes, S., & Mashour, G. A. (2015). General Relationship of Global Topology, Local Dynamics, and Directionality in Large-Scale Brain Networks. PLOS Computational Biology, 11(4), e1004225.

Newman, M. E. J. (2006). Modularity and community structure in networks. Proceedings of the National Academy of Sciences, 103(23), 8577–8582.

Nickalls, R. W. D., & Mapleson, W. W. (2003). Age-related iso-MAC charts for isoflurane, sevoflurane and desflurane in man. BJA: British Journal of Anaesthesia, 91(2), 170–174.

Palanca, B. J. A., Mitra, A., Larson-Prior, L., Snyder, A. Z., Avidan, M. S., & Raichle, M. E. (2015). Resting-state Functional Magnetic Resonance Imaging Correlates of Sevoflurane-induced Unconsciousness. Anesthesiology, 123(2), 346–356.

Purdon, P. L., Pierce, E. T., Mukamel, E. A., Prerau, M. J., Walsh, J. L., Wong, K. F. K., Salazar-Gomez, A. F., Harrell, P. G., Sampson, A. L., & Cimenser, A. (2013). Electroencephalogram signatures of loss and recovery of consciousness from propofol. Proceedings of the National Academy of Sciences, 110(12), E1142–E1151.

Ranft, A., Golkowski, D., Kiel, T., Riedl, V., Kohl, P., Rohrer, G., Pientka, J., Berger, S., Thul, A., Maurer, M., Preibisch, C., Zimmer, C., Mashour, G. A., Kochs, E. F., Jordan, D., & Ilg, R. (2016). Neural Correlates of Sevoflurane-induced Unconsciousness Identified by

Simultaneous Functional Magnetic Resonance Imaging and Electroencephalography. Anesthesiology, 125(5), 861–872.

Rubinov, M., & Sporns, O. (2010). Complex network measures of brain connectivity: Uses and interpretations. NeuroImage, 52(3), 1059–1069.

Sanders, R. D., Tononi, G., Laureys, S., Sleigh, J. W., & Warner, D. S. (2012). Unresponsiveness ≠ Unconsciousness. Anesthesiology, 116(4), 946–959.

Schnakers, C., Vanhaudenhuyse, A., Giacino, J., Ventura, M., Boly, M., Majerus, S., Moonen, G., & Laureys, S. (2009). Diagnostic accuracy of the vegetative and minimally conscious state: Clinical consensus versus standardized neurobehavioral assessment. BMC Neurology, 9(1), 1–5.

Schroeter, M. S., Spoormaker, V. I., Schorer, A., Wohlschlaeger, A., Czisch, M., Kochs, E. F., Zimmer, C., Hemmer, B., Schneider, G., Jordan, D., & Ilg, R. (2012). Spatiotemporal Reconfiguration of Large-Scale Brain Functional Networks during Propofol-Induced Loss of Consciousness. Journal of Neuroscience, 32(37), 12832–12840.

Shen, K., Bezgin, G., Hutchison, R. M., Gati, J. S., Menon, R. S., Everling, S., & McIntosh, A. R. (2012). Information Processing Architecture of Functionally Defined Clusters in the Macaque Cortex. Journal of Neuroscience, 32(48), 17465–17476.

Shin, J., Mashour, G. A., Ku, S., Kim, S., & Lee, U. (2013). Subgraph "Backbone" Analysis of Dynamic Brain Networks during Consciousness and Anesthesia. PloS One, 8(8), e70899.

Sporns, O. (2018). Graph theory methods: Applications in brain networks. Dialogues in Clinical Neuroscience, 20(2), 111–121.

Sporns, O., & Kötter, R. (2004). Motifs in Brain Networks. PLOS Biology, 2(11), e369.

Stam, C. J., & van Straaten, E. C. W. (2012). Go with the flow: Use of a directed phase lag index (dPLI) to characterize patterns of phase relations in a large-scale model of brain dynamics. NeuroImage, 62(3), 1415–1428.

Stam, Cornelis J., Nolte, G., & Daffertshofer, A. (2007). Phase lag index: Assessment of functional connectivity from multi channel EEG and MEG with diminished bias from common sources. Human Brain Mapping, 28(11), 1178–1193.

Staniek, M., & Lehnertz, K. (2008). Symbolic transfer entropy. Physical Review Letters, 100(15), 158101.

Tinker, J. H., Sharbrough, F. W., & Michenfelder, J. D. (1977). Anterior shift of the dominant EEG rhytham during anesthesia in the Java monkey: Correlation with anesthetic potency. Anesthesiology, 46(4), 252–259.

Tononi, G. (2004). An information integration theory of consciousness. BMC Neuroscience, 5(1), 42.

Tononi, G. (2012). The Integrated Information Theory of Consciousness: An Updated Account. Archives Italiennes de Biologie, 150(2/3), 56–90.

Vacanti, C. J., VanHOUTEN, R. J., & Hill, R. C. (1970). A Statistical Analysis of the Relationship of Physical Status to Postoperative Mortality in 68,388 Cases. Anesthesia & Analgesia, 49(4), 564–566.

Vecchio, F., Miraglia, F., Gorgoni, M., Ferrara, M., Iberite, F., Bramanti, P., Gennaro, L. D., & Rossini, P. M. (2017). Cortical connectivity modulation during sleep onset: A study via graph theory on EEG data. Human Brain Mapping, 38(11), 5456–5464.

Vijayan, S., Ching, S., Purdon, P. L., Brown, E. N., & Kopell, N. J. (2013). Thalamocortical Mechanisms for the Anteriorization of Alpha Rhythms during Propofol-Induced Unconsciousness. Journal of Neuroscience, 33(27), 11070–11075.

Vinck, M., Oostenveld, R., van Wingerden, M., Battaglia, F., & Pennartz, C. M. A. (2011). An improved index of phase-synchronization for electrophysiological data in the presence of volume-conduction, noise and sample-size bias. NeuroImage, 55(4), 1548–1565.

Watts, D. J., & Strogatz, S. H. (1998). Collective dynamics of ‘small-world’networks. Nature, 393(6684), 440.

Wei, Y., Liao, X., Yan, C., He, Y., & Xia, M. (2017). Identifying topological motif patterns of human brain functional networks. Human Brain Mapping, 38(5), 2734–2750.

Acknowledgements

This work was funded by the James S. McDonnell Foundation, St. Louis, MO (GM, MK and MA); the Canadian Institute for Health Research (FRN 152562, CD; Fredrick Banting and Charles Best Canada Graduate Scholarship – Masters, DN); the Fonds de Recherche du Québec – Nature et technologies (YM); the Fonds de Recherche du Québec – Santé (DN); and the Natural Science and Engineering Research Council of Canada (Discovery Grant RGPIN-2016-03817; SBM).

Author Contributions

MA, MK, and GM conceived the study; VT, PP, GV, GG, EJ and SBM collected the experimental data; YM, DN, CD, and SBM analyzed the experimental data; CD, YM, DN, and SBM interpreted the findings; CD and SBM wrote the manuscript; DN and GM constructively reviewed the manuscript; all authors reviewed and approved the final version of the manuscript.

Supplementary Information

Supplementary information accompanies this paper at https://www.nature.com/articles/s41598-021-83482-9#Sec30.

Figure Legends

Figure 1. Experimental design and timeline

Timeline of anesthetic protocol and EEG data epochs. Participants received a stepwise increasing infusion rate of propofol for 15 min: 100 mcg/kg/min × 5 min increasing to 200 mcg/kg/min × 5 min, and then to 300 mcg/kg/min × 5 min. Participant then received 1.3 age-adjusted minimum alveolar concentration inhaled isoflurane anesthesia for 3 h. Blue rectangles represent the eight 5-min EEG epochs during which network properties and motifs were calculated: 1) Baseline; 2) Induction; 3) Unconscious; 4) 30 min pre-recovery of responsiveness (ROR); 5) 10 min pre-ROR; 6) 5 min pre-ROR; 7) 30 min post-ROR; and 8) 180 min post-ROR.

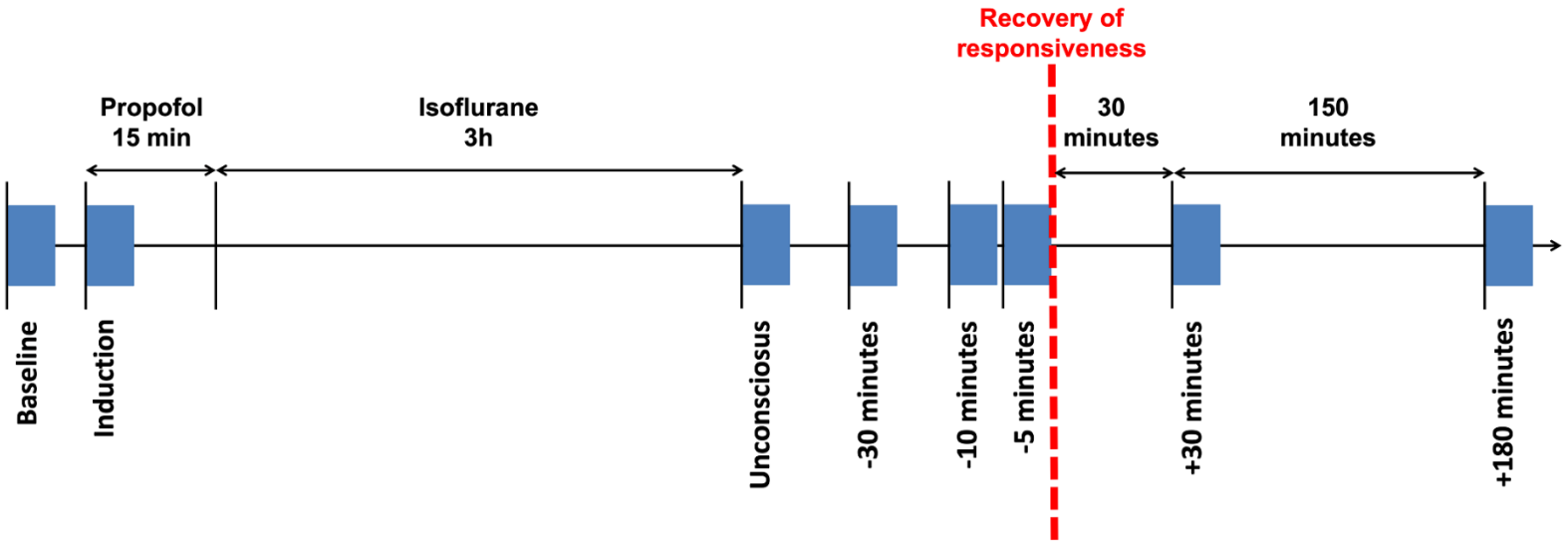

Figure 2. Possible 3-node network motifs

A 3-node motif represents a specific pattern of interconnection between three electrodes Five 3-node motifs can exist when unidirectional connections are assessed. These five 3-node motifs are assessed in this study. Dark circles represent nodes (i.e. individual electrodes), while black lines represent the edges linking the nodes. Arrows indicate the direction of phase-lead relationship.

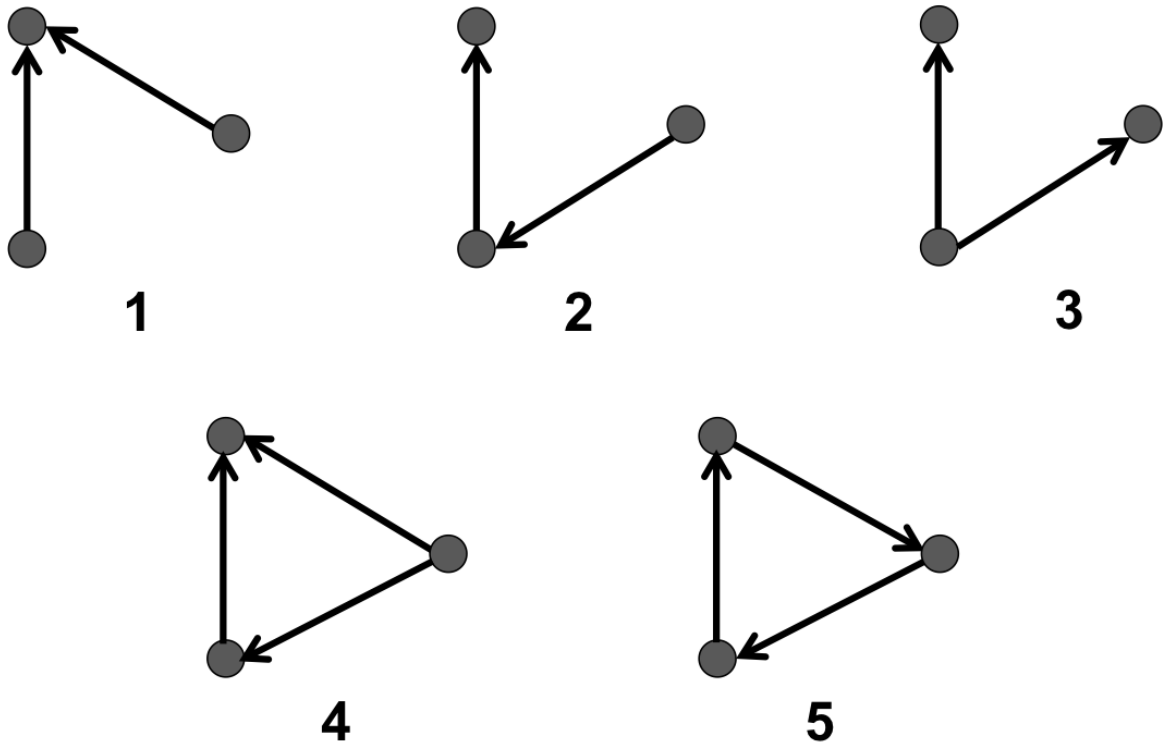

Figure 3. Motif significance across epochs and participants

For each motif, the total aggregate frequency of motifs in the network was calculated by summing across all channels. A z-score was calculated for the frequency of each motif in each network by comparing the total number of motifs in a given network to the distribution of motif frequency in 100 null networks. Motifs that were statistically significance per participant and time point are represented by orange (motif 1), purple (motif 2) and green (motif 5) rectangles. Motifs not statistically significant are left grey. Motif significance varied across time points and participants. Percentages in the right column represent the frequency of motif significance. A frequency of 98.6% indicates that this motif was significant throughout all participants and time points, except one participant, at one time point.

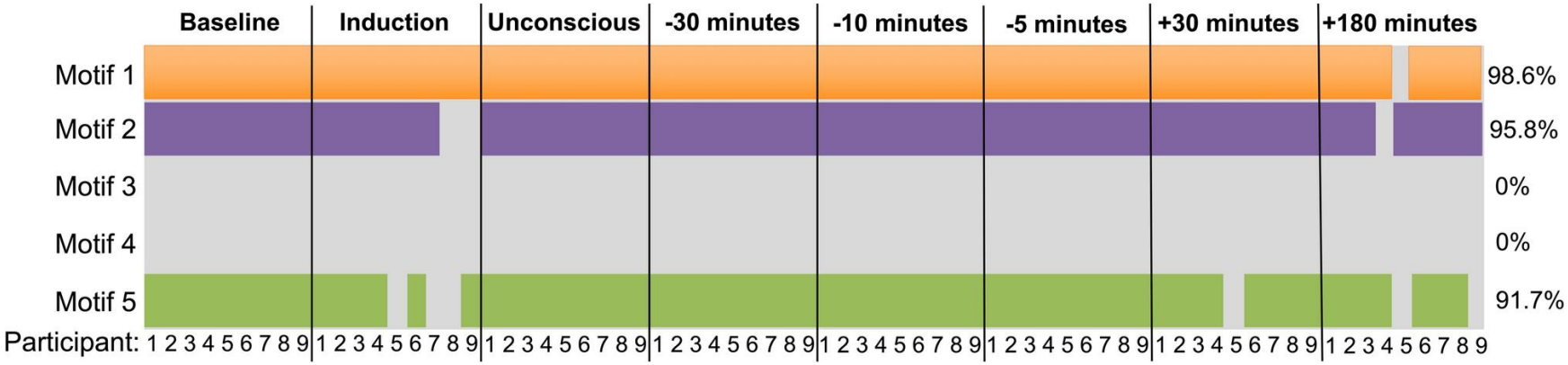

Figure 4. Motif topology across states of consciousness

(A) and (C) Topographic maps of the frequency of participation of nodes in alpha motif 1 (M1) and motif 5 (M5) across the eight analysis epochs. Orange rectangles highlight the epochs that are significantly distinct from Baseline ($p < 0.05$). The colormap represents the Z-score comparing the frequency of motif participation for each electrode to the distribution of frequency of motif participation for all electrodes in the network. (B) Topographic maps depicting the distribution of nodes acting as sources of information flow (i.e. nodes that have a phase-lead relationship with regards to the other nodes within the motif), in every instance of motif 1 within the EEG network, across the eight time points of the anesthetic protocol. The colormap represents the Z-score comparing the total number of times a given node is a source, compared to the distribution of this feature for all nodes in the network. (D) Alpha power topographic maps across the eight analysis epochs. There is a significant, small-to-medium positive correlation between alpha power the frequency of motif 1 ($R = 0.26$, $p < 0.001$) and motif 5 ($R = 0.22$, $p < 0.001$). (E) Differences in cosine similarity values between Baseline, Unconsciousness, and 180 min post-recovery of responsiveness. Thin grey lines depict single participants, while the thicker red line depicts average cosine similarity value across all participants. (F) Across participants and epochs, nodes participating in motif 1 form longer-range connections than those participating in motif 5.

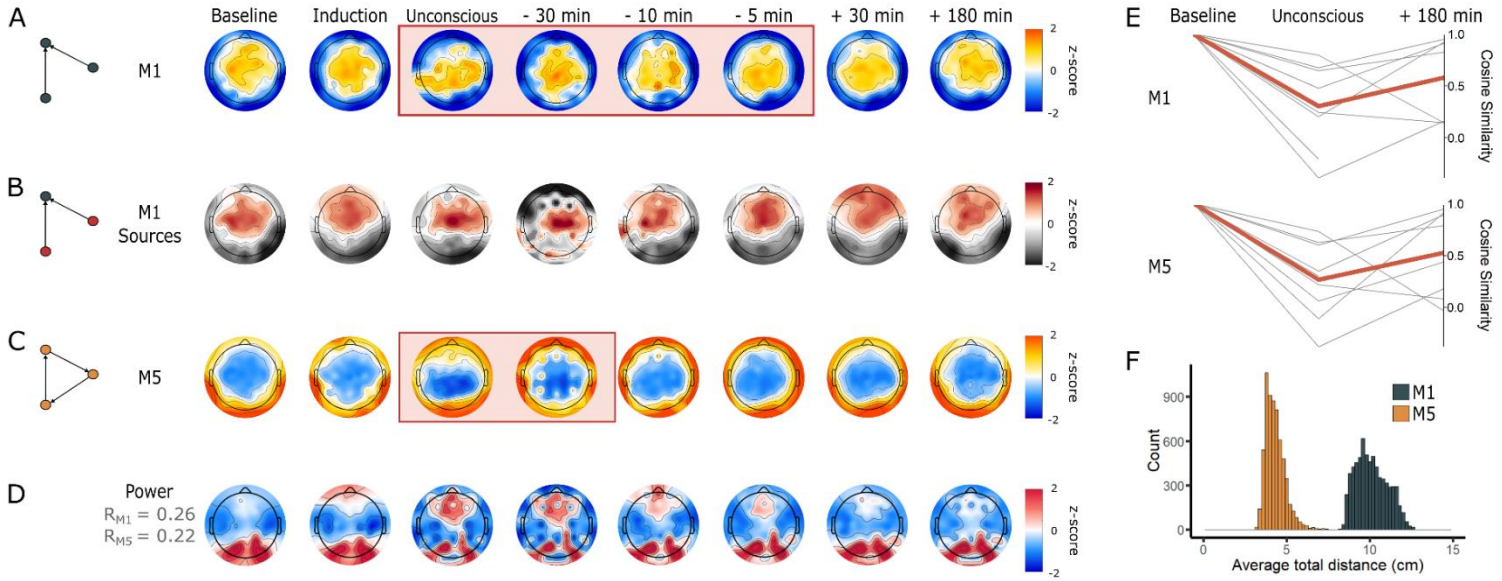

Figure 5. Global brain network properties across the experimental period

The functional brain network of each participant was constructed using a binarized wPLI matrix. From this network, we calculated global graph theoretical network properties, including global efficiency (A), clustering coefficient (B), binary small-worldness and modularity (C), across the eight analysis epochs. Changes in binary small-worldness were driven by changes in the clustering coefficient; this metric was therefore also significantly increased from Baseline at Unconscious, 30-, 10-, and 5-min pre-recovery of consciousness epochs (not plotted due to redundancy). Boxes represent the interquartile range, with the lower and upper limit of boxes indicating 1st and 3rd quartiles, respectively. The median is marked by the black horizontal line inside the boxes. The whiskers outside the boxes extend to the lowest and highest observations that are not outliers, while outliers are marked by a cross, and are defined as values greater than ±1.5 times the interquartile range.

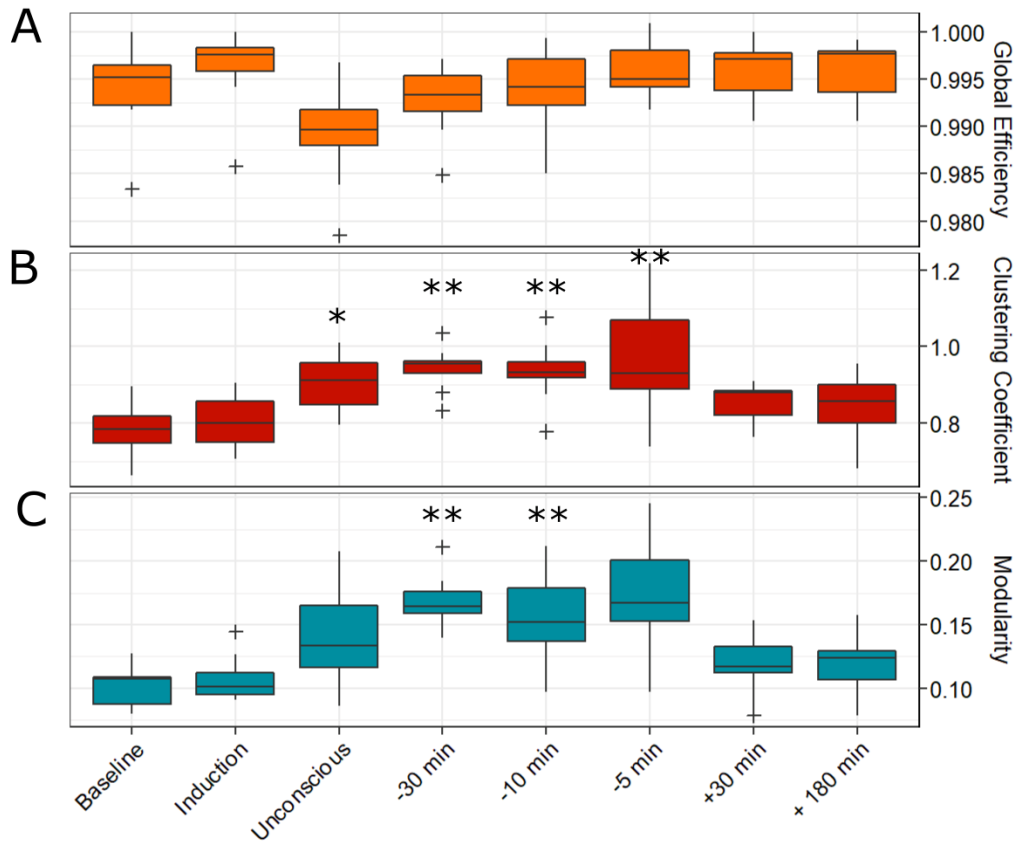

+: outliers (greater than median +/- 1.5*IQR)
*: significantly different from Baseline ($p<0.05$)
**: significantly different from Baseline ($p<0.01$)

Figure 6. Pipeline for extracting network properties and motifs EEG time series

Each 5-min EEG epoch was used to construct a wPLI and dPLI matrix. Network properties were then calculated based on the wPLI matrix, while the dPLI matrix was used to create a phase-lead matrix, which set all non-phase-leading values to 0 (black), and normalized the remaining non-zero values between 0 and 1. Motifs were then extracted from the phase lead matrix, and their frequency (i.e frequency of participation of each node in each of the possible types of motifs) and topology (i.e. topological distribution of participating nodes in each motifs) were calculated.

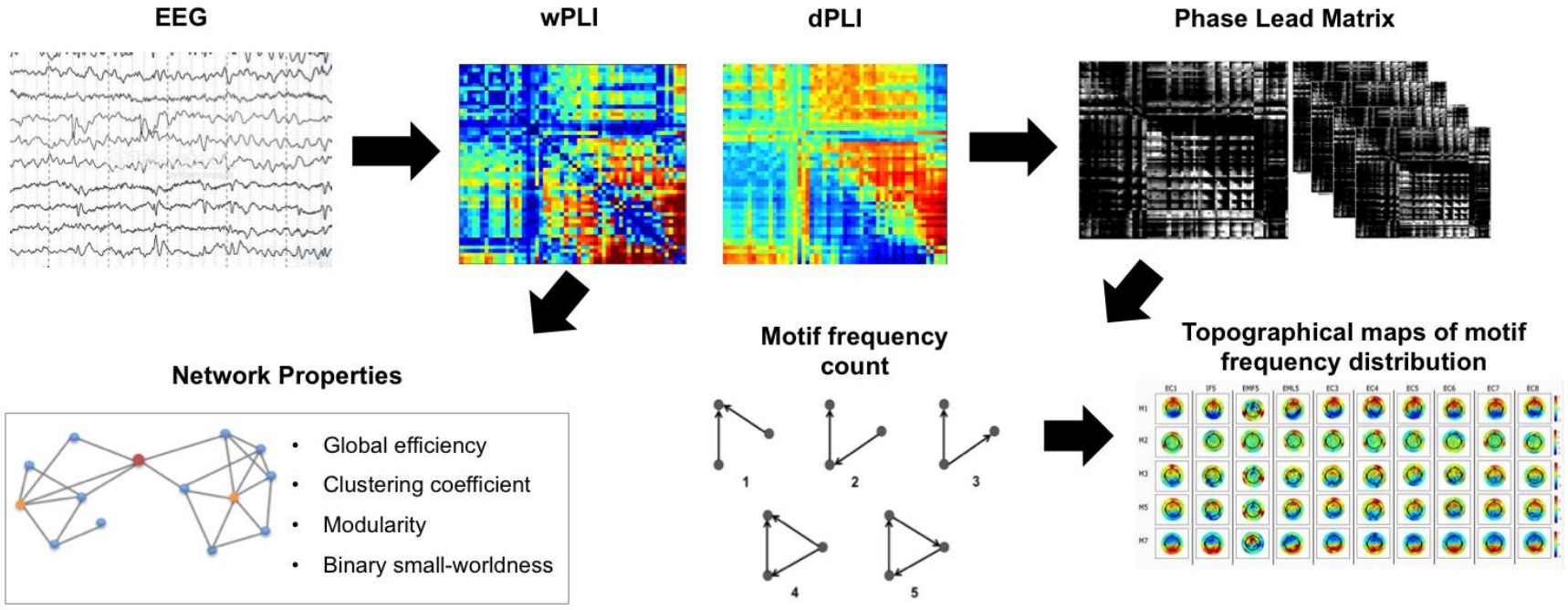

EEG: electroencephalography; wPLI: weighted phase lag index; dPLI: directed phase lag index

Chapter 3: Brain Network Motif Topography May Predict Emergence from Disorders of Consciousness: A Case Series

Danielle Nadin[1,2], Catherine Duclos[1,3], Yacine Mahdid[1,2], Alexander Rokos[1,2], Mohamed Badawy[4,5], Justin Letourneau[4,5], Caroline Arbour[6,7], Gilles Plourde[4,5], Stefanie Blain-Moraes[1,3*]

1. Montreal General Hospital, McGill University Health Center Research Institute, Montreal, QC, Canada
2. Integrated Program in Neuroscience, Faculty of Medicine, McGill University, Montreal, QC, Canada
3. School of Physical and Occupational Therapy, Faculty of Medicine, McGill University, Montreal, QC, Canada
4. Montreal Neurological Hospital and Institute, McGill University Health Center, Montreal, QC
5. Department of Anesthesia, McGill University, Montreal, QC
6. Centre de recherche, CIUSSS du-Nord-de-l'Île-de-Montréal, Montreal, QC
7. Faculty of Nursing, Université de Montréal, Montreal, QC

* Correspondence address: Montreal General Hospital, McGill University Health Center Research Institute, 1650 Cedar Ave, L11-132, Montreal, QC, H3G 1A4, Canada. Tel: 514-398-1325; Fax: 514-398-6360; E-mail: stefanie.blain-moraes@mcgill.ca

Following the evidence presented in Chapter 2 on the association of motifs with states of anesthetic-induced unconsciousness, we explore the association of this metric with prognosis in three patients with disorders of consciousness. This manuscript was published in *Neuroscience of Consciousness*. Supplemental figures can be found at: https://academic.oup.com/nc/article/2020/1/niaa017/5893032#supplementary-data

Reference: Nadin, D., Duclos, C., Mahdid, Y., Rokos, A., Badawy, M., Létourneau, J., ... & Blain-Moraes, S. (2020). Brain network motif topography may predict emergence from disorders of consciousness: a case series. *Neuroscience of Consciousness*, *2020*(1), https://doi.org/10.1093/nc/niaa017.

Abstract

Neuroimaging methods have improved the accuracy of diagnosis in patients with disorders of consciousness (DOC), but novel, clinically translatable methods for prognosticating this population are still needed. In this case series, we explored the association between topographic and global brain network properties and prognosis in patients with DOC. We recorded high-density electroencephalograms in three patients with acute or chronic DOC, two of whom also underwent an anesthetic protocol. In these two cases, we compared functional network motifs, network hubs and power topography (i.e. topographic network properties), as well as relative power and graph theoretical measures (i.e. global network properties), at baseline, during exposure to anesthesia and after recovery from anesthesia. We also compared these properties to a group of healthy, conscious controls. At baseline, the topographic distribution of nodes participating in alpha motifs resembled conscious controls in patients who later recovered consciousness and high relative power in the delta band was associated with a negative outcome. Strikingly, the reorganization of network motifs, network hubs and power topography under anesthesia followed by their return to a baseline patterns upon recovery from anesthesia, was associated with recovery of consciousness. Our findings suggest that topographic network properties measured at the single-electrode level might provide more prognostic information than global network properties that are averaged across the brain network. In addition, we propose that the brain network's capacity to reorganize in response to a perturbation is a precursor to the recovery of consciousness in DOC patients.

Keywords: disorders of consciousness, electroencephalography, anesthesia, brain networks, graph theory, network motifs, network hubs

Introduction

Brain injury often leads to loss of consciousness. Individuals who survive but fail to regain behavioural responsiveness to pain or external cues are considered to be in a disorder of consciousness (DOC). Awareness fluctuates greatly in patients with DOC according to their diagnosis: in unresponsive wakefulness syndrome (UWS), individuals exhibit spontaneous eye opening and reflexive behaviours such as eye blinking and swallowing, but are not aware of themselves or their environment (Monti, Laureys, & Owen, 2010), while those in a minimally conscious state (MCS) are inconsistently able to respond to commands and to their environment (Giacino et al., 2002). When diagnoses are made based on clinical consensus, over 40% of patients in MCS are estimated to be misdiagnosed with UWS – a phenomenon that has been attributed to variations in behavioural assessment and interpretation

(Peterson, Cruse, Naci, Weijer, & Owen, 2015; Schnakers et al., 2009). Moreover, some patients diagnosed with UWS have demonstrated awareness through willful modulation of their brain activity in a functional magnetic resonance imaging (fMRI) scanner (Monti, Vanhaudenhuyse, et al., 2010; Owen et al., 2006) and during high-density electroencephalography (EEG) recordings (Cruse et al., 2011). Such neuroimaging approaches have revealed that even when the best available behavioral assessment (Coma Recovery Scale – Revised; CRS-R) is used, there is still a misdiagnosis rate of approximately 15% (Kondziella, Friberg, Frokjaer, Fabricius, & Møller, 2016). Both the high misdiagnosis rate of behavioural assessment and the presence of "covert" consciousness in behaviourally unresponsive patients highlight the need for objective assessment tools. However, as the gold standard for the assessment of consciousness is self-report and response to commands, there will always be uncertainty associated with any new diagnostic test for unresponsive individuals (Peterson et al., 2015). An alternative approach is to develop tools for prognostication: since clinical outcomes can be reliably gathered, prognostic tools have the potential to achieve higher reliability and accuracy than diagnostic tools in this population. Such tools can have substantial impact on patient quality of life, influencing treatment and end-of-life decision-making.

Advances in neuroimaging have improved prognostication in this patient population beyond what is possible with clinical measures such as age at injury or etiology alone. Positron-emission tomography (PET) measures of brain glucose metabolism and fMRI measures of functional connectivity in the default mode and attention networks have predicted outcomes with accuracies of up to 88% (Song et al., 2018; Stender et al., 2016). EEG in particular has been extensively explored for prognosis due to its high translational potential. Spectral power ratios (Bagnato et al., 2017; Sitt et al., 2014) and the presence of long-latency event-related potentials (ERPs) have been established as predictors of recovery from DOC (F Faugeras et al., 2011; Frédéric Faugeras et al., 2012; Steppacher et al., 2013; Wijnen, Van Boxtel, Eilander, & De Gelder, 2007). More recently, brain network characteristics have been explored for their prognostic value. Network features including low functional connectivity in low frequency bandwidths (Bai, Xia, Wang, He, & Li, 2019; Sitt et al., 2014), and feedback-dominant frontoparietal connectivity and posterior-dominant network hubs (Blain-Moraes et al., 2016) have been associated with favourable outcomes in patients with DOC. Graph theory analysis of EEG has demonstrated that path length, participation coefficient, modularity and clustering of brain networks are potential prognostic markers (Chennu et al., 2017; Stefan et al., 2018). Finally, the complexity of the brain's EEG response to transcranial magnetic stimulation has been associated with the degree of recovery from DOC (Casarotto et al., 2016). While these EEG studies have established the enormous

potential of this neuroimaging technique for prognosis in this population, to date, none have achieved sufficient prognostic accuracy, specificity and sensitivity to be clinically useful (≥ 85% for all three metrics), particularly in UWS patients. There is therefore a need to explore novel EEG prognostic measures, or refine existing ones, in this population.

Brain network motifs are recurring connectivity patterns in a network that are present at numbers significantly higher than in random networks (Milo et al., 2002). These subgraphs are thought to be the building blocks of larger networks, with functional motifs representing communication channels between nodes (Sporns & Kötter, 2004). Motifs may reveal granular changes in network composition that are associated with the capacity of a network to sustain consciousness (Kafashan, Ching, & Palanca, 2016; Shin, Mashour, Ku, Kim, & Lee, 2013) and thus may have strong prognostic value for DOC patients. Our group has demonstrated in healthy participants that three-node functional motifs exhibit topographically-distinct patterns associated with states of anesthetic-induced unconsciousness (Duclos et al., 2020). We have also demonstrated the feasibility of using anesthesia to perturb the brain networks of a DOC patient, allowing us to measure changes in the network that herald the recovery of consciousness (Blain-Moraes et al., 2016). Driven by these findings, in this study, we investigate the prognostic potential of three-node functional network motifs in three DOC patients in an acute or chronic state, two of whom were exposed to anesthesia. We hypothesize that patient prognosis is associated with motif topography before, during and after exposure to anesthesia. Furthermore, we compared motif topography to other topographic network properties (network hubs and power topography) and global network properties (graph theoretical network properties and relative power). We predict that the spatial information provided by topographic network properties will be more predictive of patient outcome compared to global brain network characteristics, which are averaged across nodes in the network.

Materials and methods

Participants

A convenience sample of three patients in a DOC following acquired brain injury were recruited from the Montreal Neurological Hospital and the surrounding Montreal area. Participants were included if they were between 18 and 80 years old and were in UWS or MCS, as assessed using the CRS-R by a trained experimenter (CA). They were excluded if they presented with elevated intracranial pressure, hepatic or renal failure and/or hemodynamic instability, were receiving active vasopressor therapy, were in a medically-induced coma for intracranial hypertension or status epilepticus, had a

neurosurgical intervention in the 72 hours prior to the study (due to open-head injury or intracranial pathology), or had a documented allergy to propofol. Participants were also excluded for pregnancy, or if they were deemed medically unsuitable for the study by their attending physician. Next of kin provided written informed consent for all participants. The study was approved by the McGill University Health Center Research Ethics Board (15-996-MP-CUSM).

Experimental design

We present a series of case studies of three patients in a DOC, who underwent a high-density EEG recording. Details of each case are presented in the results section. Importantly, two patients were in an acute state (< 3 months post-injury), while one was in a chronic state. We expected that the acute patient in MCS would exhibit EEG patterns similar to healthy controls (positive control), whereas the chronic UWS patient would not (negative control). In the acute UWS patient, we tested the hypothesis that topographic network properties – particularly, network motifs – were associated with prognosis.

Two of the three patients were also exposed to anesthesia, as per the anesthetic protocol detailed in (Blain-Moraes et al., 2016). Briefly, high-density EEG was measured at baseline, during exposure to anesthesia, and after recovery from anesthesia. We followed the guidelines of the Canadian Anesthesiologists' Society in all regards, including pre-anesthetic assessment, fasting, and monitoring. An Alaris PK Carefusion pump (Carefusion, Switzerland) was used to administer propofol in a target-controlled infusion mode using the Marsh kinetic set (Marsh, White, Morton, & Kenny, 1991). The parameters to drive the pump were based on the age and weight of the patients. The effect site concentration was of 2 μg/mL and was held constant for the duration of the anesthetic exposure (40 min). The patients maintained adequate spontaneous respiration throughout. The beginning of the recovery period was defined as the moment the effect site concentration reached 0.5 μg/mL.

Global and topographic network properties in DOC patients were compared against nine healthy controls undergoing anesthetic-induced unconsciousness, induced by propofol and maintained for 3 hours using isoflurane (Duclos et al., 2020; Maier et al., 2017). Similarly to DOC patients, high-density EEG was recorded during baseline, anesthesia exposure and recovery.

Electroencephalographic data acquisition and preprocessing

EEG signals were collected from the scalp using a 128-channel electrode net (Electrical Geodesics, Inc., Eugene, OR, USA) referenced to Cz. Data were sampled at 1 kHz, and electrode impedances were kept below 50 kΩ. Pre-processing was performed in EEGLAB (Delorme & Makeig, 2004). The data

were bandpass filtered from 0.1 to 50 Hz, and non-scalp channels were discarded, leaving 99 channels for subsequent analyses. Noisy channels were also removed, and the data were re-referenced to an average reference. When present, eye blinks were removed using ICA. Five-minute segments of EEG were extracted during three analysis epochs – baseline, anesthesia and recovery – while patients were presented with auditory stimuli to induce ERPs. (The results of ERP analysis are not presented in this publication.) Upon visual inspection by a trained experimenter (DN), noisy segments within each epoch were removed.

Network construction

Functional networks were constructed using custom MATLAB scripts (version R2018b). Data were first filtered into the delta (1-4 Hz), theta (4-8 Hz) or alpha (8-13 Hz) band using a Butterworth filter. Functional connectivity and directed functional connectivity were calculated across 10-second windows and averaged within each analysis epoch and frequency band to generate representative connectivity matrices for baseline, anesthesia and recovery periods. Functional connectivity was calculated using weighted phase lag index (wPLI), and directed functional connectivity using directed phase lag index (dPLI) – measures robust against the effects of volume conduction (Stam & van Straaten, 2012; Vinck, Oostenveld, van Wingerden, Battaglia, & Pennartz, 2011).

The wPLI between two channels was computed as:

$$wPLI_{ij} = \frac{\left|E\{\Im(C_{ij})\}\right|}{E\{\left|\Im(C_{ij})\right|\}} = \frac{\left|E\{\left|\Im(C_{ij})\right| sgn(\Im(C_{ij}))\}\right|}{E\{\left|\Im(C_{ij})\right|\}}$$

where $\Im(C_{ij})$ is the imaginary part of the cross-spectrum C_{ij} between signals i and j, and sgn is the signum function. When one signal leads the other, the wPLI is close to 1, with a value of 1 indicating perfect phase locking between signals. When there is no phase relationship between the signals, the wPLI is equal to 0.

A Hilbert transform yielded the instantaneous phase time series for each channel, and the phase difference $\Delta\phi_{ij}$ between all pairs of signals i and j was calculated. dPLI was defined as:

$$dPLI_{ij} = \frac{1}{N}\sum_{t=1}^{N} H(\Delta\phi_{ij})$$

where N is the length of the analysis segment and t is a given time point. H is the Heaviside step function, such that when i leads j, the dPLI is between 0.5 and 1; when j leads i, the dPLI is between 0 and 0.5; and, when there is no phase relationship between the signals, the dPLI is equal to 0.5. As the matrices were symmetrical, they were transformed into phase-lead matrices. dPLI values below 0.5 (i.e. phase-lag) were set to zero and the remainder (i.e. phase-lead) were normalized between 0 and 1.

The effects of spurious phase relationships in both the wPLI and dPLI connectivity matrices were controlled through a surrogate analysis, where signal i remained fixed while the phase time-series of signal j was scrambled, abolishing the phase relationship between the signals while maintaining their other (e.g. spectral) properties. wPLI and dPLI values were compared against a distribution of the means of 20 surrogate analyses and were retained if they were significantly different ($p < 0.05$ level). Non-significant connections were set to 0 (wPLI) or 0.5 (dPLI).

Global network properties

We defined global network properties as network measures which were averaged across all nodes in the network, resulting in a single value for each network. The global network properties examined in this study were relative power, and a set of graph theoretical network properties.

Relative power analysis

Spectral power in the delta, theta, alpha and broadband (1-13 Hz) frequency bands was computed over 10-second windows using a multi-taper power spectral density estimate (number of tapers = 3, time-bandwidth product = 2, spectrum window size = 3 seconds) from the Chronux package (Partha Mitra, 2007; Partha Mitra et al.). Power was averaged across time windows and all electrodes. Relative spectral power was equal to the ratio between the average delta, theta or alpha power and the average broadband power.

Graph theoretical network properties

In each network, four graph theoretical properties were computed using the Brain Connectivity Toolbox (BCT) (Rubinov & Sporns, 2010): 1) Global efficiency - the inverse of the average path length ($\frac{1}{L_w}$), where L_w is the average shortest path length between all pairs of nodes in the network (Latora & Marchiori, 2001). A high global efficiency reflects a more integrated network, where nodes across the network are connected using short paths. 2) Clustering coefficient (C_w) - the ratio between the number of connections between a node's neighbors, and the number of possible connections these neighbors

could make, averaged across all nodes (Watts & Strogatz, 1998). A high clustering coefficient indicates a more segregated network with high local efficiency, where nodes tend to cluster together. 3) Modularity - the sum of the strength of connections within a module, where modules are computed using Louvain's algorithm (Rubinov & Sporns, 2010). High modularity indicates a more segregated network, with strong within-module connections and weak between-module connections (Newman, 2006). 4) Binary small-worldness - the ratio between the clustering coefficient and the average path length ($\frac{C_w}{L_w}$). This measure reflects both the segregation and integration required in an efficient network (Watts & Strogatz, 1998).

Prior to computing these properties, networks constructed using wPLI (see section 2.4) were binarized by thresholding them at the top n% of connectivity values. To determine the optimal threshold n for each participant, custom MATLAB scripts were used to explore thresholds ranging from 1 to 90%. Specifically, for each participant's baseline network, n was decreased from 90% in steps of 1% until at least one node became disconnected from the rest of the graph. Disconnection was assessed using path length; when disconnected, nodes had an infinite path length. The smallest n that did not result in node disconnection was selected for each participant (n's ranged from 13 to 59 for healthy controls and from 33 to 48 for DOC patients). This procedure resulted in networks which had a minimal number of connections but no isolated nodes (H. Kim et al., 2018), corresponding to what we would expect in a human brain network with no isolated brain regions and an economical number of connections. When connectivity values fell above the selected optimal threshold, connections were set to 1, while all others were set to 0.

Network properties for baseline, anesthesia and recovery epochs were calculated by averaging the properties across 10-second windows within each epoch. To account for spurious measurements, 10 random binary networks where the degree distribution of connections was fixed, but the connections were randomized, were-computed. Connections were randomly rewired 10 times while preserving node degree (Maslov & Sneppen, 2002). Global efficiency and clustering coefficient were normalized by taking the ratio between the properties of the original network and the properties of the average random network.

Topographic network properties

We defined topographic network properties as measures that were computed at the single-node level and visualized on a topographic head map. Topographic maps were plotted using EEGLAB's *topoplot* function (Delorme & Makeig, 2004).

Power analysis

As described previously, spectral power in the delta, theta and alpha frequency bands was computed using the multi-taper method (see "Relative power analysis"). Power topography was mapped as the power at each node relative to all the other nodes in its network. Specifically, the z-score for each node was calculated using the mean and standard deviation of power across all nodes in the network.

Hub analysis

From the binarized wPLI networks (see "Graph theoretical network properties"), the degree of each node in each network was calculated to assess the location of high-degree network hubs, using the BCT. The topographic distribution of hubs was mapped as the degree of each node relative to all the other nodes in its network. Specifically, the z-score for each node was calculated using the mean and standard deviation of the degrees of all nodes in the network. For clarity, hub topographic maps were visualized using wPLI matrices binarized at the top 5% of connections.

Motif analysis

While motifs can theoretically be calculated for any number of nodes in a network, the exponentially increasing computational cost – and reduction in clinical translatability – associated with higher numbers of nodes were motivators to focus this analysis on three-node motifs. Of the 13 possible three-node motifs, only five (ID = 1, 2, 3, 5, 7) can be constructed based on the unidirectional connectivity between nodes as calculated by dPLI (Figure 1).

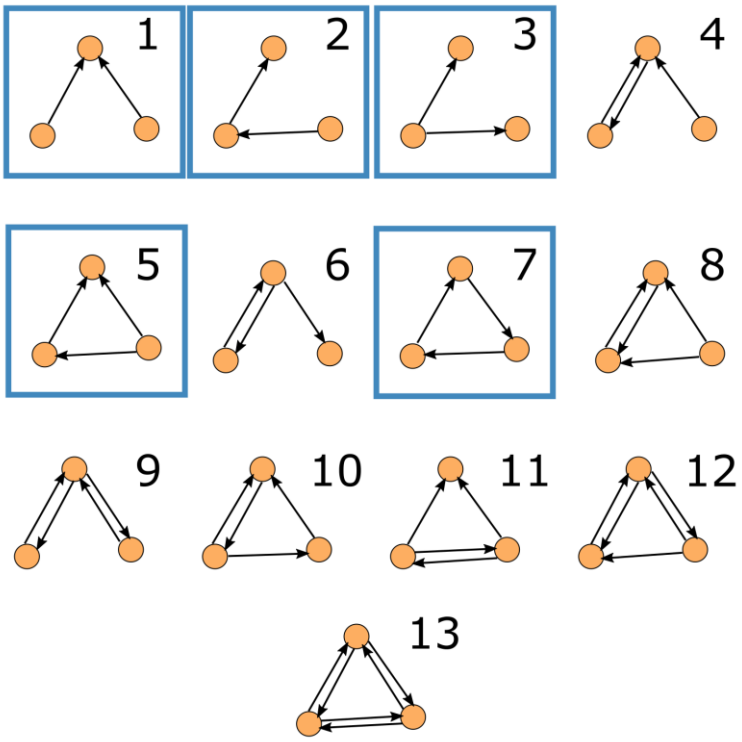

Figure 1. Three-node unidirectional network motifs explored during motif analysis.

Only unidirectional motifs can be computed using the directed phase-lag index (dPLI) and are surrounded by boxes. Circles indicate nodes in the network and arrows represent functional relationships between nodes.

Motifs were computed on the dPLI networks (see "Network construction") using custom MATLAB scripts and the BCT. The motif topography for each analysis epoch was calculated based on motif frequency – the number of times a given node in the network participated in a given motif with any other node in the network. Spurious connectivity was accounted for by comparing the sum of motif frequencies across all nodes in each network against 100 surrogate networks using a z-score. Surrogate networks were generated by randomly shuffling connections while preserving the degree and weight distributions of each node in the network. When the sum of motif frequencies was non-significant ($p > 0.05$), the frequency for all nodes in that network was set to zero.

The topographic distribution of each motif was mapped as the motif frequency at each node relative all the other nodes in its network. Specifically, the z-score for each node was calculated using the mean and standard deviation of the motif frequencies across all nodes in the network.

Comparison of electroencephalographic measures across states of anesthesia exposure and against conscious controls

Comparison across states of anesthesia exposure

Within each subject, topographic network properties across baseline, anesthesia and recovery were compared using cosine similarity (s):

$$s = \frac{b_1 \cdot b_2}{\|b_1\|\|b_2\|}$$

where b_1 and b_2 are the z-scores corresponding to motif frequency, node degree or power for states 1 and 2. Cosine similarity ranges between -1 and 1, with 1 indicating identical and -1 indicating completely opposite topographic distributions. A value of 0 indicates orthogonality or decorrelation.

Comparison against conscious controls

For topographic properties, cosine similarity was used to compare motif, hub and power topographies between DOC patients and each healthy control. The median cosine similarity value was used as a representative quantitative measure of the comparison between each patient and the group of controls.

For global properties, DOC patients' properties were plotted relative to the distribution of properties for the control population. This allowed us to estimate whether DOC patients were outliers (greater or less than the median ± 1.57 times the interquartile range), and whether changes in global network properties across baseline, anesthesia and recovery were similar between patients and controls.

Results

The ability of topographic and global network properties to distinguish between consciousness and anesthetic-induced unconsciousness was first validated in the healthy control dataset. Then, for each DOC patient, a case report, followed by the results of each analysis is presented. A summary of patients' demographic and clinical data is shown in Table 1. For clarity, results for the alpha band are presented in the main body of the paper, while results for the theta and delta bands are presented in the Supplemental Material.

Validation of analysis techniques in conscious controls

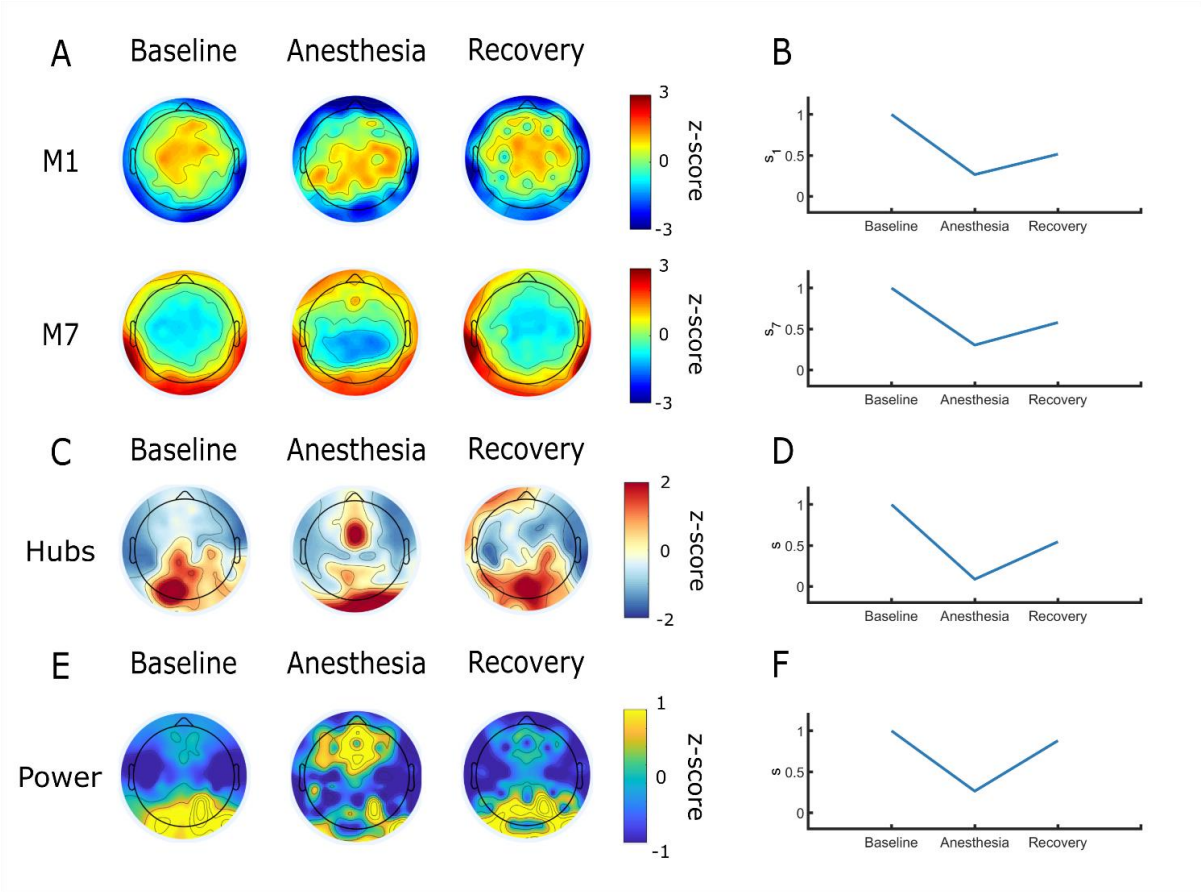

Figure 2. Topographic network properties in the alpha band distinguish between consciousness and anesthetic-induced unconsciousness in healthy controls.

Adapted from Duclos et al. (2020). In a cohort of 9 healthy controls, the average topographies of alpha motif frequency, node degree and power undergo anterior-posterior shifts across stages of anesthetic-induced unconsciousness. Topographic maps represent z-scores comparing motif frequency (A), node degree (C) and power (E) of each electrode to the distribution across all electrodes. Cosine similarity to baseline quantitatively reflects these shifts (B, D and F, respectively). M1 = motif 1, M7 = motif 7.

Topographic network properties

Motif analysis: Motifs 1, 2 and 7 were present at frequencies statistically higher than in random networks across participants. On average, in the alpha band, motif 1 was centrally dominant during consciousness and shifted posteriorly during unconsciousness, while motif 7 demonstrated the reverse pattern (i.e. posterior-dominant during consciousness, both posterior- and anterior-dominant during

unconsciousness) (Figure 2A). These visual changes were reflected by a decrease in cosine similarity during anesthesia, and an increase post-anesthesia (Figure 2B). Motifs in the theta band exhibited similar patterns (Suppl. Figure 1A), while motifs in the delta band did not clearly reorganize across states (Suppl. Figure 2A). Motif 2 did not reflect changes in states of consciousness, and therefore was not discussed in this paper.

Hub analysis: Network hubs underwent topographic shifts associated with states of consciousness. On average, alpha hubs were posterior-dominant during consciousness, and anterior-dominant during unconsciousness (Figure 2C). Visually observed changes were captured by cosine similarity (Figure 2D). Theta hubs exhibited similar patterns (Suppl. Figure 1B), while delta hubs exhibited the opposite pattern (i.e. anterior-dominant during consciousness, posterior-dominant during unconsciousness) (Suppl. Figure 2B).

Power analysis: Alpha power topography distinguished between states of consciousness. On average, alpha power was concentrated posteriorly during consciousness and shifted anteriorly under anesthesia (Figure 2E). These changes were captured by cosine similarity (Figure 2F). In the theta band, power was concentrated anteriorly at baseline, and was suppressed under anesthesia (Suppl. Figure 1C). There were no anesthetic-induced topographical shifts in power in the delta band (Suppl. Figure 2C).

Global network properties

Graph theoretical network properties: In the alpha band, there was an increase in clustering coefficient, binary-small worldness and modularity during anesthesia, and no change in global efficiency (Figure 6A, blue boxes).

Relative power analysis: During anesthesia, there was a decrease in relative alpha power, as well as an increase in relative theta and delta power (Figure 6B, blue boxes).

Table 1. Demographic and clinical data of patients.

Case	Age	Sex	Etiology	Time post-injury	State	Clinical diagnosis	CRS-R score						
							Auditory	Visual	Motor	Oromotor	Communication	Arousal	Total
1	35	F	Stroke	53 d	Acute	MCS	2	3*	4*	1	0	2	12
2	50	F	Stroke	25 d	Acute	UWS	1	1	1	0	0	0	3
3	24	M	Anoxia	8 y 6 mo	Chronic	UWS	1	0	2	1	0	1	5

* denotes MCS

Case 1: Motif patterns in minimally conscious state are similar to healthy controls

Case report

A 35-year-old female presented with a ponto-mesencephalic intracerebral hemorrhage due to a ruptured arteriovenous malformation (AVM). After an initial partial recovery (with complete return of her level of consciousness), she went to a rehabilitation center where, five months later, she experienced a second intraparenchymal hemorrhage in the pons and midbrain, extending to the 4th ventricle, complicated by seizures and hydrocephalus. Once more, she regained consciousness following this second hemorrhage and underwent a surgical resection of her AVM eighteen days after the second ictus. During the operation, she suffered from a hemorrhage in the 4th ventricle and in the pontine surgical cavity. Post-operatively, she developed obstructive hydrocephalus which was treated with extra-ventricular drainage. However, she failed to regain normal consciousness during the weeks that followed. She was recruited to the study 53 days post-operation, when she was in a minimally conscious state (MCS) (CRS-R = 12, Table 1). This patient was excluded from the anesthetic protocol as she was persistently febrile. Two weeks after data collection, she began obeying commands with her right foot and left arm. Upon discharge, 5 months and 23 days after data collection, the patient was behaviourally responsive and communicative (CRS-R = 23).

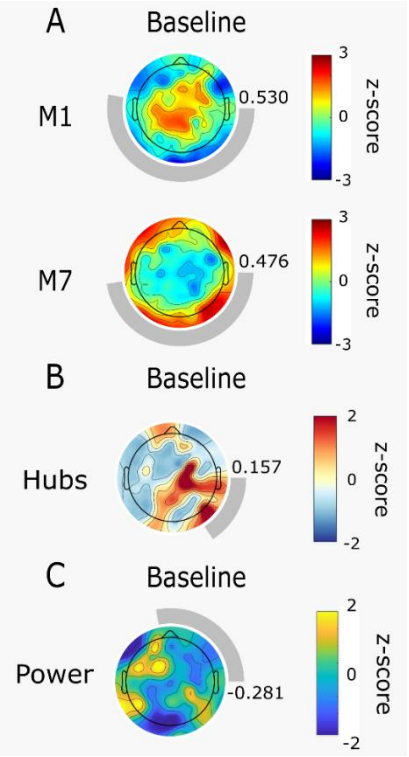

Figure 3. Alpha network motif topographies resemble those of healthy controls in an individual who emerged from minimally conscious state.

Topography of alpha motif frequency, but not of node degree or power, are similar to those of healthy controls at baseline. Topographic maps represent z-scores comparing motif frequency (A), node degree (B) and power (C) of each electrode to the distribution across all electrodes. Rings surrounding the topographic maps represent the median cosine similarity to conscious controls; a more complete ring corresponds to higher similarity, the value of which is also indicated to the right of each topographic map. *M1 = motif 1, M7 = motif 7.*

Topographic network properties

Motif analysis: The participant's alpha motifs had similar topographic patterns to conscious controls (Figure 3A). As they were close to emergence (CRS-R = 12), this was expected and may suggest that their brain network had the capacity to sustain consciousness. Motif 1 was concentrated in central brain regions ($s_1 = 0.530$); motif 7 was spread across peripheral electrodes ($s_7 = 0.476$). Motifs in the theta (Suppl. Figure 3A) and delta bands (Suppl. Figure 4A) were also similar to conscious controls.

Hub analysis: Alpha network hubs were dissimilar to conscious controls (s =0.157) (Figure 3B), as were hubs in the theta (Suppl. Figure 3B) and delta bands (Suppl. Figure 4B).

Power analysis: At baseline, alpha power topography did not resemble the distribution for conscious controls ($s = -0.281$) (Figure 3C). Neither did theta (Suppl. Figure 3C) or delta (Suppl. Figure 4C) power topography.

Global network properties

Graph theoretical network properties: At baseline, in the alpha band, global efficiency was within the range of conscious controls, while clustering coefficient, binary small-worldness and modularity were all elevated relative to conscious controls (Figure 6A, red circles). Graph theoretical properties in the theta (Suppl. Figure 9, red circles) and delta band (Suppl. Figure 10, red circles) were either lower than or within the range of conscious controls.

Relative power analysis: Relative power in the delta band was within the range of conscious controls, while relative theta power was higher and relative alpha power was lower than in conscious controls (Figure 6B, red circles).

Case 2: Motif, hub and power topographic reorganization in unresponsive wakefulness syndrome is similar to healthy controls and predicts recovery of consciousness

Case report

A 50-year-old woman presented with a high-grade subarachnoid hemorrhage (Fisher grade IV, World Federation of Neurosurgeons (WFNS) grade V, with a right frontotemporal

intraparenchymal hematoma) secondary to a ruptured right middle cerebral artery (MCA) aneurysm. She was behaviorally unresponsive upon admission (GCS = 3). The patient underwent a decompressive craniectomy and clot evacuation as well as the insertion of an extraventricular drain on the day of admission. She did not regain consciousness after this first surgery. Two days later, she underwent a second operation for clipping of her right MCA aneurysm. She did not regain normal consciousness during the four weeks that followed. At the time of data collection, 25 days post-injury, the patient was behaviourally unresponsive and in UWS (CRS-R = 3, Table 1). It is important to note that the right bone flap of the patient was resected prior to data collection. As the electrode net lacked tension on this side of the skull, their brain networks' topographic patterns were skewed. Three months and seven days following data collection, the patient recovered behavioural responsiveness, and was able to spontaneously open her eyes, obey commands and produce slow but oriented speech (GCS = 15).

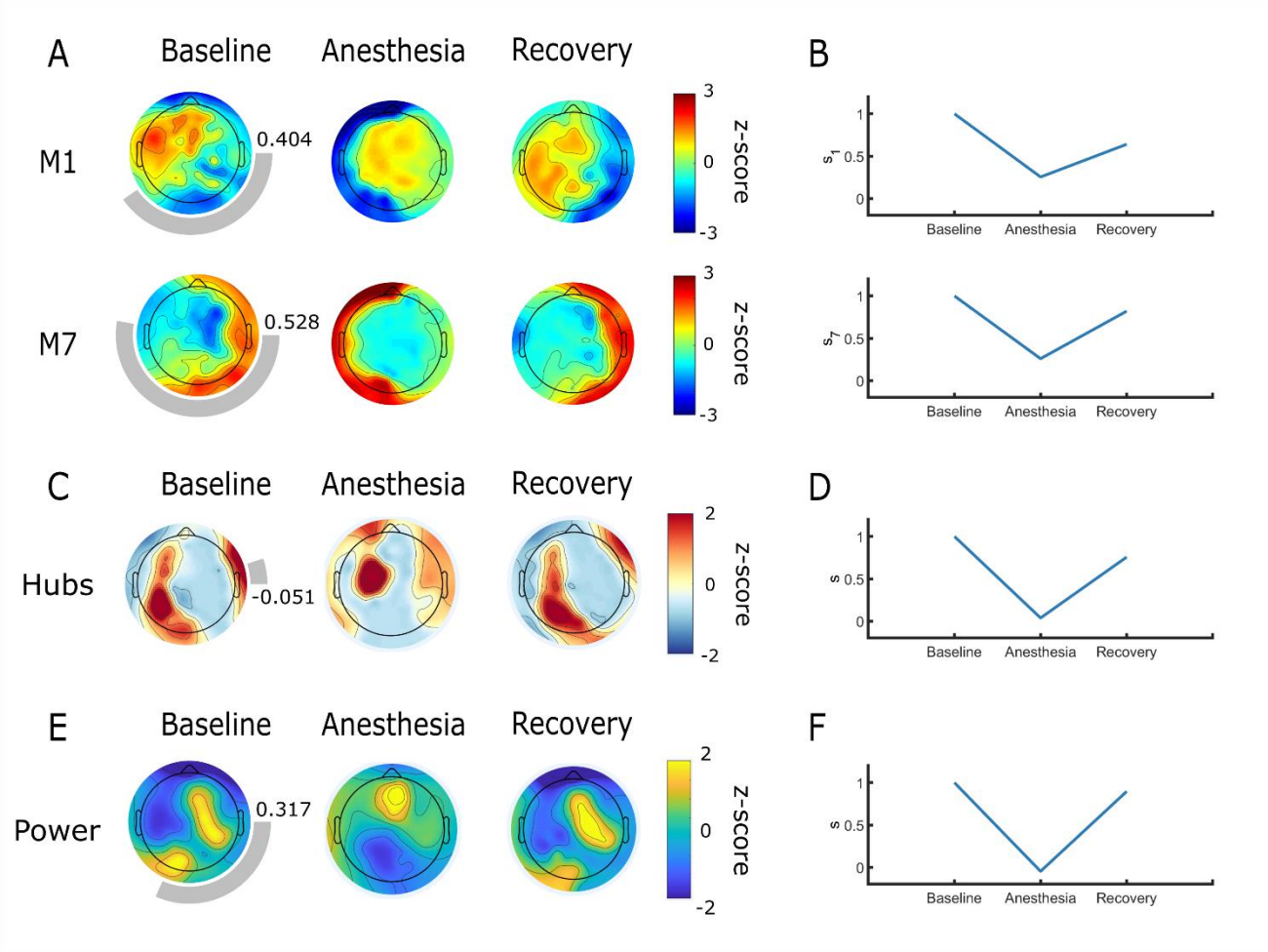

Figure 4. Alpha network motif, hub and power topographic reorganization under anesthesia in a patient who emerged from unresponsive wakefulness syndrome.

Topography of alpha motif frequency, but not of node degree or power, are similar to those of healthy controls at baseline. Motif, node degree and power distributions undergo topographic reorganization under anesthesia, similar to healthy controls. Topographic maps represent z-scores comparing motif frequency (A), node degree (C) and power (E) of each electrode to the distribution across all electrodes. Rings surrounding the topographic maps represent the median cosine similarity to conscious controls; a more complete ring corresponds to higher similarity, the value of which is also indicated to the right of each topographic map. Cosine similarity to the participant's own baseline quantitatively reflects these shifts (B, D and F, respectively). *M1 = motif 1, M7 = motif 7.*

Topographic network properties

Motif analysis: At baseline, this participant's alpha motif topography was similar to conscious controls, although skewed ($s_1 = 0.404$, $s_7 = 0.528$) (Figure 4A). Strikingly, nodes participating in motifs 1 and 7 reorganized during exposure to anesthesia (Figure 4A-B). While the topographic distribution of motifs in the anesthetized state only has a weak similarity to anesthetic-induced unconsciousness in healthy controls (i.e. not posteriorly- or anteriorly-dominant) the patient's brain network adaptively reconfigured in response to propofol and the topographic patterns returned to their baseline state upon cessation of the anesthetic, perhaps suggesting that the patient was either conscious or had the capacity for consciousness at the time of data collection. In the theta band, motif topographies are dissimilar to conscious controls at baseline but undergo similar topographic reorganization during anesthesia (Suppl. Figure 5A). Motifs in the delta band are similar to conscious controls but did not undergo clear reorganization during anesthesia (Suppl. Figure 6A).

Hub analysis: Alpha network hubs were dissimilar to conscious controls at baseline ($s = -0.051$) (Figure 4C) but reorganized under anesthesia in a similar manner as healthy individuals (i.e. posterior-to-anterior shift) (Figure 4C-D). This may once again be suggestive of consciousness or the capacity of the brain network to sustain consciousness. Theta (Suppl. Figure 5B) and delta hubs (Suppl. Figure 6B) also underwent topographic reorganization under anesthesia.

Power analysis: At baseline, alpha power topography did not resemble the distribution for conscious controls ($s = 0.317$) (Figure 4E) but reorganized under anesthesia (posterior-to-anterior) (Figure 4E-F). Neither theta (Suppl. Figure 5C) or delta (Suppl. Figure 6C) power topography shifted under anesthesia.

Global network properties

Graph theoretical network properties: In the alpha band, all global network properties were similar to conscious controls (Figure 6A, orange circles). While these properties changed across baseline, anesthesia and recovery, they did not shift in an expected pattern. This was also the case in the theta (Suppl. Figure 9, orange circles) and the delta bands (Suppl. Figure 10, orange circles).

Relative power analysis: Relative power in the delta band was within the range of conscious controls, while relative theta power was higher and relative alpha power was lower than in conscious controls (Figure 6B, orange circles).

Case 3: Motif, hub and power topographies in persistent unresponsive wakefulness syndrome are dissimilar to healthy controls

Case report

A 24-year-old male suffered from an anoxic brain injury eight years prior to this study, following cardiac arrest caused by *commotio cordis* resulting from a blow to the precordial region, leaving the patient without vital signs for approximately 30 minutes. He did not recover normal consciousness following this injury. At the time of data collection, the patient was diagnosed with UWS (CRS-R = 5, Table 1). At the time of publication, this patient remains in UWS.

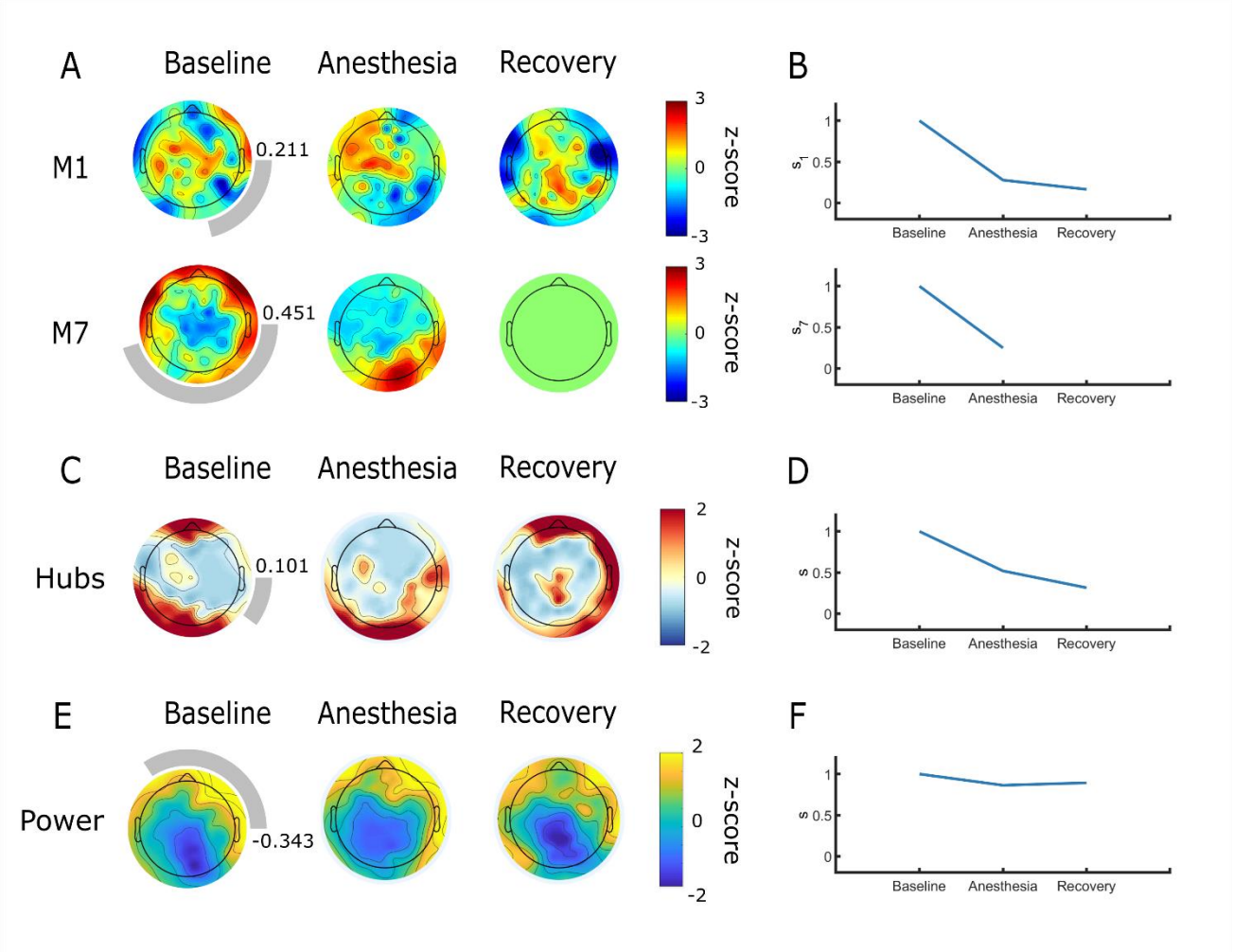

Figure 5. Alpha network motif, hub and power topographies are spatially incoherent in an individual with persistent unresponsive wakefulness syndrome.

Topography of alpha motif frequency, node degree and power are dissimilar to healthy controls at baseline. Under anesthesia, distributions either did not reorganize, or did not follow the pattern expected based on observations in healthy controls. Topographic maps represent z-scores comparing motif frequency (A), node degree (C) and power (E) of each electrode to the distribution across all electrodes. Rings surrounding the topographic maps represent the median cosine similarity to conscious controls; a more complete ring corresponds to higher similarity, the value of which is also indicated to the right of each topographic map. Cosine similarity to the participant's own baseline quantitatively reflects the failure of topographic patterns to reorganize in a clear pattern (B, D and F, respectively). *M1 = motif 1, M7 = motif 7.*

Topographic network properties

Motif analysis: At baseline, motif topographies were dissimilar to conscious controls ($s_1 = 0.211$, $s_7 = 0.451$). Motif 1 was spatially dispersed, while motif 7 exhibited the opposite polarity of topographic distribution that we would expect based on observations in healthy controls (i.e. motif 7 was anteriorly instead of posteriorly dominant) (Figure 5A). This was expected as the participant was in a chronic UWS state and might suggest that the inability of the brain network to sustain consciousness is reflected by its motif characteristics. The topographic organization of motifs 1 or 7 shifted in response to anesthesia but failed to return to baseline state post-anesthesia (Figure 5A-B). Contrary to what we would expect in a healthy individual, high-frequency nodes seemed to become more polarized towards anterior brain regions for motif 1, and posterior brain regions for motif 7. At recovery, node participation in motif 1 regained a disorganized pattern, while motif 7 became insignificant. There were no clear patterns in motif topography or reorganization in the theta (Suppl. Figure 7A) and delta bands (Suppl. Figure 8A); motifs at these frequencies were often non-significant.

Hub analysis: Alpha network hubs did not resemble conscious controls at baseline ($s = 0.101$) (Figure 5C) or return to baseline state post-anesthesia (Figure 5C-D). This may further emphasize that the inability of the brain network to sustain consciousness is associated with topographic network properties. There were no clear patterns in hub topography or reorganization in the theta band (Suppl. Figure 7B), although hubs did undergo anesthetic-induced topographic reorganization in the delta band (Suppl. Figure 8B).

Power analysis: At baseline, alpha power topography did not resemble the distribution for conscious controls ($s = -0.343$) (Figure 4E) and did not reorganize under anesthesia (Figure 4E-F). Neither theta (Suppl. Figure 7C) or delta (Suppl. Figure 8C) power topography shifted under anesthesia.

Global network properties

Graph theoretical network properties: At baseline, in the alpha band, global efficiency was within the range of conscious controls, while clustering coefficient, binary small-worldness and modularity were all elevated relative to conscious controls (Figure 6A, blue diamonds). While these properties changed across baseline, anesthesia and recovery, they did not shift in an expected

pattern. This was also the case in the theta (Suppl. Figure 9, blue diamonds) and the delta bands (Suppl. Figure 10, blue diamonds).

Relative power analysis: Relative power in the theta band was within the range of conscious controls, while relative delta power was higher and relative alpha power was lower than in conscious controls (Figure 6B, blue diamonds). Importantly, this patient, who did not recover consciousness, was the only one with elevated delta power relative to conscious controls.

Figure 6. Comparison of alpha global network properties between conscious controls and individuals with disorders of consciousness.

Graph theoretical network properties were not associated with prognosis (A), but relative power in the delta band (B) was elevated relative to conscious controls in the patient who did not recover consciousness. Boxes represent the interquartile range of the values for conscious controls, with the median indicated by a horizontal line. The whiskers extend to the minimal and maximal values which are not outliers, while outliers, defined as values greater than the median $\pm$ 1.57 times the interquartile range, are represented by crosses. Values for disorders of consciousness patients who recovered behavioural responsiveness are represented by circles, while the values for the patient who remained in unresponsive wakefulness syndrome is represented by a diamond. *CTRL = conscious controls, P = patient.*

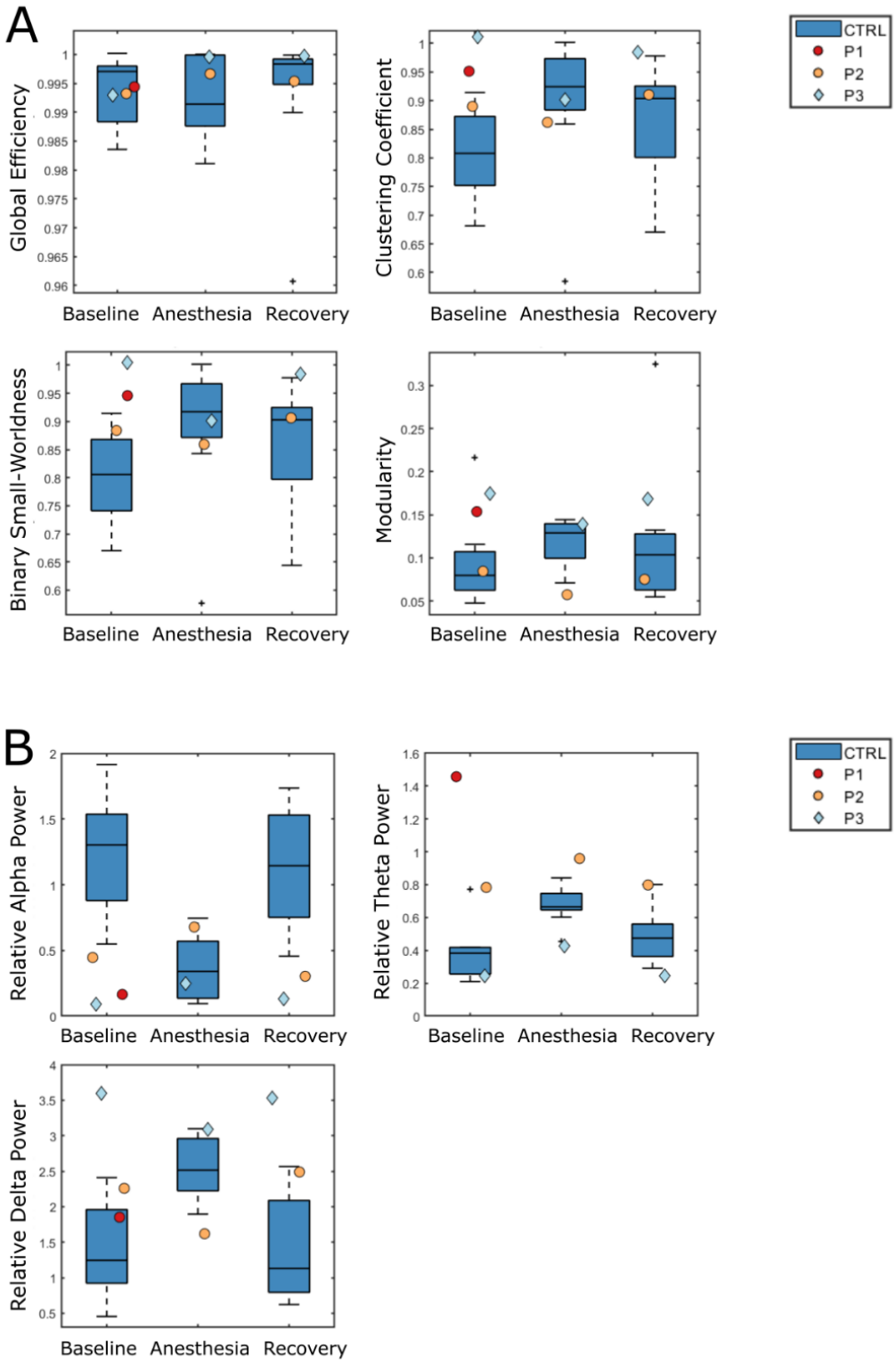
A
Global Efficiency
Clustering Coefficient
Binary Small-Worldness
Modularity
Baseline
Anesthesia
Recovery
CTRL
P1
P2
P3
B
Relative Alpha Power
Relative Theta Power
Relative Delta Power
Baseline
Anesthesia
Recovery
CTRL
P1
P2
P3

Discussion

In this study, we provide preliminary evidence through a series of three DOC cases, that network motifs may be associated with prognosis in this patient population. Further, we compared network motifs to other established topographic and global network properties. In the cases presented here, topographic network properties appear to have more prognostic value than global network properties, bringing to light issues that may arise during whole-brain averaging of brain network properties in brain-injured populations. Our findings suggest that network motifs are a promising addition to the existing repertoire of prognostic EEG measures and demonstrate that the perturbation of resting state brain networks using anesthesia can further inform prognosis.

Brain network motifs show promise as a novel prognostic measure in disorders of consciousness

In the three presented cases, the topographic distribution of three-node functional motifs resembles conscious controls at baseline in patients who later emerged from their DOC. In these cases, nodes participating in motif 1 were concentrated over central brain regions, while those participating in motif 7 were localized over lateral brain regions. Importantly, in a patient who later recovered consciousness, motif topography reconfigured under anesthesia and returned to baseline topography post-anesthesia. This was not the case in the patient in persistent UWS who underwent the same anesthetic protocol.

This is the first study to explore network motifs as prognostic markers in DOC patients. Previously, the emergence and suppression of motifs across states of anesthetic-induced unconsciousness have been observed using EEG (Shin et al., 2013) and fMRI (Kafashan et al., 2016) in healthy individuals. We build upon this emerging field of study through our use of high-density EEG, which provides greater spatial resolution, and by applying this method in a novel clinical context.

While the neural mechanisms underlying motif topography remain unclear, the specific configuration of motifs 1 and 7 informs hypotheses regarding their role in the brain. Motif 1, which consists of two nodes which converge on an apical node, has been associated with balancing between-module integration and segregation (Sporns & Kötter, 2004). In particular, the apical node is thought to integrate information as part of the “rich club”, a core network of highly-connected hubs (Gollo, Zalesky, Hutchison, van den Heuvel, & Breakspear, 2015). Motif 7 forms

a closed loop and has been implicated in fast, within-module integration, particularly in peripheral sensory brain regions (Gollo et al., 2015). Interestingly, nodes participating in motif 7 in both controls and DOC patients are located over peripheral brain regions, and their topography is complimentary to that of motif 1, supporting this theory. In the context of persistent UWS, we observed a disruption of nodes participating in motifs 1 and 7. This may be driven by a breakdown in between- and within-module integration, which has been associated with reduced consciousness (Dehaene & Changeux, 2011; Tononi, 2004). In UWS, reduced thalamocortical integration, mediated by cortical, thalamic or fiber damage, is believed to underly negative behavioural outcomes (Rosanova et al., 2012) and global network integration is thought to shift in favor of local, segregated information processing (Rizkallah et al., 2019).

Our results demonstrate that motif reorganization is not associated with anterior-posterior shifts in alpha power across states of consciousness. The anteriorization of alpha power has traditionally been considered a marker of anesthetic-induced unconsciousness (John et al., 2001; Tinker, Sharbrough, & Michenfelder, 1977). While this phenomenon can be observed in Case 2, the reorganization of network motifs in this participant do not exhibit patterns of change that are associated with the topographic shift in alpha power. Case 3 provides further evidence of the dissociation between alpha power and motifs, as alpha power remains anterior across all three states, while the motif topography reorganizes. Our results also demonstrate that motif reorganization is not associated with shifts in the global network hub location. Previous studies have shown that posterior hub locations are associated with states of consciousness, and anterior hub locations with states of unconsciousness (Blain-Moraes et al., 2016; Lee, Mashour, Noh, Kim, & Lee, 2013). In both Cases 2 and 3, the shift in the topographic distribution of network node degree are not paralleled by the topographic shift in motif 1 or 7. While these results do not provide an explanation of the motif's underlying neural mechanism, they demonstrate the added value of this granular network analysis above and beyond these more traditional markers of levels of consciousness. Motif topography in Cases 1 and 2 was more similar to conscious controls at baseline than alpha and hub topography, further suggesting the added value of motif analysis.

Topographic network properties may be more strongly associated with recovery from disorders of consciousness than global network properties

Global network properties, which are averaged across nodes in the network, were not strongly associated with prognosis. At baseline and across states of anesthesia none of the graph theoretical network properties in any of the frequency bands consistently predicted recovery of behavioural responsiveness. This is in contrast to studies demonstrating that clustering and path length in the alpha band (Stefan et al., 2018), as well as clustering and modularity in the delta band (Chennu et al., 2017) predicted outcomes in large cohorts of DOC patients. In terms of relative power, the patient who did not recover exhibited elevated relative power in the delta band as compared to conscious controls. This is in line with several studies that have associated high delta power with negative outcomes (Bagnato et al., 2017; Golkowski et al., 2017; Sitt et al., 2014; Stefan et al., 2018). On the other hand, topographic network properties were consistently associated with behavioural outcomes. In patients who eventually recovered consciousness, we observed that nodes participating in functional motifs, high-degree nodes and nodes with high alpha power were organized in distinct patterns that reconfigured under anesthesia and returned to their baseline state post-anesthesia. We replicated the finding that alpha network hub and power location shifts under anesthesia, predicting behavioural outcome in patients who will eventually recover consciousness (Blain-Moraes et al., 2016).

Interestingly, unlike global network properties, the information provided by topographic network properties had prognostic value despite the heterogeneity of types of brain injury in our sample. While global network properties provide an overall representation of network functioning, our results suggest that valuable information may be lost during spatial averaging of network properties. Motifs capture region-specific changes in brain functioning, and thus have the potential to be more attuned to granular network changes that affect the capacity for consciousness. This is especially promising in DOC patients, where the heterogeneity of pathological brain networks across individuals calls for analysis techniques that are sensitive to changes in the building blocks of a network.

The capacity of brain networks to reorganize post-perturbation may predict the recovery of consciousness

Topographic network properties provided additional prognostic information when measured in the context of anesthesia. We observed anterior-posterior shifts in network motif participation and hubs that were predictive of a patient's recovery from UWS. In the case of network hubs, perturbing the brain using anesthesia was particularly informative, as, on its own, similarity of hub topographies to controls at baseline was not predictive of patient outcome. Although this lack of prognostic ability at baseline may have been a result of the cortical lesions distorting DOC patients' brain network organization, this observation nevertheless highlights the prognostic value of applying a perturbation to patients' brain networks.

One of the greatest challenges in DOC diagnosis and prognosis is the absence of a gold standard by which to validate novel assessment tools (Athena Demertzi, Sitt, Sarasso, & Pinxten, 2017). In the absence of self-reported levels of consciousness, DOC patients are often compared to healthy controls. As we have demonstrated in this case series, baseline comparison to controls is not always sufficient for detecting patients who will recover consciousness (as was the case for network hubs and power topography in the cases presented here). The perturbation of DOC brain networks using anesthesia allows for the within-subject comparison of patients to their own baseline. In this way, we control for the heterogeneity of etiology and chronicity of brain injury, which influences between-group comparisons.

The concept of perturbing the brain with an external stimulus and measuring its capacity to adapt to that perturbation in the context of DOC is not new. In particular, transcranial magnetic stimulation has been investigated as one such perturbation. The speed and spatial distribution (Rosanova et al., 2012), as well as the complexity of the brain's response to this type of stimulation (Casali et al., 2013; Casarotto et al., 2016) have shown promise as diagnostic and prognostic markers, achieving prognostic accuracy of up to 81%. Further, right before recovery of consciousness in healthy controls undergoing anesthetic-induced unconsciousness, brain networks meet the conditions required for rapid reconfiguration and synchronization (M. Kim et al., 2016). In a similar vein, higher levels of consciousness have been associated with a higher probability of transitioning between patterns of connectivity measured using fMRI, whereas the brain networks of UWS patients showing no signs of covert consciousness tend to remain in a static pattern (A.

Demertzi et al., 2019). These findings are strongly supported by our study, as evidenced by the brain network of a patient who remained in UWS, which did not respond in an ordered way to anesthetic perturbation at the level of network hubs and alpha motifs. Here, we add to the growing body of evidence suggesting that the brain's ability to reorganize following a perturbation and to transition between states are precursors to emergence from disordered states of consciousness.

Topographic network analysis strikes a balance between the predictive power of neuroimaging and the need for clinical translatability

We found that clinical measures do not always predict recovery of behavioural responsiveness. It has been established that DOC patients who are older at the time of injury, who experience an anoxic brain injury, who are further from the date of injury, and who are diagnosed as UWS or have low CRS-R scores are less likely to recover consciousness (Chennu et al., 2017; Song et al., 2018). Consistent with these findings, in the cases presented here, the individual in UWS who did not recover was the only case of anoxic brain injury and the most chronic DOC patient at over 8 years post-injury. Clinically, this patient was therefore the most unlikely to recover consciousness and it is worth nothing that topographic network properties reaffirmed this. Our study provides further evidence that measures usually obtained in the clinic are important but insufficient to establish a definite prognosis and could be supplemented with neuroimaging assessments.

While, as previously discussed, PET and fMRI imaging achieve high prognostic accuracy, these techniques are not always amenable to clinical implementation. Both neuroimaging methods pose a financial barrier, are unsafe or distorted in the presence of metallic implants, and are highly susceptible to movement artifacts, which may result from the involuntary movements of DOC patients. Studies on DOC prognosis based on motor imagery in fMRI have labelled up to 17% of data as unusable due to excessive motion artifacts (Cruse et al., 2011; Monti, Vanhaudenhuyse, et al., 2010). Patients are often sedated using propofol to reduce movement during MRI but, as we and others have shown, anesthesia is known to impact functional connectivity (Athena Demertzi et al., 2017; Kirsch et al., 2017). With this study, we demonstrate once more that EEG – through its cost efficiency, portability and limited contraindications – is an attractive middle-ground between strictly clinical assessment and PET or fMRI imaging.

Limitations and future directions

In this study, we presented a series of three exploratory DOC cases to demonstrate the feasibility and prognostic potential of motif analysis in this population, as well as the potential advantages of topographic versus global network analysis and within-subject comparisons. Our findings are preliminary and will need to be validated in a larger cohort of patients with diverse behavioural and demographic profiles, types of brain injury and chronicity of injury. For instance, the third patient presented was the most clinically unlikely to recover due to the chronicity and mechanism of their brain injury. Our results confirm the poor prognosis, demonstrating the validity of motif analysis in this case, but do not add any additional information beyond the what can be discerned from the clinical profile. In addition, results were influenced by a missing bone flap in one patient; similarly, differences in brain lesions in our patient population may have skewed topographic maps. Future studies might employ source-localized EEG to evaluate functional connectivity between specific brain regions, mapped onto the individual brain anatomy of patients, in order to infer the neural mechanisms underlying the observed topographic reorganization and to account for heterogeneity of brain lesions. Furthermore, connectivity measures other than dPLI, such as symbolic transfer entropy (Staniek & Lehnertz, 2008), could be used to measure bi-directional motifs, which were excluded from our analyses. Finally, limitations in our experimental design must be considered. DOC patients were subjected to a brief anesthetic protocol (45 min) using propofol, while healthy controls underwent propofol induction, followed by 3 hours of isoflurane maintenance. Nevertheless, despite differences in the duration and type of anesthesia, patterns of topographic reorganization in motifs, hubs and power are similar between groups.

Conclusion

In a series of three exploratory DOC cases, we found that topographic, but not global, brain network properties measured using high-density EEG were associated with prognosis. We showed that functional network motifs, network hubs and alpha power topography – and their topographical reorganization during anesthesia – may be associated with DOC patient outcomes. We propose that topographic network properties measured at the nodal level might be used to complement clinical and whole-brain global measures for the prognostication of DOC patients. In addition, our findings demonstrate that the brain's capacity to adapt to a perturbation like anesthesia may be predictive of recovery from DOC.

Conflict of Interest

The authors declare that the research was conducted in the absence of any commercial or financial relationships that could be construed as a potential conflict of interest.

Author Contributions

SBM and GP designed the study. CD, AR, CA and DN collected the data. GP, MB and JL administered the anesthetic protocol and monitored participants. YM and DN analyzed the data. CD, YM, DN and SBM interpreted the data and wrote the manuscript. All authors edited the manuscript and approved the final version.

Funding

This study was funded by the Canadian Institutes of Health Research (FRN 152562, CD; Fredrick Banting and Charles Best Canada Graduate Scholarship – Masters, DN); the Fonds de Recherche du Québec – Nature et technologies (YM); the Fonds de Recherche du Québec – Santé (DN); and the Natural Science and Engineering Research Council of Canada (Discovery Grant RGPIN-2016-03817; SBM).

Acknowledgments

We would like to thank participants and their caregivers for their involvement in this study.

Data Availability Statement: The data that support the findings of this study are available from the corresponding author upon reasonable request.

References

Bagnato, S., Boccagni, C., Prestandrea, C., Fingelkurts, A. A., Fingelkurts, A. A., & Galardi, G. (2017). Changes in Standard Electroencephalograms Parallel Consciousness Improvements in Patients With Unresponsive Wakefulness Syndrome. *Archives of Physical Medicine and Rehabilitation, 98*(4), 665-672. 2

Bai, Y., Xia, X., Wang, Y., He, J., & Li, X. (2019). Electroencephalography quadratic phase self-coupling correlates with consciousness states and restoration in patients with disorders of consciousness. *Clinical Neurophysiology, 130*(8), 1235-1242.

Blain-Moraes, S., Boshra, R., Ma, H. K., Mah, R., Ruiter, K., Avidan, M., . . . Mashour, G. A. (2016). Normal Brain Response to Propofol in Advance of Recovery from Unresponsive Wakefulness Syndrome. *Frontiers in Human Neuroscience, 10*(248).

Casali, A. G., Gosseries, O., Rosanova, M., Boly, M., Sarasso, S., Casali, K. R., . . . Tononi, G. (2013). A theoretically based index of consciousness independent of sensory processing and behavior. *Science translational medicine, 5*(198), 198ra105-198ra105.

Casarotto, S., Comanducci, A., Rosanova, M., Sarasso, S., Fecchio, M., Napolitani, M., . . . Massimini, M. (2016). Stratification of unresponsive patients by an independently validated index of brain complexity. *Annals of Neurology, 80*(5), 718-729.

Chennu, S., Annen, J., Wannez, S., Thibaut, A., Chatelle, C., Cassol, H., . . . Laureys, S. (2017). Brain networks predict metabolism, diagnosis and prognosis at the bedside in disorders of consciousness. *Brain, 140*(8), 2120-2132.

Cruse, D., Chennu, S., Chatelle, C., Bekinschtein, T. A., Fernández-Espejo, D., Pickard, J. D., . . . Owen, A. M. (2011). Bedside detection of awareness in the vegetative state: a cohort study. *The Lancet, 378*(9809), 2088-2094.

Dehaene, S., & Changeux, J. P. (2011). Experimental and theoretical approaches to conscious processing. *Neuron, 70*(2), 200-227.

Delorme, A., & Makeig, S. (2004). EEGLAB: an open source toolbox for analysis of single-trial EEG dynamics including independent component analysis. *Journal of Neuroscience methods, 134*(1), 9-21.

Demertzi, A., Sitt, J. D., Sarasso, S., & Pinxten, W. (2017). Measuring states of pathological (un)consciousness: research dimensions, clinical applications, and ethics. *Neuroscience of Consciousness, 2017*(1).

Demertzi, A., Tagliazucchi, E., Dehaene, S., Deco, G., Barttfeld, P., Raimondo, F., . . . Sitt, J. D. (2019). Human consciousness is supported by dynamic complex patterns of brain signal coordination. *Science Advances, 5*(2), eaat7603.

Duclos, C., Mahdid, Y., Nadin, D., Tarnal, V., Picton, P., Vanini, G., . . . Blain-Moraes, S. (2020). Brain network motifs are markers of loss and recovery of consciousness. *bioRxiv*.

Faugeras, F., Rohaut, B., Weiss, N., Bekinschtein, T., Galanaud, D., Puybasset, L., . . . Dehaene, S. (2011). Probing consciousness with event-related potentials in the vegetative state.

Neurology, 77(3), 264-268. Retrieved from https://www.ncbi.nlm.nih.gov/pmc/articles/PMC3136052/pdf/znl264.pdf

Faugeras, F., Rohaut, B., Weiss, N., Bekinschtein, T., Galanaud, D., Puybasset, L., . . . Dehaene, S. (2012). Event related potentials elicited by violations of auditory regularities in patients with impaired consciousness. *Neuropsychologia, 50*(3), 403-418. Retrieved from https://hal.archives-ouvertes.fr/hal-00719338/document

Giacino, J. T., Ashwal, S., Childs, N., Cranford, R., Jennett, B., Katz, D. I., . . . Zafonte, R. (2002). The minimally conscious state: definition and diagnostic criteria. *Neurology, 58*(3), 349-353. Retrieved from https://n.neurology.org/content/neurology/58/3/349.full.pdf

Golkowski, D., Merz, K., Mlynarcik, C., Kiel, T., Schorr, B., Lopez-Rolon, A., . . . Ilg, R. (2017). Simultaneous EEG–PET–fMRI measurements in disorders of consciousness: an exploratory study on diagnosis and prognosis. *Journal of Neurology, 264*(9), 1986-1995. Retrieved from https://link.springer.com/article/10.1007%2Fs00415-017-8591-z

Gollo, L. L., Zalesky, A., Hutchison, R. M., van den Heuvel, M., & Breakspear, M. (2015). Dwelling quietly in the rich club: brain network determinants of slow cortical fluctuations. *Philos Trans R Soc Lond B Biol Sci, 370*(1668). doi:10.1098/rstb.2014.0165

John, E., Prichep, L., Kox, W., Valdes-Sosa, P., Bosch-Bayard, J., Aubert, E., . . . Gugino, L. (2001). Invariant reversible QEEG effects of anesthetics. *Consciousness and Cognition, 10*(2), 165-183.

Kafashan, M., Ching, S., & Palanca, B. J. (2016). Sevoflurane Alters Spatiotemporal Functional Connectivity Motifs That Link Resting-State Networks during Wakefulness. *Frontiers in Neural Circuits, 10*, 107.

Kim, H., Hudetz, A. G., Lee, J., Mashour, G. A., Lee, U., & Re, C. S. G. (2018). Estimating the Integrated Information Measure Phi from High-Density Electroencephalography during States of Consciousness in Humans. *Frontiers in Human Neuroscience, 12*, 42-42. doi:10.3389/fnhum.2018.00042

Kim, M., Mashour, G. A., Moraes, S.-B., Vanini, G., Tarnal, V., Janke, E., . . . Lee, U. (2016). Functional and Topological Conditions for Explosive Synchronization Develop in Human Brain Networks with the Onset of Anesthetic-Induced Unconsciousness. *Frontiers in Computational Neuroscience, 10*(1). doi:10.3389/fncom.2016.00001

Kirsch, M., Guldenmund, P., Ali Bahri, M., Demertzi, A., Baquero, K., Heine, L., . . . Laureys, S. (2017). Sedation of Patients With Disorders of Consciousness During Neuroimaging: Effects on Resting State Functional Brain Connectivity. *Anesthesia and Analgesia, 124*(2),

Kondziella, D., Friberg, C. K., Frokjaer, V. G., Fabricius, M., & Møller, K. (2016). Preserved consciousness in vegetative and minimal conscious states: systematic review and meta-analysis. *Journal of Neurology, Neurosurgery & Psychiatry, 87*(5), 485-492.

Latora, V., & Marchiori, M. (2001). Efficient Behavior of Small-World Networks. *Physical Review Letters, 87*(19), 198701.

Lee, H., Mashour, G. A., Noh, G.-J., Kim, S., & Lee, U. (2013). Reconfiguration of Network Hub Structure after Propofol-induced Unconsciousness. *Anesthesiology: The Journal of the American Society of Anesthesiologists, 119*(6), 1347-1359.

Maier, K. L., McKinstry-Wu, A. R., Palanca, B. J. A., Tarnal, V., Blain-Moraes, S., Basner, M., . . . Kelz, M. B. (2017). Protocol for the reconstructing consciousness and cognition (ReCCognition) study. *Frontiers in Human Neuroscience, 11*, 284.

Marsh, B., White, M., Morton, N., & Kenny, G. (1991). Pharmacokinetic model driven infusion of propofol in children. *BJA: British Journal of Anaesthesia, 67*(1), 41-48.

Maslov, S., & Sneppen, K. (2002). Specificity and stability in topology of protein networks. *Science, 296*(5569), 910-913.

Milo, R., Shen-Orr, S., Itzkovitz, S., Kashtan, N., Chklovskii, D., & Alon, U. (2002). Network motifs: simple building blocks of complex networks. *Science, 298*(5594), 824-827.

Mitra, P. (2007). *Observed brain dynamics*: Oxford University Press.

Mitra, P., Bokil, H., Maniar, H., Loader, C., Mehta, S., Hill, D., . . . Kaur, S. Chronux. Retrieved from http://chronux.org/

Monti, M. M., Laureys, S., & Owen, A. M. (2010). The vegetative state. *BMJ, 341*, c3765.

Monti, M. M., Vanhaudenhuyse, A., Coleman, M. R., Boly, M., Pickard, J. D., Tshibanda, L., . . . Laureys, S. (2010). Willful modulation of brain activity in disorders of consciousness. *New England Journal of Medicine, 362*(7), 579-589.

Newman, M. E. J. (2006). Modularity and community structure in networks. *Proceedings of the National Academy of Sciences, 103*(23), 8577-8582.

Owen, A. M., Coleman, M. R., Boly, M., Davis, M. H., Laureys, S., & Pickard, J. D. (2006). Detecting awareness in the vegetative state. *Science, 313*(5792), 1402-1402.

Peterson, A., Cruse, D., Naci, L., Weijer, C., & Owen, A. M. (2015). Risk, diagnostic error, and the clinical science of consciousness. *NeuroImage: Clinical, 7*, 588-597.

Rizkallah, J., Annen, J., Modolo, J., Gosseries, O., Benquet, P., Mortaheb, S., . . . Thibaut, A. (2019). Decreased integration of EEG source-space networks in disorders of consciousness. *NeuroImage: Clinical*, 101841.

Rosanova, M., Gosseries, O., Casarotto, S., Boly, M., Casali, A. G., Bruno, M.-A., . . . Laureys, S. (2012). Recovery of cortical effective connectivity and recovery of consciousness in vegetative patients. *Brain, 135*(4), 1308-1320.

Rubinov, M., & Sporns, O. (2010). Complex network measures of brain connectivity: Uses and interpretations. *NeuroImage, 52*(3), 1059-1069.

Schnakers, C., Vanhaudenhuyse, A., Giacino, J., Ventura, M., Boly, M., Majerus, S., . . . Laureys, S. (2009). Diagnostic accuracy of the vegetative and minimally conscious state: clinical consensus versus standardized neurobehavioral assessment. *BMC Neurology, 9*(1), 35.

Shin, J., Mashour, G. A., Ku, S., Kim, S., & Lee, U. (2013). Subgraph "Backbone" Analysis of Dynamic Brain Networks during Consciousness and Anesthesia. *PloS one, 8*(8), e70899.

Sitt, J. D., King, J.-R., El Karoui, I., Rohaut, B., Faugeras, F., Gramfort, A., . . . Naccache, L. (2014). Large scale screening of neural signatures of consciousness in patients in a vegetative or minimally conscious state. *Brain, 137*(8), 2258-2270.

Song, M., Yang, Y., He, J., Yang, Z., Yu, S., Xie, Q., . . . Jiang, T. (2018). Prognostication of chronic disorders of consciousness using brain functional networks and clinical characteristics. *eLife, 7*.

Sporns, O., & Kötter, R. (2004). Motifs in Brain Networks. *PLOS Biology, 2*(11), e369.

Stam, C. J., & van Straaten, E. C. W. (2012). Go with the flow: Use of a directed phase lag index (dPLI) to characterize patterns of phase relations in a large-scale model of brain dynamics. *NeuroImage, 62*(3), 1415-1428.

Staniek, M., & Lehnertz, K. (2008). Symbolic transfer entropy. *Physical Review Letters, 100*(15), 158101.

Stefan, S., Schorr, B., Lopez-Rolon, A., Kolassa, I.-T., Shock, J. P., Rosenfelder, M., . . . Bender, A. (2018). Consciousness Indexing and Outcome Prediction with Resting-State EEG in Severe Disorders of Consciousness. *Brain Topography, 31*(5), 848-862.

Stender, J., Mortensen, K. N., Thibaut, A., Darkner, S., Laureys, S., Gjedde, A., & Kupers, R. (2016). The Minimal Energetic Requirement of Sustained Awareness after Brain Injury. *Current Biology, 26*(11), 1494-1499.

Steppacher, I., Eickhoff, S., Jordanov, T., Kaps, M., Witzke, W., & Kissler, J. (2013). N400 predicts recovery from disorders of consciousness. *Annals of Neurology, 73*(5), 594-602.

Tinker, J. H., Sharbrough, F. W., & Michenfelder, J. D. (1977). Anterior shift of the dominant EEG rhytham during anesthesia in the Java monkey: correlation with anesthetic potency. *Anesthesiology, 46*(4), 252-259.

Tononi, G. (2004). An information integration theory of consciousness. *BMC Neuroscience, 5*, 42-42.

Vinck, M., Oostenveld, R., van Wingerden, M., Battaglia, F., & Pennartz, C. M. A. (2011). An improved index of phase-synchronization for electrophysiological data in the presence of volume-conduction, noise and sample-size bias. *NeuroImage, 55*(4), 1548-1565.

Watts, D. J., & Strogatz, S. H. (1998). Collective dynamics of 'small-world'networks. *Nature, 393*(6684), 440.

Wijnen, V., Van Boxtel, G., Eilander, H., & De Gelder, B. (2007). Mismatch negativity predicts recovery from the vegetative state. *Clinical Neurophysiology, 118*(3), 597-605.

Chapter 4: Targeted High-Density Transcranial Direct Current Stimulation to the Left Dorsolateral Prefrontal Cortex Does Not Have Brain Network Effects

Danielle Nadin[1,2], Marie-Hélène Boudrias[3], Stefanie Blain-Moraes[1,3*]

1. Montreal General Hospital, McGill University Health Center Research Institute, Montreal, QC, Canada
2. Integrated Program in Neuroscience, Faculty of Medicine, McGill University, Montreal, QC, Canada
3. School of Physical and Occupational Therapy, Faculty of Medicine, McGill University, Montreal, QC, Canada

*Correspondence:
Stefanie Blain-Moraes, Ph.D.
1650 Cedar Ave, L11-132
Montréal, Québec
H3G 1A4
Canada
Tel: 514-398-1325
stefanie.blain-moraes@mcgill.ca

In order to inform the use of transcranial direct current stimulation as a potential treatment for disorders of consciousness, we explored the effects of transcranial direct current stimulation applied to the left dorsolateral prefrontal cortex on brain networks and behavior in a cohort of healthy young adults. This manuscript is currently in preparation.

Abstract

The neurophysiological mechanism, as well as the non-linear relationship between stimulation intensity and effects on brain networks and behavior, are still poorly understood in the field of transcranial direct current stimulation (tDCS). In this study, fifteen young, healthy adults underwent a targeted, high-density stimulation protocol, during which they received 20 minutes of sham, 1 and 2 mA tDCS to the left dorsolateral prefrontal cortex (L-DLPFC) over the course of 3 sessions. We compared resting-state brain networks constructed from 129-channel electroencephalograms (EEG) in the scalp and source space, before and 30 minutes post-stimulation. Specifically, we measured relative power, global graph theoretical network properties (global efficiency, clustering coefficient, modularity, binary small-worldness) and topographic graph theoretical properties (3-node functional motifs, nodal degree). We found no statistically significant changes in these metrics, although we did observe qualitatively different topographic patterns in the effects of tDCS on 3-node functional motifs and high-degree nodes. There was also no effect of tDCS on working memory performance as measured by a 2-back fractal working-memory task. Our findings highlight the need for more work which combines optimized tDCS targeting algorithms and graph theoretical network measures to assess the network-level effects of tDCS, in order to inform our understanding of heterogeneity in tDCS response.

Keywords: non-invasive brain stimulation, transcranial direct current stimulation, electroencephalography, resting state, brain networks, working memory

Introduction

Transcranial direct-current stimulation (tDCS) is a non-invasive brain stimulation technique which modulates cortical excitability through electrodes placed on the surface of the scalp. In its anodal configuration, cortical excitability is increased through a long-term potentiation-like mechanism (Stagg & Nitsche, 2011). This technique modulates motor learning and performance on cognitive tasks. In particular, anodal tDCS applied over the left dorsolateral prefrontal cortex (L-DLPFC) has been shown to increase working memory performance, as measured by reduced reaction time and increased accuracy on memory tasks (Boggio et al., 2006; Fregni et al., 2005; Teo, Hoy, Daskalakis, & Fitzgerald, 2011).

Response to tDCS depends on stimulation intensity (Boggio et al., 2006; Jamil et al., 2017; Tremblay et al., 2016), and it is unclear whether increasing the intensity of anodal stimulation leads to a linear increase in cortical excitability and task performance. While it was formerly believed that anodal tDCS always results in increased cortical excitability and that cathodal tDCS (when the cathode is placed of the target region) always results in decreased cortical excitability (Stagg & Nitsche, 2011), recent evidence suggests that this is not always the case. When applied at 2 mA for 20 min, cathodal tDCS has been shown to increase, rather than decrease, cortical excitability (Batsikadze et al., 2013; Mosayebi Samani et al., 2019). Further, dose-dependent effects of tDCS are non-linear, with low intensity anodal stimulation ($\leq$ 1 mA) showing equal or greater effects on cortical excitability as compared to high intensity stimulation ($>$ 1 mA) in the primary motor cortex (Agboada et al., 2019; Jamil et al., 2017). This may account for the large inter-individual variability observed in tDCS studies, which employ a varied and often inconsistent range of stimulation parameters (Bikson et al., 2018).

Traditionally, tDCS has been delivered through large sponge electrodes (typically 25 to 35 cm^2), with one electrode placed over the targeted area and the other placed over the supraorbital area. Target areas have long been determined using the 10-20 system, which estimates the location of brain areas based on landmarks like the bridge of the noise and the periauricular points (Jasper, 1958). More recently, high-density electrode montages using small circular electrodes have been shown to increase stimulation focality and intensity by $\geq$ 80% as compared to traditional montages (Dmochowski et al., 2011). Targeting algorithms have also been employed to take into consideration subjects' brain anatomy and head shape in order to determine the optimal electrode placement to stimulate a region of interest (Dmochowski et al., 2011; Fernández-Corazza et al., 2016, 2020). Further, only two studies have investigated the impact of L-DLPFC tDCS on connectivity in the source space, where greater insight on the specific brain regions affected by stimulation can be gained as compared to scalp-level analyses (Hermann et al., 2020; Hill et al., 2019).

Thus, network analysis, particularly in the source space, as well as targeted, high-density stimulation are underused tools that may prove useful in measuring and optimizing the effects of tDCS on the brain. In this study, we will use high-density electroencephalography (HD-EEG) and source localization techniques to determine the effects of stimulation intensity on brain networks

measured using EEG. The use of EEG allows for the direct measurement of neurophysiological response to tDCS. For instance, this strategy has revealed changes in the EEG power spectral density, mean frequency and event-related potentials during L-DLPFC stimulation and performance of the n-back working memory task (Boonstra, Nikolin, Meisener, Martin, & Loo, 2016; Hill, Rogasch, Fitzgerald, & Hoy, 2019; Keeser et al., 2011). An important advantage of our approach is the use of a novel HD-EEG cap which allows for targeted tDCS delivered through small, high-density EEG electrodes.

The primary objective of this study is to compare the effects of 20 min of 1 or 2 mA anodal tDCS applied to the L-DLPFC on brain networks as measured using EEG. The secondary objective is to determine whether changes in the EEG translate to behavioral changes, as measured by the n-back working memory task.

We hypothesize that 1 mA anodal tDCS applied through a custom electrode configuration in a HD-EEG cap will not have significantly different effects on the EEG spectral content and network properties as compared to 2 mA anodal tDCS. Our secondary hypothesis is that the neurophysiological effects of tDCS at both stimulation intensities will translate to behavior, i.e. that stimulation of the L-DLPFC will increase accuracy and reduce reaction time on the n-back task.

Findings from this study will help answer a long-standing question in the field of neuromodulation concerning the choice of the best stimulation intensity. Optimized tDCS protocols have applications for treating numerous clinical populations, such as those with disorders of consciousness (Cavaliere et al., 2016) and Parkinson's disease (Boggio et al., 2006).

Materials and methods

Participants and experimental design

A sample of 15 right-handed young adults (8 females, median age = 27 $\pm$ 6 years old, median Edinburgh right-handedness score = 90.0 $\pm$ 8.86%) were recruited to the study. Participants were excluded if they were not right-handed (Edinburgh score $\leq$ 50%) (Oldfield, 1971), had any contraindications to tDCS (e.g. pregnancy, metallic implants, pacemaker), were taking any medications which may affect cortical excitability (e.g. tricyclic antidepressants, other psychiatric

medications) or had any history of neurological disorder or severe brain injury (i.e. traumatic or anoxic brain injury). One participant had a mild traumatic brain injury (concussion) 6 years prior to enrollment in the study. The study was approved by the McGill University Health Center Research Ethics Board (#2019-5542).

Participants attended three 90-minute sessions. They received a different type of stimulation (sham, 1 mA or 2 mA) during each session, according to a predetermined, randomized, counterbalanced sequence (Latin Square). Consecutive visits were separated by 7 days to allow wash-out between tDCS sessions, and they were held at the same time of day each week. Participants were blinded to the type of stimulation they received, while the experimenter was not blinded. Five participants were withdrawn from the study after the first session due to COVID-19-related restrictions on human subject research, resulting in a total of 12 participants who received sham, 11 who received 1 mA, and 12 who received 2 mA stimulation.

An outline of the experimental protocol is shown in Figure 1. During each session, resting state, baseline 128-channel EEG was recorded. Participants then completed a computerized, fractal 2-back task. Next, they received either sham stimulation, 1 mA or 2 mA anodal tDCS over the L-DLPFC for a duration of 20 min. Participants were at rest during stimulation in order to mimic the unresponsive states experienced by patients with disorders of consciousness. Resting state EEG recording, followed by another administration of the 2-back task, was repeated immediately and 30 minutes post-stimulation.

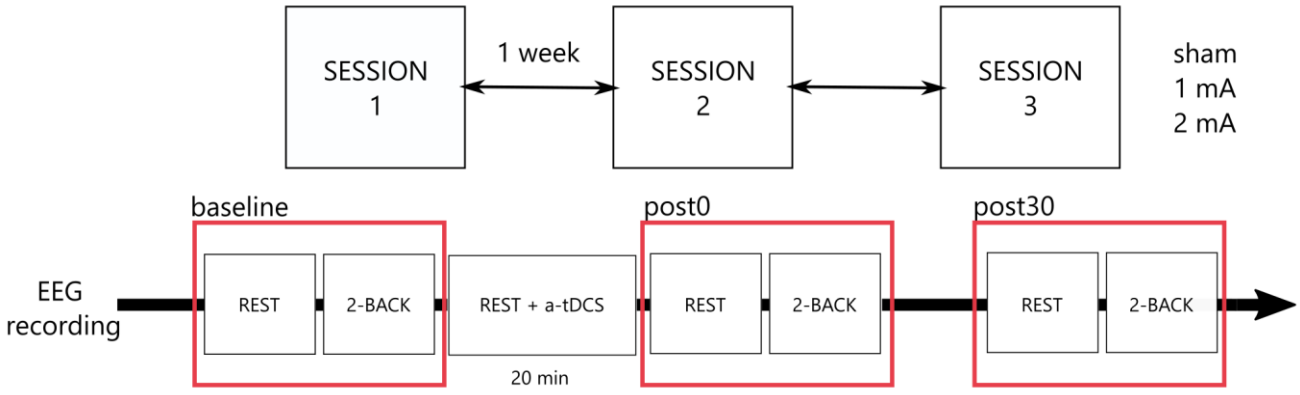

Figure 1. Schematic representation of the research protocol.

Participants took part in three sessions where they received one of sham stimulation, 1 mA or 2 mA anodal transcranial direct current stimulation (tDCS) to the left dorsolateral prefrontal cortex. These sessions were separated by a 1-week washout period. During each session, participants underwent a continuous EEG recording during resting state and while completing a 2-back fractal n-back task at baseline, immediately post-stimulation (post0) and 30 minutes post-stimulation (post30), as well as during a 20-minute session of anodal tDCS.

EEG data collection and pre-processing

High-density, 128-channel EEG (Magstim-EGI, Eugene, OR) was collected at a 1 kHz sampling frequency during resting state. Each resting-state epoch lasted 6 minutes. During 1 to 3 minutes, participants' eyes were closed. During the remaining 3 to 5 minutes, participants fixated a cross on a computer screen, with their eyes open. Electrode impedances were checked prior to each recording and were maintained below 50 kΩ. During each session, prior to removing the EEG cap, electrode and fiducial (nasion, inion, pre-auricular points) locations were registered using the Geodesic Photogrammetry System (Magstim-EGI, Eugene, OR).

Raw EEG data were filtered (0.1-50 Hz bandpass, 60 Hz notch). Non-scalp channels were removed, leaving 97 scalp channels for further analysis. Noisy channels were also removed, and independent components analysis was used to identify and remove eye movement artifacts. Data were then re-referenced to an average reference. Finally, noisy epochs (e.g. muscle, head and jaw movement artifacts) were removed manually upon visual inspection by a trained experimenter (DN). All pre-processing was performed using the open-source MATLAB toolbox, EEGLAB (Delorme & Makeig, 2004).

Transcranial Direct Current Stimulation

Stimulation was applied while EEG was simultaneously recorded through the same sensor net. Current was sent by a current regulator (GTEN 200, Magstim-EGI, Eugene, OR) to an amplifier, connected to the EEG electrode net. The 128-channel net covered the individual's entire scalp, but the stimulation was delivered through 20 of the 128 electrodes. During the stimulation period, participants were asked to keep their eyes open and minimize movement and were given the option to read a book. A lidocaine ointment was applied beneath the stimulating electrodes to reduce sensitivity to the stimulation. At the end of each stimulation period, participants reported any

experienced side-effects, and the intensity of these side-effects (linear numeric scale, 0 to 10, where 10 is the most intense). At the end of each session, they were asked to guess what type of stimulation they thought they had received, and to rate the confidence of their guess (linear numeric scale, 0 to 10, where 10 is the most confident).

Prior to the experiment, Finite Difference Method (FDM) modelling was used to determine the optimal stimulating electrode configuration for the focal brain stimulation of the L-DLPFC. Using the software Reciprocity (Magstim-EGI, Eugene, OR), a pre-loaded MRI for a canonical 40-year-old male head model (Colin27 template) (Holmes et al., 1998) was used to generate the forward and inverse models of source-localized activity using FDM and standardized low-resolution electromagnetic tomography (sLORETA) modelling. Eight dipoles perpendicular to the cortical surface, along the middle frontal gyrus and superior to the pars triangularis, were selected to target the L-DLPFC (Figure 2). Parameters were set such that the model was required to find 10 anodal electrodes and 10 cathodal electrodes that would provide the optimal stimulation for this brain area, using the Reciprocity algorithm, which optimizes for electric field intensity (Fernández-Corazza et al., 2016). These 20 electrodes (Figure 2) were used to provide tDCS for all participants. Stimulation was ramped up from 0 mA to the target intensity over 2 minutes, maintained at the target intensity for 20 minutes (for tDCS sessions only), and then ramped down to 0 mA over 30 seconds. In order to maintain blinding, during sham sessions, participants received tDCS during the ramp-up and ramp-down portions of the protocol only. During these sessions, after the ramp-up (2 minutes), the stimulation was ramped down (30 seconds) and maintained at 0 mA for 20 minutes, before being ramped-up (2 minutes) and ramped-down again (30 seconds).

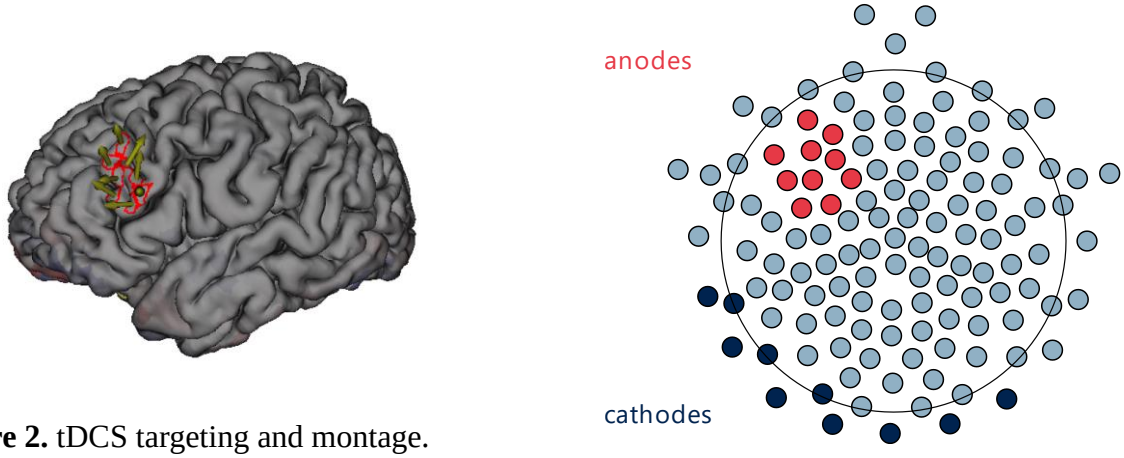

Figure 2. tDCS targeting and montage.

On the left, targeted dipoles in the left dorsolateral prefrontal cortex of the Colin27 head model are shown by yellow arrows and red outlines. On the right, the optimal stimulation montage determined by the Reciprocity algorithm is shown, with anodes in red and cathodes in dark blue.

EEG scalp analysis

Data from each session were segmented into 6 analysis epochs: (1) baseline (eyes closed); (2) baseline (eyes open); (3) immediately post-stimulation (eyes closed); (4) immediately post-stimulation (eyes open); (5) 30 min post-stimulation (eyes closed); (6) 30 min post-stimulation (eyes open). At the start of each EEG epoch, participants were asked to report their level of alertness on a linear numeric scale (0 to 10), where 10 was the highest level of alertness.

Relative power, peak alpha power topography, hub topography, network motifs and global graph theoretical network properties (global efficiency, clustering coefficient, binary small-worldness, modularity) were computed in the scalp space. First, spectral power in the delta (1-4 Hz), theta (4-8 Hz), alpha (8-13 Hz), beta (13-30 Hz) frequency bands was computed over 10-second windows using a multi-taper power spectral density estimate (number of tapers = 3, time-bandwidth product = 2, spectrum window size = 3 seconds) from the Chronux package (Mitra, 2007; Mitra et al., n.d.). Power was averaged across time windows and all electrodes. Relative spectral power was equal to the ratio between the average delta, theta, alpha or beta power and the average broadband (1-30 Hz) power. Next, the topography of the peak power in the alpha band was plotted. Then, functional connectivity in the alpha band was computed across 10-second windows using the directed and the weighted Phase Lag Index (dPLI and wPLI, respectively) (C. J. Stam & van Straaten, 2012; Vinck et al., 2011). Connectivity matrices were corrected for spurious connectivity by comparison to 20 surrogate networks, where signals were phase-shuffled to abolish phase relationships but maintain spectral properties. Non-significant connections ($p \geq 0.05$) were set to 0 (wPLI) or 0.5 (dPLI). Global graph theoretical network properties were computed on the thresholded and binarized wPLI network as described in (Nadin et al., 2020). When thresholding the network, the largest threshold between the baseline and 30 minutes post-stimulation connectivity matrices was selected in order to maintain a fully connected graph during both epochs. Finally, the topography of high-degree nodes was computed as a proxy for network hubs on the thresholded wPLI network, and 3-node functional motifs on the thresholded dPLI network, as described in (Nadin et al., 2020).

EEG source analysis

A 3-layer boundary element model of each subject's head was constructed using the Colin27 MRI template (Holmes et al., 1998), warped to the subject's head shape based on 129 head points obtained through the Geodesic scan recorded during data collection.

Source localization was performed according to (Aydin et al., 2020). For each analysis epoch (6) and stimulation condition (3), data were filtered in the alpha band (8-13 Hz) and a Hilbert transform was performed to select the 2-second segment with the lowest alpha power. This segment served as a baseline during source localization, which was performed using the wavelet Maximum Entropy on the Mean (wMEM) method, a non-linear approach which compresses data into the time-frequency space. This method is particularly effective for analyzing resting state data with a low signal-to-noise ratio (Lina et al., 2014). Resolution was set to 8 000 dipoles placed perpendicularly along the cortical surface.

Source estimates were clustered into brain regions according to the Desikan-Killiany atlas (Desikan et al., 2006). Orthogonalization was performed to correct for signal leakage (Brookes et al., 2012). Seed-based Amplitude Envelope Correlation (AEC) connectivity (Hipp et al., 2012) between dipoles in the left rostral middle-frontal region (encompassing the stimulated brain region) and all other cortical dipoles was computed. Dipoles in the ipsilateral region (right rostral middle-frontal) were not included in this connectivity map due to the nature of this method (see (Aydin et al., 2020)).

Fractal n-back task

The L-DLPFC is one of the brain regions activated by many variants of the n-back working memory task (Owen et al., 2005), and anodal tDCS applied to this region improves n-back performance (Brunoni & Vanderhasselt, 2014). In particular, the fractal n-back task has been validated and demonstrated to activate the DLPFC similarly to the more commonly used variant of the task where participants are presented with letters (Ragland et al., 2002). We therefore employed this task to measure behavioral outcomes of tDCS stimulation.

Fractal images drawn from a set of 98 images were presented for 750 msec (Maier et al., 2017). Participants left-clicked a mouse when the stimuli presented matched the one presented 2 stimuli previously (2-back condition). This was repeated for 1 block of 83 stimuli, with 21 target stimuli.

Assessment was only performed for 1 block, as the intention was to capture a metric of performance, rather than to measure learning of the task. Each letter presentation was separated by 1 ms during which the screen was blank. Performance was assessed using reaction time in milliseconds and discriminability. Reaction time was defined as the time interval between stimulus presentation and correct responses. Discriminability (d') is a measure of accuracy which assesses participants' ability to distinguish between target and non-target trials, defined in (Ragland et al., 2002) as:

$$d' = \frac{n_{TPs} + 0.5}{n_{targets} + 1} - \frac{n_{FPs} + 0.5}{n_{distractors} + 1}$$

where the first term is the hit rate, the second term is the false-alarm rate, n_{TPs} is the number of true positives, n_{FPs} is the number of false positives, $n_{targets}$ is the number of target trials (21) and $n_{distractors}$ is the number of non-target trials (62).

Statistical analyses

All statistical analyses were two-tailed and were performed in Jamovi (version 1.2.27). Normality was assessed using the Shapiro-Wilk test (significance threshold p = 0.05) and outliers were flagged when they were more than 1.5 times the interquartile range above or below the median.

Transcranial Direct Current Stimulation

Reported side-effects were grouped into four categories: hot, itching, tingling and other, and participants were assigned a Boolean value depending on whether they had reported the side-effect. Participants were also assigned a Boolean value corresponding to whether they had correctly guessed the type of stimulation they had received during a given session. The frequency of occurrence of side-effects and correct guesses were compared across stimulation conditions using a Chi-square test. When counts are less than 5, the Chi-square test is not valid. In these cases, responses for 1 mA and 2 mA were grouped into an "active stimulation" category. If counts were still below 5, Fisher's exact test, which is applicable to 2x2 contingency tables only, was used instead. Ratings of side-effect intensity and participants' confidence in perceived stimulation type were compared across stimulation conditions using a non-parametric Friedman test. Effects were deemed significant when $p < 0.05$.

EEG scalp analysis

Ratings of alertness were compared across epochs within each stimulation condition using a non-parametric Friedman test.

EEG epochs immediately post-stimulation were heavily contaminated by tDCS artifacts. The characterization and cleaning of such artifacts is a topic of ongoing debate within the neuromodulation field (Gebodh et al., 2019). We therefore excluded these epochs and compared EEG at baseline and 30 minutes post-stimulation. We believe that any effects of tDCS on the EEG will persist over 30 minutes post-stimulation, as stimulation to the primary motor cortex has been shown to effect cortical excitability 30 (Agboada et al., 2020; Jamil et al., 2017), 90 (Batsikadze et al., 2013) and 120 minutes post-stimulation (Agboada et al., 2019).

When necessary, relative power was log-transformed to obtain a normal distribution. A mixed linear model was then used to compare relative power across epochs (baseline versus 30-min post) and stimulation conditions. Epoch and stimulation condition were fixed factors, while subject was used as a random factor to account for multiple comparisons. When significant main or interaction effects were observed, Bonferroni post-hoc paired t-tests were performed.

Modularity was compared across epochs and stimulation conditions using the same mixed model approach. Global efficiency, clustering coefficient and binary small-worldness violated the normality assumption. The difference between 30-min post and baseline measures was therefore computed and compared across stimulation conditions using a non-parametric Friedman's test, for each of the above-mentioned global network properties.

Cosine similarity was used to compare the topographic distribution of peak alpha power, motifs and hubs at baseline to the distribution at 30 minutes post-stimulation, for each participant and each session. Cosine similarity values were compared across epochs and stimulation conditions using a linear mixed model. Finally, for visualization purposes, average changes in peak alpha power, motif and hub topographies were computed by subtracting the baseline topography from the 30 minutes post-stimulation topography, and averaging this difference across all participants, within each stimulation condition.

The significance threshold for all EEG scalp analyses was set to $p = 0.05$.

EEG source analysis

For each participation and stimulation condition, AEC-based connectivity to the left rostral middle-frontal area was compared between the baseline and 30 minutes post-stimulation epochs using a paired t-test, with a Bonferroni correction for the number of dipoles compared. The significance threshold was set to $p = 0.01$.

Fractal n-back task

Reaction time and discriminability were compared across stimulation conditions and epochs using a linear mixed model, with stimulation condition and epoch as fixed factors, subject as a random factor, and the significance threshold set to $p = 0.05$. When significant main or interaction effects were found, post-hoc Bonferroni-corrected paired t-tests were performed.

Results

Transcranial Direct Current Stimulation: side-effects and participant blinding

Participants primarily reported sensations of heat, itching and tingling. Three participants reported side-effects which were classified as "other," including a buzzing sensation, a cold sensation under the cathodal electrodes, headache, nausea and feelings of disorientation. There were no statistically significant differences in the number of participants who reported these side-effects, or in their ratings of side-effect intensity between stimulation conditions (Table 1).

When asked to guess which type of stimulation they had received, the number of participants who guessed correctly, and their confidence in their guess, did not differ across stimulation conditions (Table 1).

Table 1. Description of participant self-reports of stimulation side-effects and perceived stimulation type

Measure	**Sham**	**1 mA**	**2 mA**
Heat (yes/no [% yes])	6/6 [50]	4/7 [36]	6/6 [50]

Itching (yes/no [% yes]))	6/6 [50]	3/8 [27]	6/6 [50]
Tingling (yes/no [% yes]))	5/7 [42]	4/7 [36]	8/4 [67]
Other (yes/no [% yes]))	3/9 [25]	1/10 [9]	2/10 [17]
Intensity (median [min, max])	5.5 [0,8]	3.0 [0,9]	5.5 [1,10]
Correctly guessed stimulation type (yes/no [% yes])	3/9 [25]	6/5 [55]	8/4 [67]
Confidence (median [min, max])	6.5 [0,10]	6.0 [0,10]	5.5 [0,10]

EEG Scalp Analysis

Self-Reported Alertness

There was no significant effect of epoch or stimulation condition on participants' self-reported alertness, suggesting that changes in fatigue levels over the course of the experiment were not a driving factor influencing changes in the EEG.

Relative Power

During the eyes open condition, there was a significant decrease in delta power between baseline and 30 minutes post-stimulation ($F(1,49.5) = 4.431$, $p = 0.040$), but there was no effect of stimulation condition. There were no significant changes during the eyes-closed condition.

Global Graph Theoretical Network Properties

During the eyes-open condition, there were no significant changes in global efficiency, clustering coefficient, modularity or binary small-worldness across epochs and stimulation conditions. During the eyes-closed condition, there was a significantly larger baseline-30-min post stimulation change in global efficiency during the 1 mA condition as compared to the 2 mA condition ($t = 3.18$,

p = 0.005). This finding should be interpreted with caution, as this change was not significantly different from the sham condition.

Topographic Network Properties

During both the eyes-open and eyes-closed condition, there were no statistically significant effect of epoch or stimulation condition on the topographic distributions for any of the metrics investigated, as determined using cosine similarity.

Average changes in topographic maps were then visualized for the eyes-open condition. The topography for the sham condition was subtracted from the 1 mA and 2 mA topographies to facilitate interpretation.

After 1 mA stimulation, peak alpha power decreased in frontal and occipital electrodes, and increased in central electrodes (Figure 3A). After 2 mA stimulation, peak alpha power also decreased in frontal regions, with a widespread increase in power over the rest of the scale (Figure 3B).

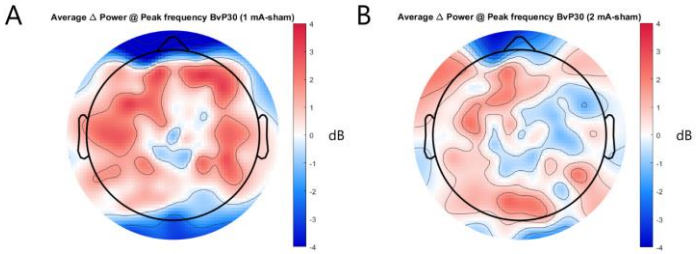

Figure 3. Average change in peak alpha power.

Topographic head maps depicting the average change in peak alpha (8-13 Hz) power from baseline to 30 minutes post-stimulation. The topography for the sham condition was subtracted from the 1 mA (panel A) and the 2 mA condition (panel B). Positive values (in red) indicate an increase in power, while negative values (in blue) represent a decrease in power.

After 1 mA stimulation, the frequency at which nodes participated in motif 1, which consists of two source nodes connected to a single sink node (see (Duclos, Mahdid, et al., 2021)), increased

around the stimulated L-DLPFC (Figure 4A). After 2 mA stimulation, there was a similar increase in the frequency of node participation in the motif around left frontocentral electrodes (Figure 4B). As for motif 5, which consists of three nodes connected in a loop (see (Duclos, Mahdid, et al., 2021)), after 1 mA stimulation, the frequency of node participation in the motif decreased over the stimulated L-DLPFC and increased over the right hemisphere (Figure 4C). Strikingly, there was an increase in node participation in motif 5 across the scalp following 2 mA stimulation (Figure 4D).

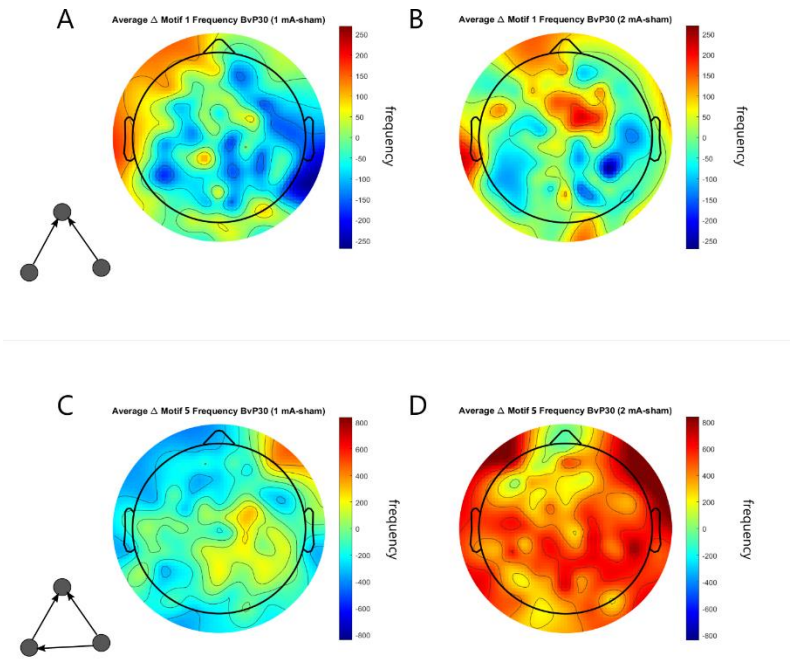

Figure 4. Average change in node participation in functional motifs.

Topographic head maps depicting the average change in the frequency of node participation in 3-node functional motifs from baseline to 30 minutes post-stimulation. The topography for the sham condition was subtracted from the 1 mA (panels A and C) and the 2 mA condition (panel B and D). Positive values (in red) indicate an increase in power, while negative values (in blue) represent a decrease in power. Participation in motif 1 is shown in panels A and B, with the motif depicted in panel A. Participation in motif 5 is shown in panels C and D, with the motif depicted in panel C.

After 1 mA stimulation, node degree increased primarily in the right frontal hemisphere (Figure 5A), whereas after 2 mA stimulation there was a diffuse increase in node degree in left temporal and central electrodes, with a decrease in right frontocentral electrodes (Figure 5B).

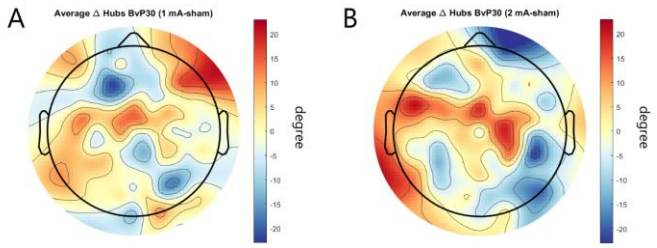

Figure 5. Average change in node degree.

Topographic head maps depicting the average change in high-degree nodes (hubs) from baseline to 30 minutes post-stimulation. The topography for the sham condition was subtracted from the 1 mA (panel A) and the 2 mA condition (panel B). Positive values (in red) indicate an increase in power, while negative values (in blue) represent a decrease in power.

EEG Source Analysis

Connectivity to the rostral middle frontal cortex (which encompasses the stimulated L-DLPFC) was plotted for each participant and stimulation condition. Inter-subject variability across conditions was extremely high, with no clear trends in the effects of epoch or stimulation condition (Figure 6).

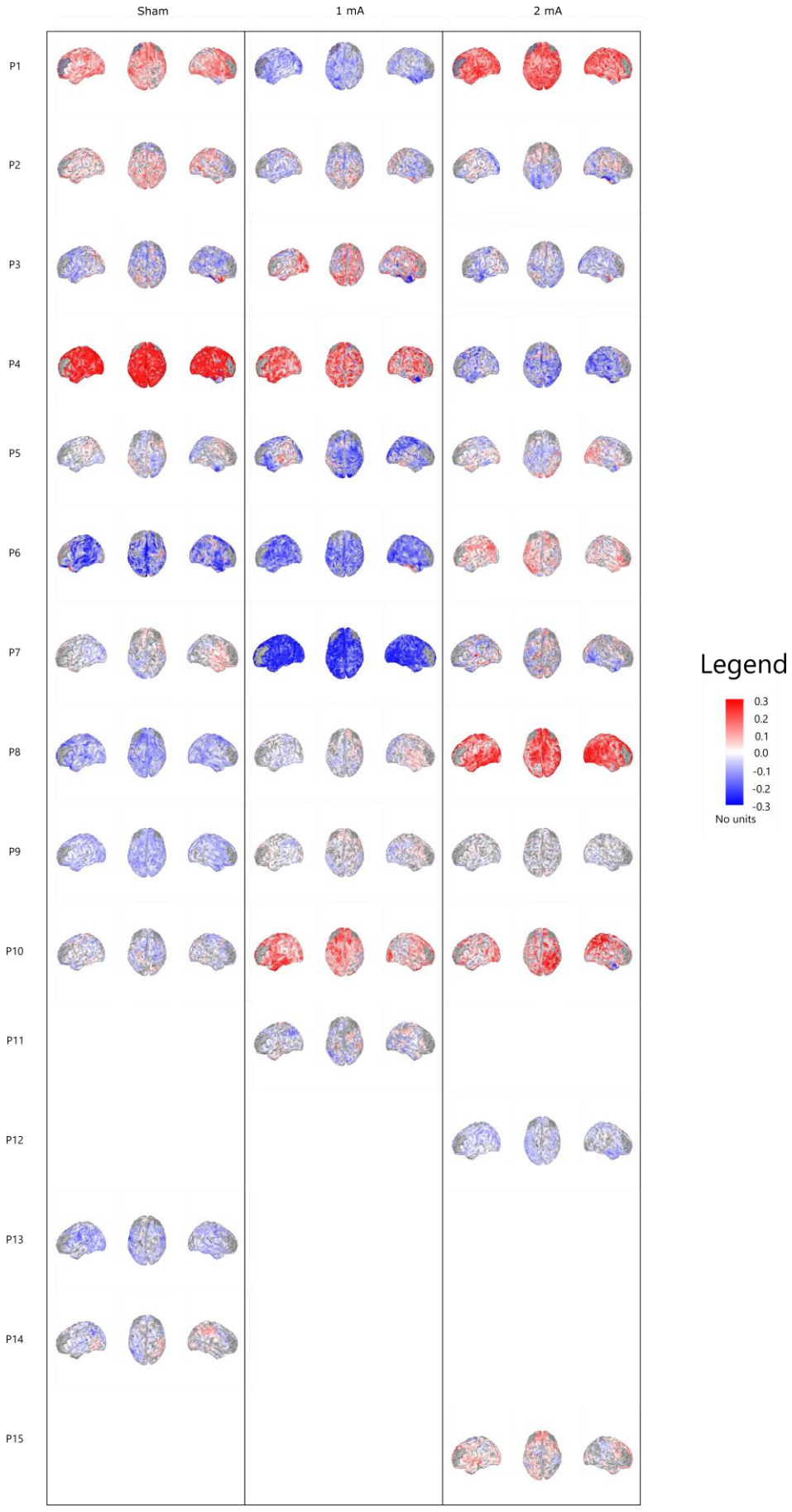
Sham
1 mA
2 mA
P1
P2
P3
P4
P5
P6
P7
P8
P9
P10
P11
P12
P13
P14
P15
Legend
0.3
0.2
0.1
0.0
-0.1
-0.2
-0.3
No units

Figure 6. Source space connectivity.

Topographic head maps depicting statistically significant changes in source space connectivity to the left rostral middle-frontal region (Desikan-Killiany atlas) from baseline to 30 minutes post-stimulation. Each row represents an individual participant, and columns represent the sham, 1 mA and 2 mA stimulation conditions (from left to right, respectively). Positive values (in red) indicate an increase in connectivity, while negative values (in blue) represent a decrease in connectivity. Grey areas represent statistically non-significant changes.

Fractal N-Back Task

There was no effect of epoch or stimulation condition on reaction time (Figure 7A). There was a significant effect of epoch on discriminability ($F(2,82.9)=4.588$, $p=0.013$) with participants' ability to discriminate between target and non-target trials increasing between baseline and 30 minutes post-stimulation ($t(82.1)=-3.02$, $p=0.010$) (Figure 7B). Stimulation condition had no effect on discriminability, suggesting that the observed improvement was a result of participants learning the task.

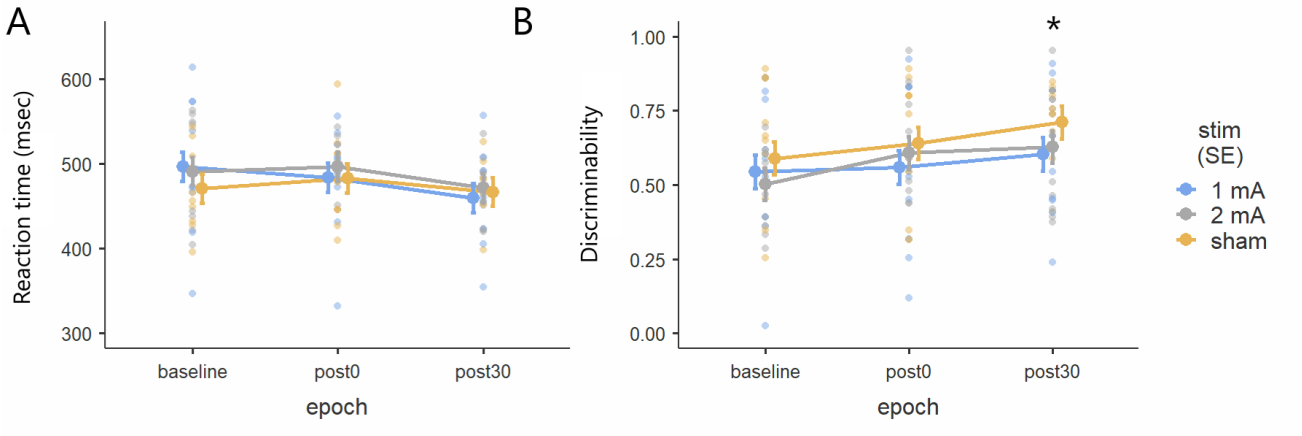

Figure 7. Effects of anodal tDCS on fractal 2-back working memory task.

Change in reaction time (panel A) and discriminability (panel B) across experimental epochs (post0 – immediately post-stimulation, post30 – 30 minutes post-stimulation) and stimulation conditions. Lines represent average values, error bars represent standard error, and dots represent individual participant values. Stimulation conditions are distinguished by colors (sham – orange, 1 mA – blue, 2 mA – grey). *: $p<0.05$.

Discussion

In this study, we applied targeted anodal tDCS to the L-DLPFC through small, circular, high-density electrodes in a group of 15 healthy young adults. We measured the impact of stimulation on scalp and source EEG networks to determine whether or not 1 and 2 mA stimulation have different effects on the brain network. Participants also completed a fractal 2-back working memory task to determine whether any network effects translated to behavior. There was not sufficient evidence to support either of our hypotheses. At the scalp level, while 1 and 2 mA stimulation qualitatively appeared to have different topographic effects on the brain network, none of these effects were significantly different between stimulation conditions. Indeed, neither 1 or 2 mA stimulation had significantly different effects on the brain network as compared to sham stimulation. At the source level, there was a high level of interindividual variability, with no clear trends in changes in connectivity to the stimulated L-DLPFC. While participants did improve their task performance over the course of the experiment, there was no effect of stimulation on 2-back reaction time or discriminability.

We observed that relative delta power decreased over the course of each session, but that tDCS had no effect on this metric. There were no statistically significant changes in relative power in the theta, alpha or beta bands. Decreases in left frontal delta power have been observed in one study using similar stimulation parameters as ours, which also reported increases in beta power (Keeser et al., 2011). Other studies have reported decreases in alpha and theta power (Zaehle et al., 2011), as well as overall decreases in low frequency (< 15 Hz) power (Boonstra et al., 2016) after a single session of offline L-DLPFC stimulation. These findings point towards the potential importance of low frequency EEG power in tDCS response, warranting further exploration in larger cohorts of participants.

We found no statistically significant effects of stimulation on global network properties, including global efficiency, clustering coefficient, modularity and binary small-worldness. Topographic network properties, including 3-node functional motifs and high-degree hubs, were not statistically different across stimulation conditions, but we did observe qualitative differences between 1 and 2 mA stimulation, when controlling for the sham condition. Very few studies have investigated the effects of tDCS on graph theoretical network properties. One study in a cohort of patients with disorders of consciousness found that patients who responded behaviorally to anodal tDCS applied

to the L-DLPFC had increased network centrality, which, like our measure of high-degree nodes, is related to the location of network hubs (Thibaut et al., 2018). In a cohort of individuals with alcohol use disorders, 5 repeated sessions of anodal tDCS to the L-DLPFC was associated with increased global efficiency and decreased clustering coefficient in resting state functional MRI networks (Holla et al., 2020). On the other hand, brief periods of low intensity anodal stimulation to the L-DLPFC have been shown to have no effect on node degree, betweenness centrality or local efficiency in EEG networks (Mancini et al., 2016). Taken together with these findings, our results highlight the need for further exploration of graph theoretical network properties following tDCS, as little work has been done in this area, and results thus far are highly heterogeneous.

We did not observe any significant changes in source space connectivity to the stimulated L-DPLFC, which is in line with one other study which found no effect of online and offline tDCS on resting state EEG source networks (Hill et al., 2019). Our negative finding should be interpreted with the caveat that source networks were constructed based on a template MRI. Current density at the L-DPLFC has been associated with response to tDCS stimulation to the same area (J.-H. Kim et al., 2014), both in healthy individuals and patient populations (Hermann et al., 2020), highlighting that interindividual differences are dependent on individual brain anatomy. There is therefore a need for future work investigated the effects of tDCS on source networks constructed from individual MRIs.

During the fractal 2-back task, we found that discriminability increased over time, but that neither reaction time nor discriminability were significantly different between stimulation conditions. As we observed no statistically significant changes in EEG networks, we did not expect any behavioral changes. The impact of tDCS on the n-back working memory task is highly variable, with reports of decreased reaction times (Brunoni & Vanderhasselt, 2014; Dedoncker et al., 2016; Teo et al., 2011), increased accuracy or discriminability (Fregni et al., 2005; Martin et al., 2014), a combination of effects on both outcome measures (Keeser et al., 2011; Zaehle et al., 2011), and null effects (Hill et al., 2018, 2019; Nikolin et al., 2018).

Importantly, we also found that there no differences in participants self-reported side-effects, side-effect intensity, ability to guess which type of stimulation they had received, or confidence of this

guess between stimulation groups. This suggests that participant blinding was sufficient, with the sham condition resulting in comparable sensations to active stimulation.

Our findings should be interpreted considering several limitations. First, stimulation was delivered offline, while participants were at rest, rather than online, while they were engaged in a task. It has been established that online stimulation of the L-DLPFC results in better acquisition of the n-back task (Martin et al., 2014), although others have observed increases in cortical excitability following both online and offline stimulation (Hill et al., 2019). Greater effects of tDCS may have been observed if stimulation was delivered online. Second, we applied only a single session of stimulation, while multiple sessions are known to have greater impacts on brain networks and behavior in clinical populations (Thibaut et al., 2017). Third, we were unable to analyse EEG networks in the epoch immediately post-stimulation due to artifacts. The characterization and cleaning of tDCS artifacts is an ongoing area of study (Gebodh et al., 2019), and future work should strive to investigate changes in brain networks at a finer time scale. Fourth, tDCS was targeted using a template MRI, as described above. We also used the reciprocity algorithm for targeting. This algorithm optimizes stimulation intensity, but there are algorithms which prioritize intensity and focality of stimulation to different degrees (Fernández-Corazza et al., 2020). Future work should explore a broad range of targeting algorithms, using individual subject MRIs to provide the most optimal stimulation montages possible.

Conclusion

In summary, we observed qualitatively but not statistically different effects of 1 and 2 mA targeted, high-density anodal tDCS to the L-DLPFC on scalp and source EEG networks. These effects were not significantly different from sham stimulation and did not translate to behavior on a fractal 2-back working memory tasks. Our findings highlight the need for the further exploration of graph theoretical network measures following tDCS stimulation, as well as the need for optimized tDCS protocols which use individual participant MRIs and a variety of targeting algorithms.

References

Agboada, D., Mosayebi Samani, M., Jamil, A., Kuo, M.-F., & Nitsche, M. A. (2019). Expanding the parameter space of anodal transcranial direct current stimulation of the primary motor cortex. Scientific Reports, 9(1), 18185.

Agboada, D., Mosayebi-Samani, M., Kuo, M.-F., & Nitsche, M. A. (2020). Induction of long-term potentiation-like plasticity in the primary motor cortex with repeated anodal transcranial direct current stimulation – Better effects with intensified protocols? Brain Stimulation, 13(4), 987–997.

Aydin, Ü., Pellegrino, G., Bin Ka'b Ali, O., Abdallah, C., Dubeau, F., Lina, J. M., Kobayashi, E., & Grova, C. (2020). Magnetoencephalography resting state connectivity patterns as indicatives of surgical outcome in epilepsy patients. Journal of Neural Engineering, 17(3), 035007–035007.

Batsikadze, G., Moliadze, V., Paulus, W., Kuo, M.-F., & Nitsche, M. A. (2013). Partially non-linear stimulation intensity-dependent effects of direct current stimulation on motor cortex excitability in humans. The Journal of Physiology, 591(7), 1987–2000.

Bikson, M., Brunoni, A. R., Charvet, L. E., Clark, V. P., Cohen, L. G., Deng, Z. D., Dmochowski, J., Edwards, D. J., Frohlich, F., Kappenman, E. S., Lim, K. O., Loo, C., Mantovani, A., McMullen, D. P., Parra, L. C., Pearson, M., Richardson, J. D., Rumsey, J. M., Sehatpour, P., … Lisanby, S. H. (2018). Rigor and reproducibility in research with transcranial electrical stimulation: An NIMH-sponsored workshop. Brain Stimulation, 11(3), 465–480.

Boonstra, T. W., Nikolin, S., Meisener, A. C., Martin, D. M., & Loo, C. K. (2016). Change in Mean Frequency of Resting-State Electroencephalography after Transcranial Direct Current Stimulation. Frontiers in Human Neuroscience, 10, 270.

Brookes, M. J., Woolrich, M. W., & Barnes, G. R. (2012). Measuring functional connectivity in MEG: a multivariate approach insensitive to linear source leakage. NeuroImage, 63(2), 910–920.

Brunoni, A. R., & Vanderhasselt, M.-A. (2014). Working memory improvement with non-invasive brain stimulation of the dorsolateral prefrontal cortex: A systematic review and meta-analysis. Brain and Cognition, 86, 1–9.

Dedoncker, J., Brunoni, A. R., Baeken, C., & Vanderhasselt, M.-A. (2016). A Systematic Review and Meta-Analysis of the Effects of Transcranial Direct Current Stimulation (tDCS) Over the Dorsolateral Prefrontal Cortex in Healthy and Neuropsychiatric Samples: Influence of Stimulation Parameters. Brain Stimulation, 9(4), 501–517.

Delorme, A., & Makeig, S. (2004). EEGLAB: an open source toolbox for analysis of single-trial EEG dynamics including independent component analysis. Journal of Neuroscience Methods, 134(1), 9–21.

Desikan, R. S., Ségonne, F., Fischl, B., Quinn, B. T., Dickerson, B. C., Blacker, D., Buckner, R. L., Dale, A. M., Maguire, R. P., Hyman, B. T., Albert, M. S., & Killiany, R. J. (2006). An automated labeling system for subdividing the human cerebral cortex on MRI scans into gyral based regions of interest. NeuroImage, 31(3), 968–980.

Dmochowski, J. P., Datta, A., Bikson, M., Su, Y., & Parra, L. C. (2011). Optimized multi-electrode stimulation increases focality and intensity at target. Journal of Neural Engineering, 8(4), 046011.

Duclos, C., Mahdid, Y., Nadin, D., Tarnal, V., Picton, P., Vanini, G., Golmirzaie, G., Janke, E., Avidan, M., Kelz, M. B., Mashour, G. A., & Blain-Moraes, S. (2021). Brain network motifs are markers of loss and recovery of consciousness. Scientific Reports, 11: 3892.

Fernández-Corazza, M., Turovets, S., Luu, P., Anderson, E., & Tucker, D. (2016). Transcranial electrical neuromodulation based on the reciprocity principle. Frontiers in Psychiatry, 7, 87.

Fernández-Corazza, M., Turovets, S., & Muravchik, C. H. (2020). Unification of optimal targeting methods in transcranial electrical stimulation. NeuroImage, 209, 116403.

Fregni, F., Boggio, P. S., Nitsche, M., Bermpohl, F., Antal, A., Feredoes, E., Marcolin, M. A., Rigonatti, S. P., Silva, M. T. A., Paulus, W., & Pascual-Leone, A. (2005). Anodal transcranial direct current stimulation of prefrontal cortex enhances working memory. Experimental Brain Research, 166(1), 23–30.

Gebodh, N., Esmaeilpour, Z., Adair, D., Chelette, K., Dmochowski, J., Woods, A. J., Kappenman, E. S., Parra, L. C., & Bikson, M. (2019). Inherent physiological artifacts in EEG during tDCS. NeuroImage, 185, 408–424.

Hermann, B., Raimondo, F., Hirsch, L., Huang, Y., Denis-Valente, M., Pérez, P., Engemann, D., Faugeras, F., Weiss, N., & Demeret, S. (2020). Combined behavioral and electrophysiological evidence for a direct cortical effect of prefrontal tDCS on disorders of consciousness. Scientific Reports, 10(1), 1–16.

Hill, A. T., Rogasch, N. C., Fitzgerald, P. B., & Hoy, K. E. (2018). Effects of single versus dual-site High-Definition transcranial direct current stimulation (HD-tDCS) on cortical

reactivity and working memory performance in healthy subjects. Brain Stimulation, 11(5), 1033–1043.

Hill, A. T., Rogasch, N. C., Fitzgerald, P. B., & Hoy, K. E. (2019). Impact of concurrent task performance on transcranial direct current stimulation (tDCS)-Induced changes in cortical physiology and working memory. Cortex, 113, 37–57.

Hipp, J. F., Hawellek, D. J., Corbetta, M., Siegel, M., & Engel, A. K. (2012). Large-scale cortical correlation structure of spontaneous oscillatory activity. Nature Neuroscience, 15(6).

Holla, B., Biswal, J., Ramesh, V., Shivakumar, V., Bharath, R. D., Benegal, V., Venkatasubramanian, G., Chand, P. K., & Murthy, P. (2020). Effect of prefrontal tDCS on resting brain fMRI graph measures in Alcohol Use Disorders: A randomized, double-blind, sham-controlled study. Progress in Neuro-Psychopharmacology & Biological Psychiatry, 102(q45, 8211617), 109950.

Holmes, C. J., Hoge, R., Collins, L., Woods, R., Toga, A. W., & Evans, A. C. (1998). Enhancement of MR Images Using Registration for Signal Averaging. Journal of Computer Assisted Tomography, 22(2), 324–333.

Jamil, A., Batsikadze, G., Kuo, H. I., Labruna, L., Hasan, A., Paulus, W., & Nitsche, M. A. (2017). Systematic evaluation of the impact of stimulation intensity on neuroplastic after-effects induced by transcranial direct current stimulation. Journal of Physiology, 595(4), 1273–1288.

Jasper, H. H. (1958). The ten-twenty electrode system of the International Federation. Electroencephalogr. Clin. Neurophysiol., 10, 370–375.

Keeser, D., Padberg, F., Reisinger, E., Pogarell, O., Kirsch, V., Palm, U., Karch, S., Möller, H.-J., Nitsche, M. A., & Mulert, C. (2011). Prefrontal direct current stimulation modulates resting EEG and event-related potentials in healthy subjects: A standardized low resolution tomography (sLORETA) study. NeuroImage, 55(2), 644–657.

Kim, J.-H., Kim, D.-W., Chang, W. H., Kim, Y.-H., Kim, K., & Im, C.-H. (2014). Inconsistent outcomes of transcranial direct current stimulation may originate from anatomical differences among individuals: Electric field simulation using individual MRI data. Neuroscience Letters, 564, 6–10.

Lina, J. M., Chowdhury, R., Lemay, E., Kobayashi, E., & Grova, C. (2014). Wavelet-based localization of oscillatory sources from magnetoencephalography data. IEEE Trans Biomed Eng, 61(8), 2350–2364.

Maier, K. L., McKinstry-Wu, A. R., Palanca, B. J. A., Tarnal, V., Blain-Moraes, S., Basner, M., Avidan, M. S., Mashour, G. A., & Kelz, M. B. (2017). Protocol for the reconstructing consciousness and cognition (ReCCognition) study. Frontiers in Human Neuroscience, 11, 284.

Mancini, M., Brignani, D., Conforto, S., Mauri, P., Miniussi, C., & Pellicciari, M. C. (2016). Assessing cortical synchronization during transcranial direct current stimulation: A graph-theoretical analysis. NeuroImage, 140, 57–65.

Martin, D. M., Liu, R., Alonzo, A., Green, M., & Loo, C. K. (2014). Use of transcranial direct current stimulation (tDCS) to enhance cognitive training: Effect of timing of stimulation. Experimental Brain Research, 232(10), 3345–3351.

Mitra, P. (2007). Observed brain dynamics. Oxford University Press.

Mitra, P., Bokil, H., Maniar, H., Loader, C., Mehta, S., Hill, D., Mitra, S., Andrews, P., Baptista, R., Gopinath, S., Nalatore, H., & Kaur, S. (n.d.). Chronux.

Mosayebi Samani, M., Agboada, D., Jamil, A., Kuo, M.-F., & Nitsche, M. A. (2019). Titrating the neuroplastic effects of cathodal transcranial direct current stimulation (tDCS) over the primary motor cortex. Cortex, 119, 350–361.

Nadin, D., Duclos, C., Mahdid, Y., Rokos, A., Badawy, M., Létourneau, J., Arbour, C., Plourde, G., & Blain-Moraes, S. (2020). Brain network motif topography may predict emergence from disorders of consciousness: A case series. Neuroscience of Consciousness, 2020(1).

Nikolin, S., Martin, D., Loo, C. K., & Boonstra, T. W. (2018). Effects of TDCS dosage on working memory in healthy participants. Brain Stimulation, 11(3), 518–527.

Oldfield, R. C. (1971). The assessment and analysis of handedness: The Edinburgh inventory. Neuropsychologia, 9(1), 97–113.

Owen, A. M., McMillan, K. M., Laird, A. R., & Bullmore, E. (2005). N-back working memory paradigm: A meta-analysis of normative functional neuroimaging studies. Human Brain Mapping, 25(1), 46–59.

Ragland, J. D., Turetsky, B. I., Gur, R. C., Gunning-Dixon, F., Turner, T., Schroeder, L., Chan, R., & Gur, R. E. (2002). Working memory for complex figures: An fMRI comparison of letter and fractal n-back tasks. Neuropsychology, 16(3), 370.

Stagg, C. J., & Nitsche, M. A. (2011). Physiological Basis of Transcranial Direct Current Stimulation. The Neuroscientist, 17(1), 37–53.

Stam, C. J., & van Straaten, E. C. W. (2012). Go with the flow: Use of a directed phase lag index (dPLI) to characterize patterns of phase relations in a large-scale model of brain dynamics. NeuroImage, 62(3), 1415–1428.

Teo, F., Hoy, K. E., Daskalakis, Z. J., & Fitzgerald, P. B. (2011). Investigating the Role of Current Strength in tDCS Modulation of Working Memory Performance in Healthy Controls. Frontiers in Psychiatry, 2.

Thibaut, A., Chennu, S., Chatelle, C., Martens, G., Annen, J., Cassol, H., & Laureys, S. (2018). Theta network centrality correlates with tDCS response in disorders of consciousness. Brain Stimulation.

Thibaut, A., Wannez, S., Donneau, A.-F., Chatelle, C., Gosseries, O., Bruno, M.-A., & Laureys, S. (2017). Controlled clinical trial of repeated prefrontal tDCS in patients with chronic minimally conscious state. Brain Injury, 31(4), 466–474.

Vinck, M., Oostenveld, R., van Wingerden, M., Battaglia, F., & Pennartz, C. M. A. (2011). An improved index of phase-synchronization for electrophysiological data in the presence of volume-conduction, noise and sample-size bias. NeuroImage, 55(4), 1548–1565.

Zaehle, T., Sandmann, P., Thorne, J. D., Jäncke, L., & Herrmann, C. S. (2011). Transcranial direct current stimulation of the prefrontal cortex modulates working memory performance: Combined behavioural and electrophysiological evidence. BMC Neuroscience, 12(1), 2.

Discussion

This thesis aimed to further our understanding of prognosis and treatment of DoC through two specific aims. First, we sought to validate functional network motifs as a novel graph theoretical metric for the prognosis of DoC. Second, we aimed to assess the impact of anodal tDCS applied to the L-DLPFC on HD-EEG networks and behavior, in a cohort of healthy controls.

In Chapter 2, our first study explored the relationship between 3-node functional network motifs and anesthetic-induced unconsciousness in a group of healthy young adults. We found that the topography of node participation in these motifs was associated with states of anesthetic-induced unconsciousness. Motif 1, composed of two sources connected to a central sink, was associated with long-range connections and feedback-dominant connectivity. Node participation in this motif was disrupted during all states of anesthetic-induced unresponsiveness and returned to its baseline state as participants recovered responsiveness. Motif 5, a loop-like motif composed of 3 connected nodes, was associated with shorter-range connections. Node participation in this motif was disrupted when anesthetic concentrations were at their highest and returned to its baseline state 10 minutes prior to participants' recovery of responsiveness. Overall, our findings suggest that functional network motifs should be further explored as a potential network correlate of consciousness.

In Chapter 3, our second study measured 3-node functional network motifs in the brain networks of three patients with DoC, two of whom underwent an anesthetic protocol. We found that, at baseline, the topography of node participation in motifs was similar to healthy controls in patients who later recovered consciousness, but that this baseline measure alone was prone to false positives. When patients were exposed to anesthesia, the ability of node participation in motifs to reconfigure in response to this perturbation, and to recover post-anesthesia, was associated with eventual recovery of consciousness, overcoming the limitation of baseline-only assessment. Network motifs appeared to provide complementary prognostic information in addition to what can be measured with more commonly used spectral or global graph theoretical network properties in this patient population.

In Chapter 4, our third and final study applied anodal tDCS to the L-DLPFC through a high-density, targeted electrode montage in a group of healthy individuals. We measured HD-EEG and

working memory performance before and 30 minutes-post tDCS to compare the effects of 1 and 2 mA tDCS to sham stimulation. We found no statistically significant effects of tDCS on EEG spectral properties, scalp-level graph theoretical network properties, source-level connectivity, or behavior, as compared to sham stimulation. While statistically non-significant, we observed qualitative differences between 1 and 2 mA tDCS which support the idea of a non-linear relationship between stimulation intensity and effects on cortical networks.

Functional network motifs as a prognostic measure for disorders of consciousness

Our promising findings for network motifs warrant the further exploration of this metric in the context of DoC. An immediate next step for this work is to perform a prospective study, in which we would aim to measure the positive predictive value, sensitivity and specificity of functional network motifs in a large sample of patients with DoC. This would allow us to better understand the complementary information provided by network motifs as compared to more commonly used graph theoretical network properties, which have been extensively explored in large cohorts of patients (Chennu et al., 2017; Sitt et al., 2014).

The use of anesthesia to measure response to perturbation in DoC patients' brain networks should also be investigated in larger cohorts of patients, as has been done for the perturbational complexity index, which leverages magnetic stimulation as a perturbation (Casarotto et al., 2016). Our group has applied anesthetic perturbations in 12 patients with DoC and observed potential prognostic value in several graph theoretical metrics (paper in preparation). A study is also underway to investigate whether withdrawing sedation in comatose patients in intensive care can provide similar prognostic information in an acute context (Duclos, Norton, et al., 2020).

tDCS as a treatment for disorders of consciousness

Several questions remain following our exploration of L-DPLFC tDCS. First, we have yet to conclude whether 1 and 2 mA anodal tDCS applied to this brain area produce different effects on brain networks and behavior. While we observed potential qualitative differences, neither of these interventions produced statistically different effects from each other, or from sham stimulation. While simulations predict a monotonic increase in electric field strength at the stimulated brain area with increased tDCS intensity, neurophysiological evidence in humans is highly variable

between individuals, suggesting a non-monotonic relationship between stimulation intensity and neurophysiological response (Esmaeilpour et al., 2018). In DoC patients, the majority of tDCS trials have used 2 mA stimulation. To our knowledge, only two studies have applied 1 mA in this patient population. The first showed no increases in CRS-R after 5 consecutive days of 1 mA anodal stimulation to either the L-DLPFC or the primary motor cortex, but did find increases after a subsequent 5-day session of 2 mA stimulation to the same area, as well as at 1-month follow-up (Angelakis et al., 2014). The other applied 1 mA anodal tDCS to the L-DLPFC in a subset of patients who had had a left craniotomy (Zhang et al., 2017). After 20 sessions of tDCS spread across 10 days, they observed increases in patients' event-related potentials in response to the sound of their own name (Zhang et al., 2017). Given the limited number of studies which apply L-DLPFC stimulation at intensities other than 2 mA, and the emerging evidence in healthy controls that there is a non-monotonic relationship between tDCS intensity and neurophysiological response, tDCS dose-response studies in DoC patients are warranted.

Second, we have focused on the L-DLPFC due to converging evidence in double-blind randomized controlled trials that stimulation of this area increases behavioral responsiveness in DoC patients (Martens et al., 2018; Thibaut et al., 2014, 2017). Despite this strong evidence, there are several other brain areas worth considering, including but not limited to the premotor and motor cortex (Angelakis et al., 2014; Martens et al., 2019; Straudi et al., 2019), the precuneus (Guo et al., 2019), the parietal cortex (Cai et al., 2019; W. Huang et al., 2017; Lin et al., 2019) and the orbitofrontal cortex (Naro et al., 2015). There is preliminary evidence supporting the application of tDCS to all of these areas, except the orbitofrontal cortex, in DoC. Further, the effects of stimulating networks rather than single brain areas are still poorly understood. One study so far has attempted bilateral fronto-parietal stimulation in patients with DoC. No group-level effects were observed, with a minority of participants exhibiting increased behavioral responsiveness, and some patients becoming less behaviorally responsive following stimulation (Martens et al., 2020). The L-DLPFC may not be the best area to stimulate in all patients, especially when considering the effects of varied brain lesions on the flow of electrical current in the cortex (Minjoli et al., 2017). Thus, more work needs to be done to inform the selection of optimal brain areas to stimulate in patients with DoC.

Third, while we have taken preliminary steps towards targeting tDCS stimulation, there are more sophisticated methods available to do so, which have yet to be explored in DoC patients. We were unable to obtain individual MRIs for participants in our study, but such scans would allow for more accurately targeted neuromodulation and would be particularly important for stimulating injured brains (Minjoli et al., 2017). Segmenting lesioned brains in order to perform such targeting remains a challenge due to abnormality in the boundaries between tissue types, but advances are being made in this area. For example, one pre-print describes deep volumetric neural networks trained on the MRIs of stroke patients, which achieved human-level tissue segmentation performance when presented with novel stroke patient MRIs (Hirsch et al., 2019). In addition, we restricted our exploration to the reciprocity targeting algorithm, but a range of algorithms exist, optimizing for stimulation intensity and focality to different degrees (Fernández-Corazza et al., 2020). These algorithms do not incorporate appropriate segmentation algorithms for lesioned brains, and it remains an open question whether available targeting algorithms are optimized for lesioned brains.

These lingering questions, paired with our and many others' highly heterogenous tDCS findings, raise two broader issues. What is tDCS really doing in the subset of DoC patients who respond to it, and what are the implications of this response for patient care?

While tDCS potentiates the cortex, making it easier for neurons to fire action potentials, spontaneous activity in the brain is still required to cause these neurons to fire. The effect of tDCS on the cortex may be smaller than the intrinsic variability of the brain at rest, resulting in no overall influence on cortical firing patterns or networks. It is likely that, while tDCS is increasing the likelihood of neural firing, a stimulus is required to ignite the specific networks targeted by stimulation. For instance, there is strong evidence that when tDCS is applied "online," in conjunction with a task that activates the stimulated area, it has more robust effects on cortical excitability and behavior (Brunoni & Vanderhasselt, 2014; Dedoncker et al., 2016; Katsoulaki et al., 2017; Martin et al., 2014). In patients with DoC, who cannot always engage in cognitive and behavioral tasks, a large, external stimulus may be needed to ignite brain networks, and may explain why some patients do not respond to tDCS. In such cases, one promising avenue for triggering cortical ignition is deep brain stimulation. A pivotal study applied deep brain stimulation in the thalamus of a patient who had been in MCS for 6 years; the patient regained consciousness

after 6 months of therapy (Schiff et al., 2007). This group hypothesized that deep brain stimulation recruited large-scale networks which were not being ignited by the frontal lobe due to the patient's brain injury (Schiff et al., 2007).

Another proposed treatment for patients with disorders of consciousness is sensory stimulation. This treatment approach has shown effects on coma, MCS and UWS patients' level of consciousness. In particular, tactile stimuli such as massage (Cheng et al., 2018; M. Lippert Grüner, 2000), cooling and warming (M. Lippert Grüner, 2000; Mitchell et al., 1990), brushes and combs (Mitchell et al., 1990; Moattari et al., 2016), as well as other stimuli such as sandpaper, fur, fabric, feathers and needles (Mitchell et al., 1990) applied to the face and body have been shown to impact levels of consciousness. It is worth noting that, when applied to the face, sensations such as warmth and the tingling experienced when a brush or feather is applied to the skin are similar to the side-effects that may result from tDCS. Many healthy controls presented in Chapter 4 experienced sensations of warmth, tingling and itching during tDCS, despite the use of a lidocaine ointment to reduce the intensity of these sensations. It is usually not possible for DoC patients to self-report any side-effects they experience during tDCS, and no studies thus far have reported signs of discomfort in DoC patients receiving stimulation. Despite this, it is possible that patients also experience these sensations, and that the sensory aspects of stimulation may contribute to observed effects on behavioral responsiveness, without any network-level changes to the EEG. This hypothesis should be interpreted with the caveat that the sensations associated with tDCS are not emotionally salient, autobiographical or non-repetitive, characteristics that have been shown to make sensory stimulation more effective as a DoC treatment (Li et al., 2020).

In many cases, the effects of L-DPLFC tDCS are not immediate. Stimulation often results in an immediate increase in CRS-R score, with only a subset of these increases leading to a change in level of consciousness (e.g. from UWS to MCS, from MCS to emergence from DoC) in the weeks or months following stimulation (Estraneo et al., 2017; Thibaut et al., 2014; Wu et al., 2019). Why, then, should we study the short-term effects of tDCS on the brain, and what purpose does tDCS serve in cases where it increases a patient's CRS-R score, but does not result in a change of behavioral diagnosis? This transient increase in CRS-R may present a window of opportunity to increase access to rehabilitative therapy or other types of treatment, such as deep brain stimulation or sensory stimulation. Amantadine, the only pharmacological agent which has been proven

effective in the treatment of acute DoC, increases patients' rate of recovery during administration, but not after cessation of the drug (Giacino et al., 2012). Similarly, tDCS may have effects on recovery rate during its administration that, when paired with other therapeutic interventions, can lead to positive outcomes for patients. Further, tDCS may also enhance the efficacy of diagnostic and prognostic interventions, such as fMRI and EEG command-following paradigms (Cruse et al., 2011; Monti, Vanhaudenhuyse, et al., 2010).

Limitations of this thesis

In addition to the limitations presented in Chapters 2 to 4, several overarching limitations must be considered when interpreting the results of this thesis. I have presented exploratory analyses but have not comprehensively explored the range of analytic methods available for quantifying HD-EEG-derived brain networks. First, connectivity was primarily measured using phase-based measures of connectivity (wPLI and dPLI). In one analysis presented in Chapter 4, amplitude-based connectivity was used (AEC). As phase-based and amplitude-based connectivity measures result in completely different brain networks, a comparison of both types of connectivity is warranted for all analyses presented in this thesis. In particular, AEC connectivity maps are closely tied to networks constructed from fMRI (Brookes et al., 2012). The use of this connectivity metric would therefore allow results to be more closely tied into the fMRI literature. Further, measures of information transfer, such as Symbolic Transfer Entropy and Symbolic Mutual Information would allow for a better approximation of causal relationships between nodes in EEG networks. Second, in Chapters 2 to 4, I presented graph theoretical network properties which were derived from thresholded graphs. Thresholds were selected in order to maintain a sparse but fully connected graph, but there are multiple approaches to thresholding graphs. For instance, orthogonalized minimally spanning trees may prove a more robust approach to constructing a minimally spanning graph (Dimitriadis et al., 2017).

Conclusion and Summary

This thesis aimed to address issues of prognosis and treatment in patients with DoC, for whom limited options are available. The first two studies, presented in Chapters 2 and 3, explored 3-node functional network motifs as a prognostic measure. In a group of healthy controls, we found that the spatial organization of node participation in motifs was associated with states of anesthetic-induced unconsciousness. A motif formed of long-range, source-sink connections was associated with participants' level of responsiveness, while a loop-like, short-range motif heralded participants' recovery of responsiveness. In three patients with DoC, the spatial organization of node participation in these motifs provided complimentary prognostic information to what could be derived from more commonly used clinical and network properties. The similarity of motif topography to healthy controls, as well as ability of the network to reconfigure in response to anesthetic perturbation, were both associated with eventual recovery of consciousness. In the third and final study, presented in Chapter 3, we measured the effects of 1 and 2 mA tDCS applied to the L-DPLFC on scalp and source-level brain networks constructed from HD-EEG, as well as working memory performance. We found no statistically significant effects of tDCS on brain networks or behavior as compared to sham stimulation. We observed qualitative differences in the network effects of 1 and 2 mA stimulation, tying into evidence of a non-monotonic relationship between tDCS intensity and effects on cortical excitability. Future work should explore functional network motifs and brain network responses to perturbation for the prognosis of DoC. To develop optimized stimulation protocols for DoC patients which will reduce heterogeneity in patient response to this potential treatment, a better understanding of tDCS dosage and targeting is required.

Bibliography

Agboada, D., Mosayebi Samani, M., Jamil, A., Kuo, M.-F., & Nitsche, M. A. (2019). Expanding the parameter space of anodal transcranial direct current stimulation of the primary motor cortex. *Scientific Reports*, *9*(1), 18185.

Agboada, D., Mosayebi-Samani, M., Kuo, M.-F., & Nitsche, M. A. (2020). Induction of long-term potentiation-like plasticity in the primary motor cortex with repeated anodal transcranial direct current stimulation – Better effects with intensified protocols? *Brain Stimulation*, *13*(4), 987–997.

Akeju, O., Westover, M. B., Pavone, K. J., Sampson, A. L., Hartnack, K. E., Brown, E. N., & Purdon, P. L. (2014). Effects of Sevoflurane and Propofol on Frontal Electroencephalogram Power and Coherence. *Anesthesiology: The Journal of the American Society of Anesthesiologists*, *121*(5), 990–998.

Angelakis, E., Liouta, E., Andreadis, N., Korfias, S., Ktonas, P., Stranjalis, G., & Sakas, D. E. (2014). Transcranial Direct Current Stimulation Effects in Disorders of Consciousness. *Archives of Physical Medicine and Rehabilitation*, *95*(2), 283–289.

Avidan, M. S., Jacobsohn, E., Glick, D., Burnside, B. A., Zhang, L., Villafranca, A., Karl, L., Kamal, S., Torres, B., O'Connor, M., Evers, A. S., Gradwohl, S., Lin, N., Palanca, B. J., & Mashour, G. A. (2011). Prevention of Intraoperative Awareness in a High-Risk Surgical Population. *New England Journal of Medicine*, *365*(7), 591–600.

Aydin, Ü., Pellegrino, G., Bin Ka'b Ali, O., Abdallah, C., Dubeau, F., Lina, J. M., Kobayashi, E., & Grova, C. (2020). Magnetoencephalography resting state connectivity patterns as indicatives of surgical outcome in epilepsy patients. *Journal of Neural Engineering*, *17*(3), 035007–035007.

Bai, Y., Xia, X., Wang, Y., Guo, Y., Yang, Y., He, J., & Li, X. (2018). Fronto-parietal coherence response to tDCS modulation in patients with disorders of consciousness. *International Journal of Neuroscience*, *128*(7), 587–594.

Batsikadze, G., Moliadze, V., Paulus, W., Kuo, M.-F., & Nitsche, M. A. (2013). Partially non-linear stimulation intensity-dependent effects of direct current stimulation on motor cortex excitability in humans. *The Journal of Physiology*, *591*(7), 1987–2000.

Bayne, T., Hohwy, J., & Owen, A. M. (2016). Are There Levels of Consciousness? *Trends in Cognitive Sciences*, *20*(6), 405–413.

Berger, M., & Garcia, P. (2016). Anesthetic Suppression of Thalamic High Frequency Oscillations: Evidence that the Thalamus is More than Just a Gateway to Consciousness? *Anesthesia and Analgesia*, *122*(6), 1737–1739.

Betzel, R. F., Medaglia, J. D., & Bassett, D. S. (2018). Diversity of meso-scale architecture in human and non-human connectomes. *Nature Communications*, *9*(1), 346.

Bikson, M., Brunoni, A. R., Charvet, L. E., Clark, V. P., Cohen, L. G., Deng, Z. D., Dmochowski, J., Edwards, D. J., Frohlich, F., Kappenman, E. S., Lim, K. O., Loo, C., Mantovani, A., McMullen, D. P., Parra, L. C., Pearson, M., Richardson, J. D., Rumsey, J. M., Sehatpour, P., … Lisanby, S. H. (2018). Rigor and reproducibility in research with transcranial electrical stimulation: An NIMH-sponsored workshop. *Brain Stimulation*, *11*(3), 465–480.

Blain-Moraes, S., Boshra, R., Ma, H. K., Mah, R., Ruiter, K., Avidan, M., Connolly, J. F., & Mashour, G. A. (2016). Normal Brain Response to Propofol in Advance of Recovery from Unresponsive Wakefulness Syndrome. *Frontiers in Human Neuroscience*, *10*(248).

Blain-Moraes, S., Lee, U., Ku, S., Noh, G., & Mashour, G. A. (2014). Electroencephalographic effects of ketamine on power, cross-frequency coupling, and connectivity in the alpha bandwidth. *Frontiers in Systems Neuroscience*, *8*(114).

Blain-Moraes, S., Tarnal, V., Vanini, G., Alexander, A., Rosen, D., Shortal, B., Janke, E., & Mashour, G. A. (2015). Neurophysiological Correlates of Sevoflurane-induced Unconsciousness. *Anesthesiology: The Journal of the American Society of Anesthesiologists*, *122*(2), 307–316.

Blain-Moraes, S., Tarnal, V., Vanini, G., Bel-Behar, T., Janke, E., Picton, P., Golmirzaie, G., Palanca, B. J. A., Avidan, M. S., Kelz, M. B., & Mashour, G. A. (2017). Network Efficiency and Posterior Alpha Patterns Are Markers of Recovery from General Anesthesia: A High-Density Electroencephalography Study in Healthy Volunteers. *Frontiers in Human Neuroscience*, *11*, 328.

Blumenfeld, H. (2010). *Neuroanatomy through clinical cases*. Sinauer Associates Sunderland.

Boggio, P. S., Ferrucci, R., Rigonatti, S. P., Covre, P., Nitsche, M., Pascual-Leone, A., & Fregni, F. (2006). Effects of transcranial direct current stimulation on working memory in patients with Parkinson's disease. *Journal of the Neurological Sciences*, *249*(1), 31–38.

Bonhomme, V., Vanhaudenhuyse, A., Demertzi, A., Bruno, M.-A., Jaquet, O., Bahri, M. A., Plenevaux, A., Boly, M., Boveroux, P., Soddu, A., Brichant, J. F., Maquet, P., & Laureys, S. (2016). Resting-state Network-specific Breakdown of Functional Connectivity during Ketamine Alteration of Consciousness in Volunteers. *Anesthesiology*, *125*(5), 873–888.

Boonstra, T. W., Nikolin, S., Meisener, A. C., Martin, D. M., & Loo, C. K. (2016). Change in Mean Frequency of Resting-State Electroencephalography after Transcranial Direct Current Stimulation. *Frontiers in Human Neuroscience*, *10*, 270.

Boveroux, P., Vanhaudenhuyse, A., Bruno, M.-A., Noirhomme, Q., Lauwick, S., Luxen, A., Degueldre, C., Plenevaux, A., Schnakers, C., Phillips, C., Brichant, J.-F., Bonhomme, V., Maquet, P., Greicius, M. D., Laureys, S., & Boly, M. (2010). Breakdown of within- and between-network Resting State Functional Magnetic Resonance Imaging Connectivity during Propofol-induced Loss of Consciousness. *Anesthesiology*, *113*(5), 1038–1053.

Brookes, M. J., Woolrich, M. W., & Barnes, G. R. (2012). Measuring functional connectivity in MEG: a multivariate approach insensitive to linear source leakage. *NeuroImage*, *63*(2), 910–920.

Brunoni, A. R., & Vanderhasselt, M.-A. (2014). Working memory improvement with non-invasive brain stimulation of the dorsolateral prefrontal cortex: A systematic review and meta-analysis. *Brain and Cognition*, *86*, 1–9.

Bullmore, E., & Sporns, O. (2009). Complex brain networks: Graph theoretical analysis of structural and functional systems. *Nature Reviews Neuroscience*, *10*, 186.

Cai, T., Xia, X., Zhang, H., Guo, Y., & Bai, Y. (2019). High-definition transcranial direct current stimulation modulates neural activities in patients with prolonged disorders of consciousness. *Brain Stimulation*.

Casarotto, S., Comanducci, A., Rosanova, M., Sarasso, S., Fecchio, M., Napolitani, M., Pigorini, A., Casali, A. G., Trimarchi, P. D., Boly, M., Gosseries, O., Bodart, O., Curto, F., Landi, C., Mariotti, M., Devalle, G., Laureys, S., Tononi, G., & Massimini, M. (2016).

Stratification of unresponsive patients by an independently validated index of brain complexity. *Annals of Neurology*, *80*(5), 718–729.

Castaigne, P., Lhermitte, F., Buge, A., Escourolle, R., Hauw, J. J., & Lyon-Caen, O. (1981). Paramedian thalamic and midbrain infarcts: Clinical and neuropathological study. *Annals of Neurology*, *10*(2), 127–148.

Cheng, L., Cortese, D., Monti, M. M., Wang, F., Riganello, F., Arcuri, F., Di, H., & Schnakers, C. (2018). Do Sensory Stimulation Programs Have an Impact on Consciousness Recovery?. *Frontiers in Neurology*, *9*(101546899), 826.

Chennu, S., Annen, J., Wannez, S., Thibaut, A., Chatelle, C., Cassol, H., Martens, G., Schnakers, C., Gosseries, O., Menon, D., & Laureys, S. (2017). Brain networks predict metabolism, diagnosis and prognosis at the bedside in disorders of consciousness. *Brain*, *140*(8), 2120–2132.

Chennu, S., Finoia, P., Kamau, E., Allanson, J., Williams, G. B., Monti, M. M., Noreika, V., Arnatkeviciute, A., Canales-Johnson, A., Olivares, F., Cabezas-Soto, D., Menon, D. K., Pickard, J. D., Owen, A. M., & Bekinschtein, T. A. (2014). Spectral Signatures of Reorganised Brain Networks in Disorders of Consciousness. *PLOS Computational Biology*, *10*(10).

Chennu, S., O'Connor, S., Adapa, R., Menon, D. K., & Bekinschtein, T. A. (2016). Brain Connectivity Dissociates Responsiveness from Drug Exposure during Propofol-Induced Transitions of Consciousness. *PLOS Computational Biology*, *12*(1).

Ching, S., Cimenser, A., Purdon, P. L., Brown, E. N., & Kopell, N. J. (2010). Thalamocortical model for a propofol-induced α-rhythm associated with loss of consciousness. *Proceedings of the National Academy of Sciences*, *107*(52), 22665–22670.

Crone, Julia S, Lutkenhoff, E. S., Vespa, P. M., & Monti, M. M. (2020). A systematic investigation of the association between network dynamics in the human brain and the state of consciousness. *Neuroscience of Consciousness*, *2020*(niaa008).

Crone, Julia Sophia, Soddu, A., Höller, Y., Vanhaudenhuyse, A., Schurz, M., Bergmann, J., Schmid, E., Trinka, E., Laureys, S., & Kronbichler, M. (2014). Altered network

properties of the fronto-parietal network and the thalamus in impaired consciousness. *NeuroImage: Clinical*, *4*, 240–248.

Cruse, D., Chennu, S., Chatelle, C., Bekinschtein, T. A., Fernández-Espejo, D., Pickard, J. D., Laureys, S., & Owen, A. M. (2011). Bedside detection of awareness in the vegetative state: A cohort study. *The Lancet*, *378*(9809), 2088–2094.

Daniel, M., Weiskopf, R. B., Noorani, M., & Eger, E. I. (1998). Fentanyl Augments the Blockade of the Sympathetic Response to Incision (MAC-BAR) Produced by Desflurane and Isoflurane: Desflurane and Isoflurane MAC-BAR without and with Fentanyl. *Anesthesiology*, *88*(1), 43–49.

Dedoncker, J., Brunoni, A. R., Baeken, C., & Vanderhasselt, M.-A. (2016). A Systematic Review and Meta-Analysis of the Effects of Transcranial Direct Current Stimulation (tDCS) Over the Dorsolateral Prefrontal Cortex in Healthy and Neuropsychiatric Samples: Influence of Stimulation Parameters. *Brain Stimulation*, *9*(4), 501–517.

Dehaene, S., & Naccache, L. (2001). Towards a cognitive neuroscience of consciousness: Basic evidence and a workspace framework. *Cognition*, *79*(1), 1–37.

Dell'Italia, J., Johnson, M. A., Vespa, P. M., & Monti, M. M. (2018). Network Analysis in Disorders of Consciousness: Four Problems and One Proposed Solution (Exponential Random Graph Models). *Frontiers in Neurology*, *9*.

Delorme, A., & Makeig, S. (2004). EEGLAB: an open source toolbox for analysis of single-trial EEG dynamics including independent component analysis. *Journal of Neuroscience Methods*, *134*(1), 9–21.

Desikan, R. S., Ségonne, F., Fischl, B., Quinn, B. T., Dickerson, B. C., Blacker, D., Buckner, R. L., Dale, A. M., Maguire, R. P., Hyman, B. T., Albert, M. S., & Killiany, R. J. (2006). An automated labeling system for subdividing the human cerebral cortex on MRI scans into gyral based regions of interest. *NeuroImage*, *31*(3), 968–980.

Dimitriadis, S. I., Salis, C., Tarnanas, I., & Linden, D. E. (2017). Topological Filtering of Dynamic Functional Brain Networks Unfolds Informative Chronnectomics: A Novel Data-Driven Thresholding Scheme Based on Orthogonal Minimal Spanning Trees (OMSTs). *Frontiers in Neuroinformatics*, *11*.

Dmochowski, J. P., Datta, A., Bikson, M., Su, Y., & Parra, L. C. (2011). Optimized multi-electrode stimulation increases focality and intensity at target. *Journal of Neural Engineering*, *8*(4), 046011.

Duclos, C., Mahdid, Y., Nadin, D., Tarnal, V., Picton, P., Vanini, G., Golmirzaie, G., Janke, E., Avidan, M., Kelz, M. B., Mashour, G. A., & Blain-Moraes, S. (2020). Brain network motifs are markers of loss and recovery of consciousness. *Scientific Reports, Under Review.*

Duclos, C., Norton, L., Laforge, G., Frantz, A., Maschke, C., Badawy, M., Letourneau, J., Slessarev, M., Gofton, T., Debicki, D., Owen, A. M., & Blain-Moraes, S. (2020). Protocol for the Prognostication of Consciousness Recovery Following a Brain Injury. *Frontiers in Human Neuroscience*, *14*.

Eger, E. I. I. (2001). Age, Minimum Alveolar Anesthetic Concentration, and Minimum Alveolar Anesthetic Concentration-Awake. *Anesthesia & Analgesia*, *93*(4), 947–953.

Esmaeilpour, Z., Marangolo, P., Hampstead, B. M., Bestmann, S., Galletta, E., Knotkova, H., & Bikson, M. (2018). Incomplete evidence that increasing current intensity of tDCS boosts outcomes. *Brain Stimulation*, *11*(2), 310–321.

Estraneo, A., Pascarella, A., Moretta, P., Masotta, O., Fiorenza, S., Chirico, G., Crispino, E., Loreto, V., & Trojano, L. (2017). Repeated transcranial direct current stimulation in prolonged disorders of consciousness: A double-blind cross-over study. *Journal of the Neurological Sciences*, *375*, 464–470.

Fernández-Corazza, M., Turovets, S., Luu, P., Anderson, E., & Tucker, D. (2016). Transcranial electrical neuromodulation based on the reciprocity principle. *Frontiers in Psychiatry*, *7*, 87.

Fernández-Corazza, M., Turovets, S., & Muravchik, C. H. (2020). Unification of optimal targeting methods in transcranial electrical stimulation. *NeuroImage*, *209*, 116403.

Feshchenko, V. A., Veselis, R. A., & Reinsel, R. A. (2004). Propofol-Induced Alpha Rhythm. *Neuropsychobiology*, *50*(3), 257–266.

Fregni, F., Boggio, P. S., Nitsche, M., Bermpohl, F., Antal, A., Feredoes, E., Marcolin, M. A., Rigonatti, S. P., Silva, M. T. A., Paulus, W., & Pascual-Leone, A. (2005). Anodal

transcranial direct current stimulation of prefrontal cortex enhances working memory. *Experimental Brain Research*, *166*(1), 23–30.

Gebodh, N., Esmaeilpour, Z., Adair, D., Chelette, K., Dmochowski, J., Woods, A. J., Kappenman, E. S., Parra, L. C., & Bikson, M. (2019). Inherent physiological artifacts in EEG during tDCS. *NeuroImage*, *185*, 408–424.

Giacino, J. T., Fins, J. J., Laureys, S., & Schiff, N. D. (2014). Disorders of consciousness after acquired brain injury: The state of the science. *Nature Reviews Neurology*, *10*(2), 99.

Giacino, J. T., Katz, D. I., Schiff, N. D., Whyte, J., Ashman, E. J., Ashwal, S., Barbano, R., Hammond, F. M., Laureys, S., & Ling, G. S. (2018). Practice guideline update recommendations summary: Disorders of consciousness. Report of the Guideline Development, Dissemination, and Implementation Subcommittee of the American Academy of Neurology; the American Congress of Rehabilitation Medicine; and the National Institute on Disability, Independent Living, and Rehabilitation Research. *Neurology*, *91*, 450–460.

Giacino, J. T., Whyte, J., Bagiella, E., Kalmar, K., Childs, N., Khademi, A., Eifert, B., Long, D., Katz, D. I., & Cho, S. (2012). Placebo-controlled trial of amantadine for severe traumatic brain injury. *New England Journal of Medicine*, *366*(9), 819–826.

Giattino, C. M., Gardner, J. E., Sbahi, F. M., Roberts, K. C., Cooter, M., Moretti, E., Browndyke, J. N., Mathew, J. P., Woldorff, M. G., Berger, M., Investigators, the M.-P., Berger, M., Brigman, B. E., Browndyke, J. N., Bullock, W. M., Carter, J., Chapman, J., Colin, B., Cooter, M., … Young, C. (2017). Intraoperative Frontal Alpha-Band Power Correlates with Preoperative Neurocognitive Function in Older Adults. *Frontiers in Systems Neuroscience*, *11*.

Gloor, P. (1985). Neuronal Generators and the Problem of Localization in Electroencephalography: Application of Volume Conductor Theory to Electroencephalography. *Journal of Clinical Neurophysiology*, *2*(4), 327–354.

Gollo, L. L., Zalesky, A., Hutchison, R. M., van den Heuvel, M., & Breakspear, M. (2015). Dwelling quietly in the rich club: Brain network determinants of slow cortical fluctuations. *Philos Trans R Soc Lond B Biol Sci*, *370*(1668).

Gollo, Leonardo L., & Breakspear, M. (2014). The frustrated brain: From dynamics on motifs to communities and networks. *Philosophical Transactions of the Royal Society B: Biological Sciences*, *369*(1653), 20130532.

Guo, Y., Bai, Y., Xia, X., Li, J., Wang, X., Dai, Y., Dang, Y., He, J., Liu, C., & Zhang, H. (2019). Effects of Long-Lasting High-Definition Transcranial Direct Current Stimulation in Chronic Disorders of Consciousness: A Pilot Study. *Frontiers in Neuroscience*, *13*, 412.

Hämäläinen, M., Hari, R., lmoniemi, R., Knuutila, J., & Lounasmaa, O. (1993). Magnetoencephalography. Theory, instrumentation and applications to the noninvasive study of human brain function. *Rev. Mod. Phys.*, *65*, 413–497.

Hashmi, J. A., Loggia, M. L., Khan, S., Gao, L., Kim, J., Napadow, V., Brown, E. N., & Akeju, O. (2017). Dexmedetomidine Disrupts the Local and Global Efficiencies of Large-scale Brain Networks. *Anesthesiology*, *126*(3), 419–430.

Hassan, M., & Wendling, F. (2018). Electroencephalography Source Connectivity: Aiming for High Resolution of Brain Networks in Time and Space. *IEEE Signal Processing Magazine*, *35*(3), 81–96.

Hassan, Mahmoud, Dufor, O., Merlet, I., Berrou, C., & Wendling, F. (2014). EEG Source Connectivity Analysis: From Dense Array Recordings to Brain Networks. *PLOS One*, *9*(8), e105041.

Hermann, B., Raimondo, F., Hirsch, L., Huang, Y., Denis-Valente, M., Pérez, P., Engemann, D., Faugeras, F., Weiss, N., & Demeret, S. (2020). Combined behavioral and electrophysiological evidence for a direct cortical effect of prefrontal tDCS on disorders of consciousness. *Scientific Reports*, *10*(1), 1–16.

Hill, A. T., Rogasch, N. C., Fitzgerald, P. B., & Hoy, K. E. (2018). Effects of single versus dual-site High-Definition transcranial direct current stimulation (HD-tDCS) on cortical reactivity and working memory performance in healthy subjects. *Brain Stimulation*, *11*(5), 1033–1043.

Hill, A. T., Rogasch, N. C., Fitzgerald, P. B., & Hoy, K. E. (2019). Impact of concurrent task performance on transcranial direct current stimulation (tDCS)-Induced changes in cortical physiology and working memory. *Cortex*, *113*, 37–57.

Hipp, J. F., Hawellek, D. J., Corbetta, M., Siegel, M., & Engel, A. K. (2012). Large-scale cortical correlation structure of spontaneous oscillatory activity. *Nature Neuroscience*, *15*(6).

Hirsch, L., Huang, Y., & Parra, L. C. (2019). Segmentation of lesioned brain anatomy with deep volumetric neural networks and multiple spatial priors achieves human-level performance. *ArXiv*.

Holla, B., Biswal, J., Ramesh, V., Shivakumar, V., Bharath, R. D., Benegal, V., Venkatasubramanian, G., Chand, P. K., & Murthy, P. (2020). Effect of prefrontal tDCS on resting brain fMRI graph measures in Alcohol Use Disorders: A randomized, double-blind, sham-controlled study. *Progress in Neuro-Psychopharmacology & Biological Psychiatry*, *102*(q45, 8211617), 109950.

Holmes, C. J., Hoge, R., Collins, L., Woods, R., Toga, A. W., & Evans, A. C. (1998). Enhancement of MR Images Using Registration for Signal Averaging. *Journal of Computer Assisted Tomography*, *22*(2), 324–333.

Huang, W., Wannez, S., Fregni, F., Hu, X., Jing, S., Martens, G., He, M., Di, H., Laureys, S., & Thibaut, A. (2017). Repeated stimulation of the posterior parietal cortex in patients in minimally conscious state: A sham-controlled randomized clinical trial. *Brain Stimulation: Basic, Translational, and Clinical Research in Neuromodulation*, *10*(3),

Huang, Y., Datta, A., Bikson, M., & Parra, L. C. (2018). *ROAST: An Open-Source, Fully-Automated, Realistic Volumetric-Approach-Based Simulator For TES*. 3072–3075.

Humphries, M. D., & Gurney, K. (2008). Network 'Small-World-Ness': A Quantitative Method for Determining Canonical Network Equivalence. *PLoS ONE*, *3*(4), e0002051.

Jamil, A., Batsikadze, G., Kuo, H. I., Labruna, L., Hasan, A., Paulus, W., & Nitsche, M. A. (2017). Systematic evaluation of the impact of stimulation intensity on neuroplastic after-effects induced by transcranial direct current stimulation. *Journal of Physiology*, *595*(4), 1273–1288.

Jasper, H. H. (1958). The ten-twenty electrode system of the International Federation. *Electroencephalogr. Clin. Neurophysiol.*, *10*, 370–375.

John, E. R., Prichep, L. S., Kox, W., Valdes-Sosa, P., Bosch-Bayard, J., Aubert, E., Tom, M., & Gugino, L. D. (2001). Invariant reversible QEEG effects of anesthetics. *Consciousness and Cognition*, *10*(2), 165–183.

Jordan, D., Ilg, R., Riedl, V., Schorer, A., Grimberg, S., Neufang, S., Omerovic, A., Berger, S., Untergehrer, G., Preibisch, C., Schulz, E., Schuster, T., Schröter, M., Spoormaker, V., Zimmer, C., Hemmer, B., Wohlschläger, A., Kochs, E. F., & Schneider, G. (2013). Simultaneous Electroencephalographic and Functional Magnetic Resonance Imaging Indicate Impaired Cortical Top–Down Processing in Association with Anesthetic-induced Unconsciousness. *Anesthesiology*, *119*(5), 1031–1042.

Kafashan, M., Ching, S., & Palanca, B. J. (2016). Sevoflurane Alters Spatiotemporal Functional Connectivity Motifs That Link Resting-State Networks during Wakefulness. *Frontiers in Neural Circuits*, *10*, 107.

Katsoulaki, M., Kastrinis, A., & Tsekoura, M. (2017). The Effects of Anodal Transcranial Direct Current Stimulation on Working Memory. *Advances in Experimental Medicine and Biology*, *987*, 283–289.

Keeser, D., Padberg, F., Reisinger, E., Pogarell, O., Kirsch, V., Palm, U., Karch, S., Möller, H.-J., Nitsche, M. A., & Mulert, C. (2011). Prefrontal direct current stimulation modulates resting EEG and event-related potentials in healthy subjects: A standardized low resolution tomography (sLORETA) study. *NeuroImage*, *55*(2), 644–657.

Kim, H., Hudetz, A. G., Lee, J., Mashour, G. A., Lee, U., & Re, Cc. S. G. (2018). Estimating the Integrated Information Measure Phi from High-Density Electroencephalography during States of Consciousness in Humans. *Frontiers in Human Neuroscience*, *12*, 42–42.

Kim, H., & Lee, U. (2019). Criticality as a Determinant of Integrated Information Φ in Human Brain Networks. *Entropy*, *21*(10), 981.

Kim, J.-H., Kim, D.-W., Chang, W. H., Kim, Y.-H., Kim, K., & Im, C.-H. (2014). Inconsistent outcomes of transcranial direct current stimulation may originate from anatomical

differences among individuals: Electric field simulation using individual MRI data. *Neuroscience Letters*, *564*, 6–10.

Kim, M., Mashour, G. A., Moraes, S.-B., Vanini, G., Tarnal, V., Janke, E., Hudetz, A. G., & Lee, U. (2016). Functional and Topological Conditions for Explosive Synchronization Develop in Human Brain Networks with the Onset of Anesthetic-Induced Unconsciousness. *Frontiers in Computational Neuroscience*, *10*(1).

Knapp, R. M. (2017). A Deeper Look at Anesthesia Depth. *Anesthesiology*, *127*(5), 904–905.

Kondziella, D., Bender, A., Diserens, K., van Erp, W., Estraneo, A., Formisano, R., Laureys, S., Naccache, L., Ozturk, S., & Rohaut, B. (2020). European Academy of Neurology guideline on the diagnosis of coma and other disorders of consciousness. *European Journal of Neurology*.

Kondziella, D., Friberg, C. K., Frokjaer, V. G., Fabricius, M., & Møller, K. (2016). Preserved consciousness in vegetative and minimal conscious states: Systematic review and meta-analysis. *Journal of Neurology, Neurosurgery & Psychiatry*, *87*(5), 485–492.

Lachaux, J.-P., Rodriguez, E., Martinerie, J., & Varela, F. J. (1999). Measuring phase synchrony in brain signals. *Human Brain Mapping*, *8*(4), 194–208.

Lee, H., Mashour, G. A., Noh, G.-J., Kim, S., & Lee, U. (2013). Reconfiguration of Network Hub Structure after Propofol-induced Unconsciousness. *Anesthesiology: The Journal of the American Society of Anesthesiologists*, *119*(6), 1347–1359.

Lee, M., Sanders, R. D., Yeom, S.-K., Won, D.-O., Seo, K.-S., Kim, H. J., Tononi, G., & Lee, S.-W. (2017). Network Properties in Transitions of Consciousness during Propofol-induced Sedation. *Scientific Reports*, *7*(1), 16791.

Lee, U., & Mashour, G. A. (2018). Role of Network Science in the Study of Anesthetic State Transitions. *Anesthesiology*, *129*(5), 1029–1044.

Lee, U., Muller, M., Noh, G.-J., Choi, B., & Mashour, G. A. (2011). Dissociable network properties of anesthetic state transitions. *Anesthesiology*, *114*(4), 872–881.

Li, J., Cheng, Q., Liu, F.-K., Huang, Z., & Feng, S.-S. (2020). Sensory stimulation to improve arousal in comatose patients after traumatic brain injury: A systematic review of the

literature. *Neurological Sciences : Official Journal of the Italian Neurological Society and of the Italian Society of Clinical Neurophysiology*, *41*(9), 2367–2376.

Liang, Z., Cheng, L., Shao, S., Jin, X., Yu, T., Sleigh, J. W., & Li, X. (2020). Information Integration and Mesoscopic Cortical Connectivity during Propofol Anesthesia. *Anesthesiology*, *132*(3), 504–524.

Lin, Y., Liu, T., Huang, Q., Su, Y., Chen, W., Gao, D., Tian, X., Huang, T., Zhen, Z., Han, T., Ye, H., & Wang, Y. (2019). Electroencephalography and functional magnetic resonance imaging-guided simultaneous transcranial direct current stimulation and repetitive transcranial magnetic stimulation in a patient with minimally conscious state. *Frontiers in Neuroscience*, *10*(JUL), 746.

Lina, J. M., Chowdhury, R., Lemay, E., Kobayashi, E., & Grova, C. (2014). Wavelet-based localization of oscillatory sources from magnetoencephalography data. *IEEE Trans Biomed Eng*, *61*(8), 2350–2364.

Lotto, M. L., Banoub, M., & Schubert, A. (2004). Effects of Anesthetic Agents and Physiologic Changes on Intraoperative Motor Evoked Potentials. *Journal of Neurosurgical Anesthesiology*, *16*(1), 32–42.

Luppi, A. I., Craig, M. M., Pappas, I., Finoia, P., Williams, G. B., Allanson, J., Pickard, J. D., Owen, A. M., Naci, L., Menon, D. K., & Stamatakis, E. A. (2019). Consciousness-specific dynamic interactions of brain integration and functional diversity. *Nature Communications*, *10*(1), 4616.

M. Lippert Grüner, D. T. (2000). Multimodal early onset stimulation (MEOS) in rehabilitation after brain injury. *Brain Injury*, *14*(6), 585–594.

Maier, K. L., McKinstry-Wu, A. R., Palanca, B. J. A., Tarnal, V., Blain-Moraes, S., Basner, M., Avidan, M. S., Mashour, G. A., & Kelz, M. B. (2017). Protocol for the reconstructing consciousness and cognition (ReCCognition) study. *Frontiers in Human Neuroscience*, *11*, 284.

Mancini, M., Brignani, D., Conforto, S., Mauri, P., Miniussi, C., & Pellicciari, M. C. (2016). Assessing cortical synchronization during transcranial direct current stimulation: A graph-theoretical analysis. *NeuroImage*, *140*, 57–65.

Martens, G., Fregni, F., Carrière, M., Barra, A., Laureys, S., & Thibaut, A. (2019). Single tDCS session of motor cortex in patients with disorders of consciousness: A pilot study. *Brain Injury*, 1–5.

Martens, G., Kroupi, E., Bodien, Y., Frasso, G., Annen, J., Cassol, H., Barra, A., Martial, C., Gosseries, O., Lejeune, N., Soria-Frisch, A., Ruffini, G., Laureys, S., & Thibaut, A. (2020). Behavioral and electrophysiological effects of network-based frontoparietal tDCS in patients with severe brain injury: A randomized controlled trial. *NeuroImage: Clinical*, *28*, 102426.

Martens, G., Lejeune, N., O'Brien, A. T., Fregni, F., Martial, C., Wannez, S., Laureys, S., & Thibaut, A. (2018). Randomized controlled trial of home-based 4-week tDCS in chronic minimally conscious state. *Brain Stimulation*, *11*(5), 982–990.

Martial, C., Cassol, H., Laureys, S., & Gosseries, O. (2020). Near-Death Experience as a Probe to Explore (Disconnected) Consciousness. *Trends in Cognitive Sciences*, *24*.

Martin, D. M., Liu, R., Alonzo, A., Green, M., & Loo, C. K. (2014). Use of transcranial direct current stimulation (tDCS) to enhance cognitive training: Effect of timing of stimulation. *Experimental Brain Research*, *232*(10), 3345–3351.

Mashour, G. A., Orser, B. A., Avidan, M. S., & Warner, D. S. (2011). Intraoperative Awareness: From Neurobiology to Clinical Practice. *Anesthesiology*, *114*(5), 1218–1233.

Maslov, S., & Sneppen, K. (2002). Specificity and stability in topology of protein networks. *Science*, *296*(5569), 910–913.

Milo, R., Shen-Orr, S., Itzkovitz, S., Kashtan, N., Chklovskii, D., & Alon, U. (2002). Network motifs: Simple building blocks of complex networks. *Science*, *298*(5594), 824–827.

Minjoli, S., Saturnino, G. B., Blicher, J. U., Stagg, C. J., Siebner, H. R., Antunes, A., & Thielscher, A. (2017). The impact of large structural brain changes in chronic stroke patients on the electric field caused by transcranial brain stimulation. *NeuroImage: Clinical*, *15*, 106–117.

Mitchell, S., Bradley, V. A., Welch, J. L., & Britton, P. G. (1990). Coma arousal procedure: A therapeutic intervention in the treatment of head injury. *Brain Injury*, *4*(3), 273–279.

Mitra, P. (2007). *Observed brain dynamics*. Oxford University Press.

Mitra, P., Bokil, H., Maniar, H., Loader, C., Mehta, S., Hill, D., Mitra, S., Andrews, P., Baptista, R., Gopinath, S., Nalatore, H., & Kaur, S. (n.d.). *Chronux*.

Moattari, M., Alizadeh Shirazi, F., Sharifi, N., & Zareh, N. (2016). Effects of a Sensory Stimulation by Nurses and Families on Level of Cognitive Function, and Basic Cognitive Sensory Recovery of Comatose Patients With Severe Traumatic Brain Injury: A Randomized Control Trial. *Trauma Monthly*, *21*(4).

Monti, M. M., Laureys, S., & Owen, A. M. (2010). The vegetative state. *BMJ*, *341*, c3765.

Monti, M. M., Vanhaudenhuyse, A., Coleman, M. R., Boly, M., Pickard, J. D., Tshibanda, L., Owen, A. M., & Laureys, S. (2010). Willful modulation of brain activity in disorders of consciousness. *New England Journal of Medicine*, *362*(7), 579–589.

Moon, J.-Y., Lee, U., Blain-Moraes, S., & Mashour, G. A. (2015). General Relationship of Global Topology, Local Dynamics, and Directionality in Large-Scale Brain Networks. *PLOS Computational Biology*, *11*(4), e1004225.

Mosayebi Samani, M., Agboada, D., Jamil, A., Kuo, M.-F., & Nitsche, M. A. (2019). Titrating the neuroplastic effects of cathodal transcranial direct current stimulation (tDCS) over the primary motor cortex. *Cortex*, *119*, 350–361. https://doi.org/10.1016/j.cortex.2019.04.016

Nadin, D., Duclos, C., Mahdid, Y., Rokos, A., Badawy, M., Létourneau, J., Arbour, C., Plourde, G., & Blain-Moraes, S. (2020). Brain network motif topography may predict emergence from disorders of consciousness: A case series. *Neuroscience of Consciousness*, *2020*(1).

Naro, A., Calabrò, R. S., Russo, M., Leo, A., Pollicino, P., Quartarone, A., & Bramanti, P. (2015). Can transcranial direct current stimulation be useful in differentiating unresponsive wakefulness syndrome from minimally conscious state patients? *Restorative Neurology and Neuroscience*, *33*(2), 159–176.

Newman, M. E. J. (2006). Modularity and community structure in networks. *Proceedings of the National Academy of Sciences*, *103*(23), 8577–8582.

Nickalls, R. W. D., & Mapleson, W. W. (2003). Age-related iso-MAC charts for isoflurane, sevoflurane and desflurane in man. *BJA: British Journal of Anaesthesia*, *91*(2), 170–174.

Nikolin, S., Martin, D., Loo, C. K., & Boonstra, T. W. (2018). Effects of TDCS dosage on working memory in healthy participants. *Brain Stimulation*, *11*(3), 518–527.

Oldfield, R. C. (1971). The assessment and analysis of handedness: The Edinburgh inventory. *Neuropsychologia*, *9*(1), 97–113.

Owen, A. M., McMillan, K. M., Laird, A. R., & Bullmore, E. (2005). N-back working memory paradigm: A meta-analysis of normative functional neuroimaging studies. *Human Brain Mapping*, *25*(1), 46–59.

Palanca, B. J. A., Mitra, A., Larson-Prior, L., Snyder, A. Z., Avidan, M. S., & Raichle, M. E. (2015). Resting-state Functional Magnetic Resonance Imaging Correlates of Sevoflurane-induced Unconsciousness. *Anesthesiology*, *123*(2), 346–356.

Peterson, A., Cruse, D., Naci, L., Weijer, C., & Owen, A. M. (2015). Risk, diagnostic error, and the clinical science of consciousness. *NeuroImage: Clinical*, *7*, 588–597.

Purdon, P. L., Pierce, E. T., Mukamel, E. A., Prerau, M. J., Walsh, J. L., Wong, K. F. K., Salazar-Gomez, A. F., Harrell, P. G., Sampson, A. L., & Cimenser, A. (2013). Electroencephalogram signatures of loss and recovery of consciousness from propofol. *Proceedings of the National Academy of Sciences*, *110*(12), E1142–E1151.

Ragland, J. D., Turetsky, B. I., Gur, R. C., Gunning-Dixon, F., Turner, T., Schroeder, L., Chan, R., & Gur, R. E. (2002). Working memory for complex figures: An fMRI comparison of letter and fractal n-back tasks. *Neuropsychology*, *16*(3), 370.

Ranft, A., Golkowski, D., Kiel, T., Riedl, V., Kohl, P., Rohrer, G., Pientka, J., Berger, S., Thul, A., Maurer, M., Preibisch, C., Zimmer, C., Mashour, G. A., Kochs, E. F., Jordan, D., & Ilg, R. (2016). Neural Correlates of Sevoflurane-induced Unconsciousness Identified by Simultaneous Functional Magnetic Resonance Imaging and Electroencephalography. *Anesthesiology*, *125*(5), 861–872.

Rubinov, M., & Sporns, O. (2010). Complex network measures of brain connectivity: Uses and interpretations. *NeuroImage*, *52*(3), 1059–1069.

Sanders, R. D., Tononi, G., Laureys, S., Sleigh, J. W., & Warner, D. S. (2012). Unresponsiveness ≠ Unconsciousness. *Anesthesiology*, *116*(4), 946–959.

Schiff, N. D., Giacino, J. T., Kalmar, K., Victor, J. D., Baker, K., Gerber, M., Fritz, B., Eisenberg, B., O'Connor, J., Kobylarz, E. J., Farris, S., Machado, A., McCagg, C., Plum, F., Fins, J. J., & Rezai, A. R. (2007). Behavioural improvements with thalamic stimulation after severe traumatic brain injury. *Nature*, *448*(7153), 600–603.

Schnakers, C., Vanhaudenhuyse, A., Giacino, J., Ventura, M., Boly, M., Majerus, S., Moonen, G., & Laureys, S. (2009a). Diagnostic accuracy of the vegetative and minimally conscious state: Clinical consensus versus standardized neurobehavioral assessment. *BMC Neurology*, *9*(1), 35.

Schnakers, C., Vanhaudenhuyse, A., Giacino, J., Ventura, M., Boly, M., Majerus, S., Moonen, G., & Laureys, S. (2009b). Diagnostic accuracy of the vegetative and minimally conscious state: Clinical consensus versus standardized neurobehavioral assessment. *BMC Neurology*, *9*(1), 1–5.

Schroeter, M. S., Spoormaker, V. I., Schorer, A., Wohlschlaeger, A., Czisch, M., Kochs, E. F., Zimmer, C., Hemmer, B., Schneider, G., Jordan, D., & Ilg, R. (2012). Spatiotemporal Reconfiguration of Large-Scale Brain Functional Networks during Propofol-Induced Loss of Consciousness. *Journal of Neuroscience*, *32*(37), 12832–12840.

Shen, K., Bezgin, G., Hutchison, R. M., Gati, J. S., Menon, R. S., Everling, S., & McIntosh, A. R. (2012). Information Processing Architecture of Functionally Defined Clusters in the Macaque Cortex. *Journal of Neuroscience*, *32*(48), 17465–17476.

Shin, J., Mashour, G. A., Ku, S., Kim, S., & Lee, U. (2013). Subgraph "Backbone" Analysis of Dynamic Brain Networks during Consciousness and Anesthesia. *PloS One*, *8*(8), e70899.

Sitt, J. D., King, J.-R., El Karoui, I., Rohaut, B., Faugeras, F., Gramfort, A., Cohen, L., Sigman, M., Dehaene, S., & Naccache, L. (2014). Large scale screening of neural signatures of consciousness in patients in a vegetative or minimally conscious state. *Brain*, *137*(8), 2258–2270.

Song, M., Yang, Y., He, J., Yang, Z., Yu, S., Xie, Q., Xia, X., Dang, Y., Zhang, Q., Wu, X., Cui, Y., Hou, B., Yu, R., Xu, R., & Jiang, T. (2018). Prognostication of chronic disorders of consciousness using brain functional networks and clinical characteristics. *ELife*, *7*.

Sporns, O. (2018). Graph theory methods: Applications in brain networks. *Dialogues in Clinical Neuroscience*, *20*(2), 111–121.

Sporns, O., & Kötter, R. (2004). Motifs in Brain Networks. *PLOS Biology*, *2*(11), e369.

Stagg, C. J., & Nitsche, M. A. (2011). Physiological Basis of Transcranial Direct Current Stimulation. *The Neuroscientist*, *17*(1), 37–53.

Stam, C. J., & van Straaten, E. C. W. (2012). Go with the flow: Use of a directed phase lag index (dPLI) to characterize patterns of phase relations in a large-scale model of brain dynamics. *NeuroImage*, *62*(3), 1415–1428.

Stam, Cornelis J., Nolte, G., & Daffertshofer, A. (2007). Phase lag index: Assessment of functional connectivity from multi channel EEG and MEG with diminished bias from common sources. *Human Brain Mapping*, *28*(11), 1178–1193.

Staniek, M., & Lehnertz, K. (2008). Symbolic transfer entropy. *Physical Review Letters*, *100*(15), 158101.

Stender, J., Mortensen, K. N., Thibaut, A., Darkner, S., Laureys, S., Gjedde, A., & Kupers, R. (2016). The Minimal Energetic Requirement of Sustained Awareness after Brain Injury. *Current Biology*, *26*(11), 1494–1499.

Straudi, S., Bonsangue, V., Mele, S., Craighero, L., Montis, A., Fregni, F., Lavezzi, S., & Basaglia, N. (2019). Bilateral M1 anodal transcranial direct current stimulation in post traumatic chronic minimally conscious state: A pilot EEG-tDCS study. *Brain Injury*, *33*(4), 490–495.

Teo, F., Hoy, K. E., Daskalakis, Z. J., & Fitzgerald, P. B. (2011). Investigating the Role of Current Strength in tDCS Modulation of Working Memory Performance in Healthy Controls. *Frontiers in Psychiatry*, *2*.

Thibaut, A., Bruno, M.-A., Ledoux, D., Demertzi, A., & Laureys, S. (2014). tDCS in patients with disorders of consciousness: Sham-controlled randomized double-blind study. *Neurology*, *82*(13), 1112–1118.

Thibaut, A., Chennu, S., Chatelle, C., Martens, G., Annen, J., Cassol, H., & Laureys, S. (2018). Theta network centrality correlates with tDCS response in disorders of consciousness. *Brain Stimulation*.

Thibaut, A., Di Perri, C., Chatelle, C., Bruno, M.-A., Bahri, M. A., Wannez, S., Piarulli, A., Bernard, C., Martial, C., Heine, L., Hustinx, R., & Laureys, S. (2015). Clinical Response to tDCS Depends on Residual Brain Metabolism and Grey Matter Integrity in Patients With Minimally Conscious State. *Brain Stimulation*, *8*(6), 1116–1123.

Thibaut, A., Schiff, N., Giacino, J., Laureys, S., & Gosseries, O. (2019). Therapeutic interventions in patients with prolonged disorders of consciousness. *The Lancet Neurology*.

Thibaut, A., Wannez, S., Donneau, A.-F., Chatelle, C., Gosseries, O., Bruno, M.-A., & Laureys, S. (2017). Controlled clinical trial of repeated prefrontal tDCS in patients with chronic minimally conscious state. *Brain Injury*, *31*(4), 466–474.

Tinker, J. H., Sharbrough, F. W., & Michenfelder, J. D. (1977). Anterior shift of the dominant EEG rhytham during anesthesia in the Java monkey: Correlation with anesthetic potency. *Anesthesiology*, *46*(4), 252–259.

Tononi, G. (2004). An information integration theory of consciousness. *BMC Neuroscience*, *5*(1), 42.

Tononi, G. (2012). The Integrated Information Theory of Consciousness: An Updated Account. *Archives Italiennes de Biologie*, *150*(2/3), 56–90.

Vacanti, C. J., VanHOUTEN, R. J., & Hill, R. C. (1970). A Statistical Analysis of the Relationship of Physical Status to Postoperative Mortality in 68,388 Cases. *Anesthesia & Analgesia*, *49*(4), 564–566.

Vecchio, F., Miraglia, F., Gorgoni, M., Ferrara, M., Iberite, F., Bramanti, P., Gennaro, L. D., & Rossini, P. M. (2017). Cortical connectivity modulation during sleep onset: A study via graph theory on EEG data. *Human Brain Mapping*, *38*(11), 5456–5464.

Vijayan, S., Ching, S., Purdon, P. L., Brown, E. N., & Kopell, N. J. (2013). Thalamocortical Mechanisms for the Anteriorization of Alpha Rhythms during Propofol-Induced Unconsciousness. *Journal of Neuroscience*, *33*(27), 11070–11075.

Vinck, M., Oostenveld, R., van Wingerden, M., Battaglia, F., & Pennartz, C. M. A. (2011). An improved index of phase-synchronization for electrophysiological data in the presence of volume-conduction, noise and sample-size bias. *NeuroImage*, *55*(4), 1548–1565.

Watts, D. J., & Strogatz, S. H. (1998). Collective dynamics of 'small-world'networks. *Nature*, *393*(6684), 440.

Wei, Y., Liao, X., Yan, C., He, Y., & Xia, M. (2017). Identifying topological motif patterns of human brain functional networks. *Human Brain Mapping*, *38*(5), 2734–2750.

Wu, M., Yu, Y., Luo, L., Wu, Y., Gao, J., Ye, X., & Luo, B. (2019). Efficiency of repetitive transcranial direct current stimulation of the dorsolateral prefrontal cortex in disorders of consciousness: A randomized sham-controlled study. *Neural Plasticity*, *2019*, 7089543.

Zaehle, T., Sandmann, P., Thorne, J. D., Jäncke, L., & Herrmann, C. S. (2011). Transcranial direct current stimulation of the prefrontal cortex modulates working memory performance: Combined behavioural and electrophysiological evidence. *BMC Neuroscience*, *12*(1), 2.

Zhang, Y., Song, W., Du, J., Huo, S., Shan, G., & Li, R. (2017). Transcranial Direct Current Stimulation in Patients with Prolonged Disorders of Consciousness: Combined Behavioral and Event-Related Potential Evidence. *Frontiers in Neurology*, *8*, 620.

Appendix 1: Supplemental Material – Brain Network Motifs are Markers of Loss and Recovery of Consciousness

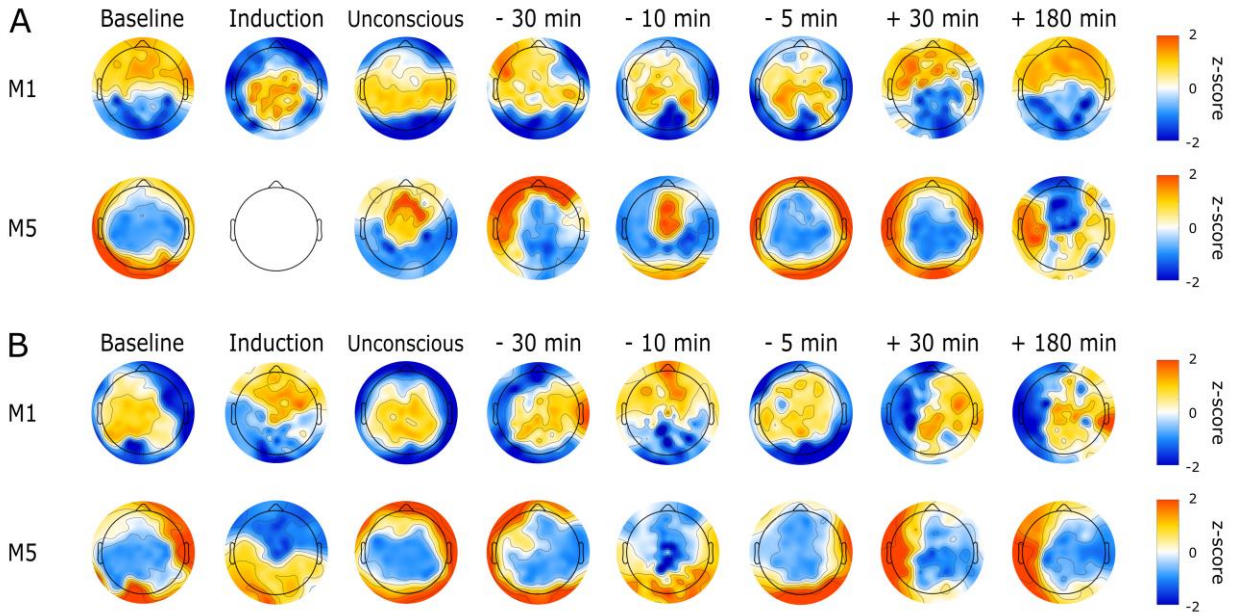

Supplemental Figure 1. Topography of motif frequency in the alpha band (8–13 Hz) across states of consciousness.

Visually compelling examples of motifs 1 and 5 (evident in 7/9 participants) are shown in panel A, while examples of non-compelling examples (evident in 2/9 participants) are in panel B. While the specific motif frequency distributions are different between individuals, motif 1 is central- or anterior-dominant during consciousness and shifts posteriorly during unconsciousness, while motif 5 is posterior-dominant during responsive states and involves anterior electrodes during unresponsive states.

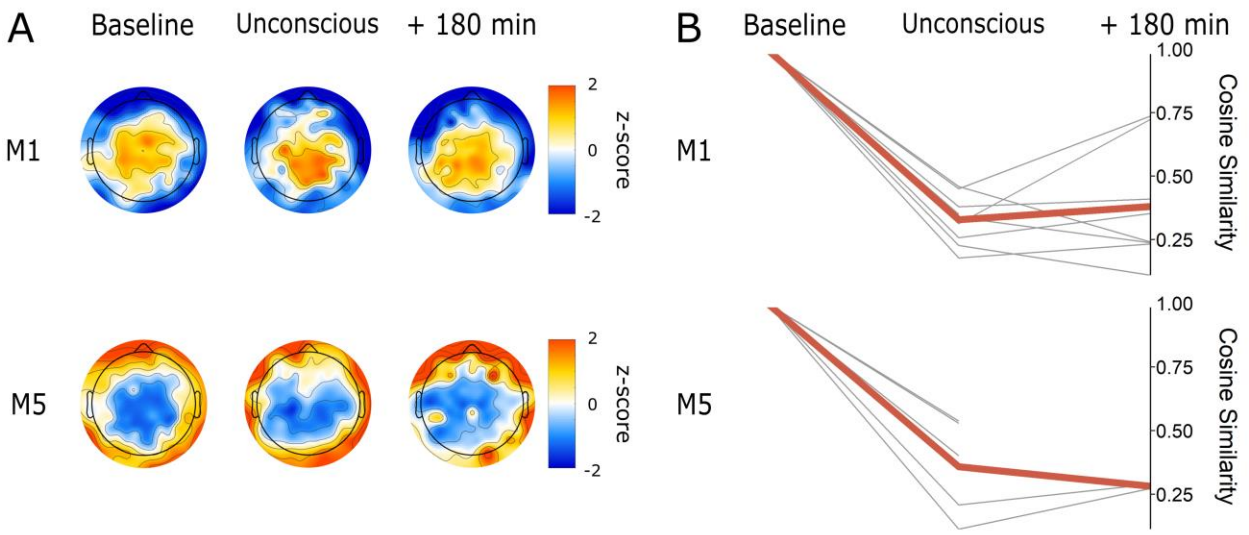

Supplemental Figure 2. Motif frequency averaged across participants in the delta band (1–4 Hz).

(A) Topographic maps indicate z-normalized motif frequency. (B) Cosine similarity between motif topographies at baseline, unconsciousness and 180-minutes post-return of responsiveness. Thin lines represent individual participants, while the thicker line represents cosine similarity averaged across participants. A reduced number of thin lines (< 9) indicates that motifs were non-significant for some participants. Here, cosine similarity shows that while motif topography shifts during unconsciousness, it does not return to its baseline state upon recovery of behavioral responsiveness. *M1 = motif 1*, *M5 = motif 5*.

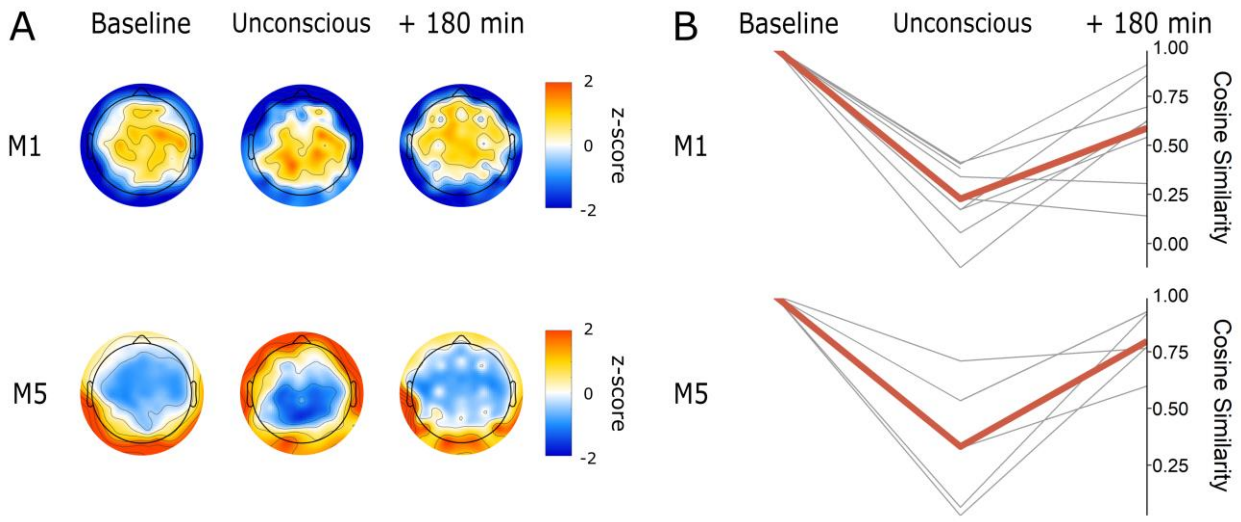

Supplemental Figure 3. Motif frequency averaged across participants in the theta band (4–8 Hz).

(A) Topographic maps indicate z-normalized motif frequency. (B) Cosine similarity between motif topographies at baseline, unconsciousness and 180-minutes post-return of responsiveness. Thin lines represent individual participants, while the thicker line represents cosine similarity averaged across participants. Cosine similarity supports what can be observed visually: motif 1 shifts slightly posteriorly while motif 5 shifts anteriorly during unconsciousness. Upon recovery of behavioral responsiveness, both motifs return to their baseline topography. *M1 = motif 1, M5 = motif 5.*

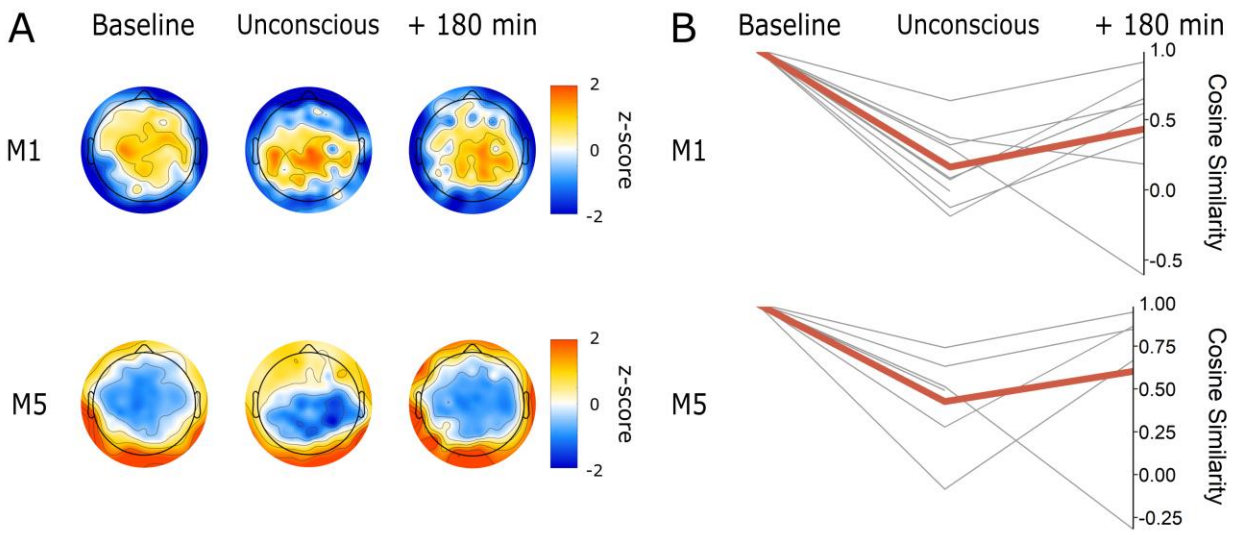

Supplemental Figure 4. Motif frequency averaged across participants in the beta band (13–30 Hz).

(A) Topographic maps indicate z-normalized motif frequency. (B) Cosine similarity between motif topographies at baseline, unconsciousness and 180-minutes post-return of responsiveness. Thin lines represent individual participants, while the thicker line represents cosine similarity averaged across participants. A reduced number of thin lines (< 9) indicates that motifs were non-significant for some participants. Here, cosine similarity shows that while motif topography shifts during unconsciousness, it does not return to its baseline state upon recovery of behavioral responsiveness. *M1 = motif 1, M5 = motif 5.*

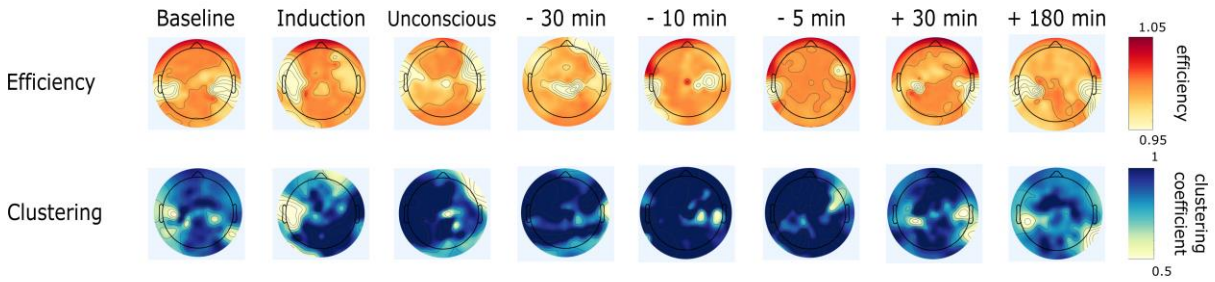

Supplemental Figure 5. Topography of efficiency and clustering coefficient in the alpha band (8–13 Hz) across states of consciousness for two individual participants.

The same participant as in Supplemental Figure 1 Panel A Motif 1 was used, to allow for comparison to their individual Motif 1 topography. Efficiency represents the inverse of the average path length between each node and all other nodes in the network. Clustering represents the clustering coefficient at each node. Both metrics were corrected against 10 random networks. There is no clear topographic organization of these metrics at baseline, or across epochs. We can observe a slight decrease in the magnitude of efficiency and an increase in the magnitude of clustering, which is in line with what we observe when analyzing the global efficiency and clustering coefficient (averaged across all nodes).